Structure-based design of hyaluronidase inhibitors

Dissertation

zur Erlangung des Doktorgrades der Naturwissenschaften (Dr. rer. nat.)
der Naturwissenschaftlichen Fakultät IV – Chemie und Pharmazie –
der Universität Regensburg

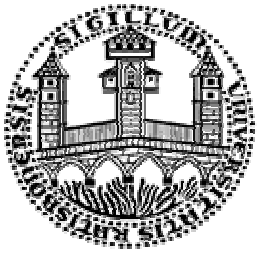

vorgelegt von

Alexander Botzki

aus München

2004

Die vorliegende Arbeit entstand in der Zeit von Juni 2000 bis März 2004 unter der Leitung von Herrn Prof. Dr. A. Buschauer und Herrn Prof. Dr. S. Dove am Institut für Pharmazie der Naturwissenschaftlichen Fakultät IV – Chemie und Pharmazie – der Universität Regensburg.

Das Promotionsgesuch wurde eingereicht im März 2004.

Tag der mündlichen Prüfung: 11. Mai 2004

Prüfungsausschuss:	Prof. Dr. W. Wiegrebe	(Vorsitzender)
	Prof. Dr. A. Buschauer	(Erstgutachter)
	Prof. Dr. S. Dove	(Zweitgutachter)
	Prof. Dr. C. Steinem	(Prüfer)

To whom it may concern

… pinki

Der Blick des Forschers fand nicht selten mehr, als er zu finden wünschte.

Ludwig Uhland

Ich bedanke mich bei Herrn Prof. Dr. A. Buschauer für die interessante Themenstellung, seine wissenschaftlichen Anregungen sowie für seine Förderung und die Durchsicht beim Verfassen dieser Arbeit.

Herrn Prof. Dr. S. Dove danke ich für die interessante Themenstellung, seine wissenschaftlichen Anregungen und Diskussionen sowie für die konstruktive Kritik bei der Durchsicht dieser Arbeit.

Bedanken möchte ich mich auch bei Herrn Dr. G. Bernhardt für seine Unterstützung bei der Lösung experimentell-pharmakologischer Probleme.

Bei Herrn M. J. Jedrzejas (Children's Hospital Oakland Research Institute, Oakland, California 94609, USA) und Herrn D. J. Rigden (National Centre of Genetic Resources and Biotechnology, Cenargen/Embrapa, Brasília, D.F. 70770-900, Brazil) bedanke ich mich für die Durchführung der Kokristallisations- Experimente und für die Aufnahme und Aufklärung der Röntgenkristallstrukturen.

Frau Dr. S. Salmen danke ich ganz besonders für die Synthese der vorgeschlagenen Substanzen, deren pharmakologische Testung sowie für die zahlreichen wertvollen Diskussionen und Anregungen. Herrn S. Braun und Herrn M. Spickenreither danke ich für die synthetisierten Verbindungen.

Herrn Dr. Christian Neiß danke ich für zahlreiche Diskussionen über theoretische Problemstellungen (Parameterschlachten, (Un)Sinn der Theorie, etc.).

Frau A. Roithmeier, Frau S. Bollwein und Frau J. Hoechstetter danke ich für die Unterstützung bei der Durchführung der pharmakologischen Testung.

Frau S. Heinrich und Herrn P. Richthammer danke ich für die Hilfsbereitschaft und Unterstützung in vielen organisatorischen und technischen Dingen und Herrn Dr. H.-J. Wittmann für tatkräftige Hilfe bei Computernotfällen.

Allen Mitgliedern des Lehrstuhls danke ich für die Kollegialität und das gute Arbeitsklima.

Bei den Firmen Tripos GmbH, Unterschleißheim, und Accelrys Inc., Unterschleißheim, bedanke ich mich für die Bereitstellung der Rohdaten zur Datenbankerzeugung sowie für die kostenlosen Probelizenzen.

Bei der Studienstiftung des deutschen Volkes bedanke ich mich für ideelle und finanzielle Förderung.

Besonderer Dank gilt auch meinen Freunden Sunny, Christian und Martin, Thomas und Andrea, Stephan, Uta & Albert & Jona, meiner Spielegruppe (Britta, Ralf, Christian und Martin) sowie meiner gesamten Familie.

Bedanken möchte ich mich auch bei meinen Kollegen Frau J. Hoechstetter, Frau Dr. S. Salmen, Herrn S. Braun, Herrn A. Brennauer und Herrn H. Preuß für die Unterstützung bei fachlichen Problemen, das heitere Laborklima sowie für die vielen Aufheiterungen im (Labor-) Alltag.

Contents

Chapter 1 Introduction

1.1 Hyaluronic acid

1.1.1 Structure and physicochemical properties

Hyaluronic acid (HA), first isolated from the vitreous humour of bovine eyes by Karl Meyer in 1934,[1] consists of repeating disaccharide units of [-> 4)-β-D-glucuronic acid(1-> 3)-β-D-*N*-acetylglucosamine(1->]$_n$, where *n* can be up to 20000 and larger (Figure 1.1).

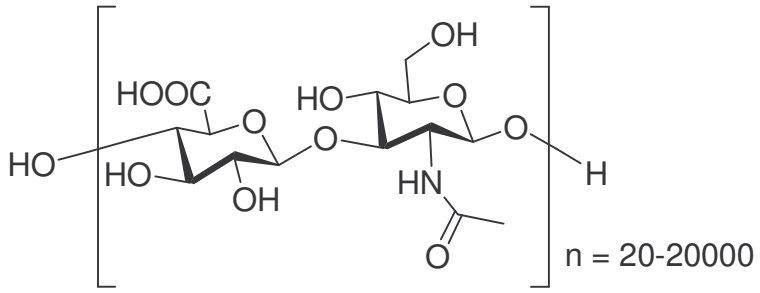

Figure 1.1. Chemical structure of hyaluronic acid

Hyaluronic acid (hyaluronan), along with chondroitin-, keratan- and dermatane sulfate, heparin and heparan sulfate, is a member of the family of glycosaminoglycanes which are mostly linear polymers of high molecular weight composed of aminosugars (*N*-acetylglucosamine or *N*-acetylgalactosamine) and uronic acids (glucuronic or iduronic acid). In contrast to the other glycosaminoglycanes, HA is not subjected to any type of covalent modification, especially sulfation, during its synthesis.

For decades, it was assumed that hyaluronan chains in solution were random coils. However, nuclear magnetic resonance studies of the shape of HA performed by J. E. Scott[2] have shown that the HA chain may be stabilised in a helical conformation via internal hydrogen bonds. Each disaccharide unit is twisted by 180 degrees with respect to both the preceding and the subsequent one. The total orientation of the hyaluronan chain is achieved by a second twist resulting in an overall two-fold helix. The striking feature of this helix is an extensive hydrophobic patch of about 8 CH-groups of 3 carbohydrate units. In addition to the two-fold helix, based on X-ray fibre diffraction studies with stretched, semi-hydrated fibres and films of different salts of

hyaluronic acid, three-fold and four-fold single helices were detected.[3] Molecular dynamics simulations of HA decasaccharide fragments revealed high flexibility and fast interconversion of hyaluronan conformations. In solution, high molecular weight sodium hyaluronate can be modelled as a highly extended structure with similar local conformations to those obtained from X-ray diffraction analysis and predicted by molecular dynamics.[4]

These properties lead to very viscous solutions of high molecular weight HA, i.e. by binding water, the volume of HA increases by about 1000-fold compared to the non-hydrated state.[5] In the hydrated state, the diffusion of e.g. proteins and electrolytes is substantially facilitated.

1.1.2 Occurrence and physiological importance

As major constituent of the extracellular matrix, hyaluronan is present in the skin (about 50 % of the total HA in the body) but also in the vitreous humour of the eye (0.1-0.4 mg/g wet weight), in the synovial joint fluid (3-4 mg/ml), in the matrix produced by the cumulus cells around the oocyte prior to ovulation (~0.5 mg/ml), or in the pathological matrix that occludes the artery in coronary restenosis.[6] Hyaluronan is synthesised by all vertebrates, some *Streptococci* strains, and viruses.

Hyaluronan as an essential structural element in the matrix plays an important role for tissue architecture by immobilising specific proteins (aggrecan, versican, neurocan, brevican, CD44 etc.) in desired locations within the body. Furthermore, hyaluronan is involved in many (patho)physiological processes, like reproduction, cell growth and migration as well as tumour spread. Increased levels of hyaluronan are observed during morphogenesis, embryonic development, wound healing and inflammation.[5,7] The function of HA may be partly regulated dependent on its chain length, e.g. angiogenesis is presumably induced by small HA oligosaccharides, whereas high molecular weight HA exerts inhibitory effects.[8]

Cell behaviour like migration etc. is affected by the interaction of hyaluronic acid with a variety of receptors and binding proteins on the surface of cells.[7,9] The most studied hyaluronan receptor to date is CD44 (lymphocyte homing receptor). Several other hyaluronan binding proteins have been identified including the RHAMM (receptor for hyaluronan which mediates motility), ICAM-1 (intercellular adhesion molecule-1) and the LEC receptor (Liver Endothelial Cell clearance receptor).[5,6]

1.2 Hyaluronidases

1.2.1 History and occurrence

Hyaluronidase was first identified in an extract of mammalian testes and other tissues as a 'spreading factor' that facilitated diffusion of antiviral vaccines, dyes and toxins injected subcutaneously.[10] After the first isolation of hyaluronan by Meyer et al.[1] and the identification of a HA degrading enzyme in bacteria,[11] it could be shown that the mammalian spreading factor was also an enzyme degrading hyaluronan.[12] Similar hyaluronidase-like enzymes were detected and/or isolated from a large number of tissues, e.g. liver, kidney, spleen, testes, uterus, placenta, from the venom of snakes, lizards, fish, bees, wasps, scorpions, spiders as well as from some bacteria, fungi and invertebrate animals. The isolated hyaluronidases differ in their molecular weight, substrate specificity and pH optima.[13-15] Although ubiquitously found, hyaluronidases are not well characterised and are a group of disregarded enzymes due to difficult purification and lack of scientific interest over a large period of time.

1.2.2 Classification of hyaluronidases

The first classification scheme for hyaluronidases was established in 1971 by K. Meyer. According to their catalytic mechanism, the hyaluronidases are grouped into three main families (Figure 1.2).[16]

The first group of hyaluronidases are the hyaluronate 4-glycanohydrolases (EC 3.2.1.35) degrading hyaluronan by cleavage of the β-1,4-glycosidic bond to the tetrasaccharide as the main product. As a special characteristic, these enzymes also catalyse transglycosylation reactions.[17,18] The best known enzymes are the testicular, the lysosomal and the bee venom hyaluronidase.

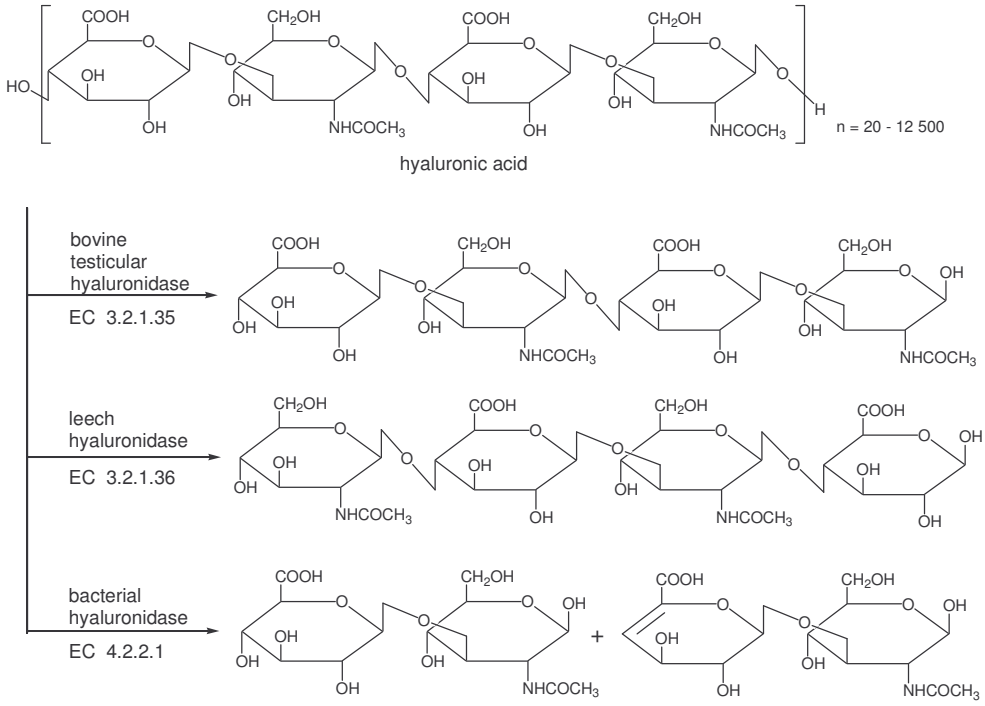

Figure 1.2. Classification of hyaluronidases according to Meyer.[16]

The second type is represented by hyaluronidases from leeches and from hookworms. These enzymes are hyaluronate 3-glycanohydrolases (EC 3.2.1.36) which degrade HA by cleavage of the β-1,3-glycosidic bond. The main product of this reaction is a tetrasaccharide, too.

The third group, the bacterial hyaluronidases (EC 4.2.2.1) are actually hyaluronate lyases. These enzymes degrade hyaluronan by a β-elimination reaction to yield the unsaturated disaccharide 2-acetamido-2-deoxy-3-*O*-(β-*D*-gluco-4-enepyranosyluronic acid)-*D*-glucose as main product.[15,16,19]

As an alternative to the classification according to Meyer, hyaluronidases are divided in two main families – the hyaluronidases from eukaryotes and from prokaryotes – according to amino acid sequence homology.[13,20]

1.2.3 Hyaluronidases from eukaryotes

In the last years, many human hyaluronidase genes located on human chromosomes 3p21.3 and 7q31.3.[20] were identified and the corresponding proteins were expressed in different cell lines. Several isoforms (Hyal1, Hyal2, Hyal3, Hyal4 and PH-20/Spam1) sharing about 40 % amino acid sequence identity have been found. The human testicular hyaluronidase, PH-20 protein, was first expressed by Gmachl et

al.[21] and is essential for penetration of the hyaluronan-rich cumulus mass that surrounds the oocyte and for fertilisation.[22] It is a multifunctional protein with a separate domain that binds to the zona pellucida.[23] Hyal1 and Hyal2 are found in most tissues and body fluids and are believed to act in succession on degrading hyaluronan. Hyal2, either anchored to the plasma membrane by a glycosylphosphatidylinositol link or occurring in a soluble form, cleaves HA to a product of approximately 20 kDa, whereas Hyal1, a lysosomal as well as a plasma enzyme, produces small oligosaccharides with tetrasaccharides as major products.

Mutations in the gene *hyal1* cause a newly described lysosomal disorder, mucopolysaccharidosis IX.[24,25] Furthermore, Hyal1 and Hyal2 appear to play a role in tumour formation. Hyal1 is a candidate tumour suppressor gene product, deleted in many tobacco-related lung tumours.[26,27] Hyal2 might share an oncogenic and a tumour suppressor gene function. At the one hand, overexpression of Hyal2 accelerates tumour formation of murine astrocytoma cells[28] and on the other hand, Hyal2 seems to accelerate apoptosis.[29] Additionally, a distinct influence of the size of HA degradation products on proliferation and, to a lesser extent, on migration could be assumed in vitro,[8] often referred to as angiogenic switch. In the beginning of tumour formation, high molecular weight HA is necessary to provide the flow of nutrients at the primary site and subsequently, intermediate HA fragments produced by Hyal2 induce angiogenesis.[30]

Very little is known about Hyal3 found in testis and bone marrow and about Hyal4 which appears to be a chondroitinase.[31] All known hyaluronidases are active at acidic pH, consistent with a lysosomal location, except PH-20 which also exhibits activity at neutral pH. All of these enzymes were barely investigated up to now[15] due to problems on isolation, purification and activity assays and to their instability.

By contrast, the bovine testicular hyaluronidase (BTH, bovine PH-20 protein) as well known representative of the mammalian hyaluronidases has been used in several medical fields for many years, e.g. orthopaedia, ophthalmology and internal medicine.[32,33] It is an endo-glycanohydrolase that cleaves the β-1,4 glycosidic bond of hyaluronan. In addition to hyaluronic acid, BTH degrades chondroitin and chondroitin 4- and 6-sulfate, which are structurally related to HA. By using ion-spray mass spectrometry, tetrasaccharide and saturated disaccharide fragments could be identified as major and as smallest hydrolysis products, respectively.[18] The pH optimum of hyal-

uronidase activity is dependent on the mostly heterogeneous enzyme composition of the BTH preparations,[34,35] the used substrate, the hyaluronidase assay and the incubation conditions.[16,34,36,37]

In addition to hydrolase activity, the bovine testicular hyaluronidase exhibits transglycosylase activity if oligosaccharides with 6 to 12 monomer units are available, leading to saturated HA oligosaccharides with *N*-acetylglucosamine at the reducing end.[17] Transglycosylation reactions are dependent on the pH value and the salt content of the incubation buffer. The optimal pH value for hydrolase activity is about 4-5, whereas pH 7 appears to be optimal for transglycosylation reactions. In the presence of NaCl, transglycosylase activity is nearly completely inhibited at concentrations higher than 0.5 M.[38]

Bee venom hyaluronidase (BVH) is a member of the hyaluronate 4-glycanohydrolases (EC 3.2.1.35) like the bovine testicular hyaluronidase. The sequence identity between mammalian hyaluronidases and bee venom hyaluronidase amounts to ca. 30 %. BVH lacks a C-terminal domain of ca. 120-150 amino acid residues present in the human and bovine hyaluronidases.[39] In 2000, the crystal structure of the bee venom hyaluronidase in complex with a HA–based tetrasaccharide was elucidated by Markovic-Housley et al.[40] The analysis of the crystal structure reveals an unusual overall fold, a $(\beta/\alpha)_7$ barrel instead of a regular $(\beta/\alpha)_8$ barrel. The HA binding site is situated at the C-terminal end of the β barrel and is lined with many conserved amino acids, e.g. both catalytic amino acids Asp111 and Glu113 along with Arg116 and Arg244 etc. Similar folds were identified for other carbohydrate degrading enzymes with a regular $(\beta/\alpha)_8$ barrel fold like β-amylase from soybean,[41] β-glucuronidase[42] etc. With respect to the active site architecture, similarity with BVH was only observed for the bacterial chitinase A.[43] In particular, the catalytic acids and several aromatic residues are located at spatially equivalent positions.[40,44]

Due to the co-crystallised HA tetrasaccharide fragment, the catalytic mechanism of HA degradation could be elucidated. In general, glycosidases act via a double or a single nucleophilic displacement mechanism which results in either retention or inversion of the configuration of the anomeric carbon atom.[44,45] In both cases, the glycosidic bond to be cleaved is positioned between two carboxylates, one acting as acid/base and the other originally suggested as nucleophile. In the crystal structure of BVH, Glu113 appears to be the catalytic acid since it forms a hydrogen bond (2.6 Å)

with the the glycosidic bond oxygen O1 of *N*-acetylglucosamine in subsite -1*. The proximate Asp111 seems to keep Glu113 in proper orientation for catalysis via a short hydrogen bond between both carboxylates, but is not in an adequate spatial position to act as enzymatic nucleophile. Therefore a substrate-assisted mechanism is proposed. The *N*-acetylglucosamine in subsite -1 (**1**) is distorted to a $^{4,1}C$ boat conformation (Figure 1.3) so that the *N*-acetyl group of the residue can attack the anomeric carbon atom forming a covalent oxazolinium ion intermediate (**2**). In a probably concerted action, Glu113 donates the proton to release the cleaved sugar residue. The ionic intermediate is hydrolysed to the product **3** with retention of the configuration at C1 of the *N*-acetylglucosamine at the reducing end.[44] A very similar mechanism has been postulated for retaining β glycosyl hydrolases of family 18 on basis of structural data[47-49] as well as theoretical calculations.[50]

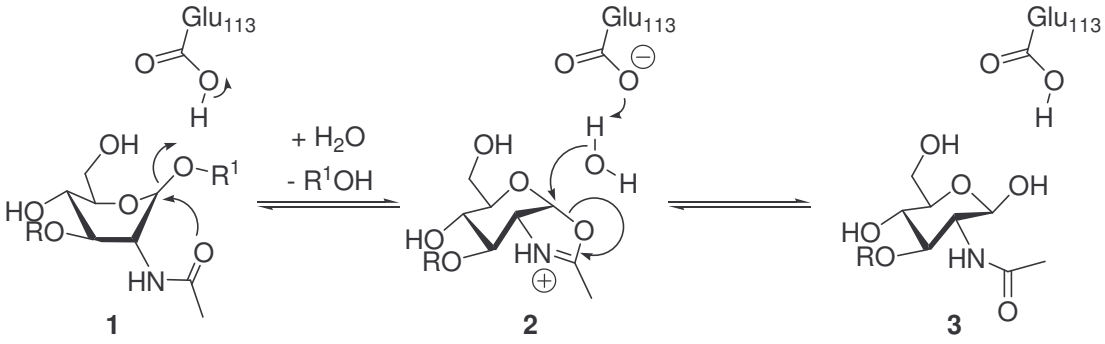

Figure 1.3. Double-displacement substrate assisted mechanism of bee venom hyaluronidase. The saccharide in subsite –1 (**1**) binds in boat conformation, and catalysis is proposed to occur via a formation of a covalent oxazolinium ion intermediate **2** to the product **3**. Adapted from reference [44].

BVH is a major allergen of bee venom, and knowledge of the structural determinants responsible for the allergenic potency is expected to lead to clinical implications.

1.2.4 Hyaluronidases from prokaryotes

To date, the amino acid sequences of a variety of hyaluronidases from prokaryotes have been decoded.[51] The best known and characterised bacterial hyaluronidases are *Streptococcus pneumoniae* and *S. agalactiae* hyaluronate lyases.[19,52,53] Both enzymes degrade hyaluronic acid at the β-1,4-glycosidic linkage between D-glucuronic acid and *N*-acetyl-D-glucosamine. The product of this elimination reaction is the un-

* By convention, the sugar residue subsites are labelled from *-n* to *+n*, with *-n* at the non-reducing end and *+n* at the reducing end of the substrate. Cleavage occurs between the -1 and +1 subsites.[46]

saturated disaccharide 2-acetamido-2-deoxy-3-*O*-(β-D-gluco-4-enepyranosyluronic acid)-D-glucose.[15,16,19,54] Recently, the 3D structures of *S. pneumoniae* and *S. agalactiae* strain 3502 hyaluronidases were elucidated by X-ray analyses.[52,53,55,56] The active site of *S. pneumoniae* hyaluronidase (hylSpn) is composed of two main parts, a catalytic triad responsible for the substrate degradation and an aromatic patch responsible for the selection and the positioning of cleavage sites on the polymeric substrate.[56] The residues that form the aromatic patch of the enzyme are Trp291, Trp292 and Phe343, those of the catalytic triad are His399, Tyr408 and Asn349.

Based on the crystal structure and mechanistical studies, the mechanism of the elimination reaction was revealed.[52,53,55,57] In the first step, the positively charged cleft of the enzyme attracts and binds the negatively charged substrate chain. Three disaccharide units can be accommodated into the cleft (see Figure 1.4, only two, HA1 and HA2, of the three units are drawn). In the second step, the aromatic patch of the active site interacts with the substrate chain and anchors it in optimal position. In the third step, the glucuronic acid of HA1 is deprotonated at C5 by His399 (Figure 1.4). At the same time, Tyr408 donates a proton to the glycosidic oxygen connecting D-glucuronic acid of HA1 and *N*-acetyl-D-glucosamine of HA2. The glycosidic bond is cleaved by 1,2-elimination forming the double bond of the unsaturated final product (fourth step). Finally (fifth step), the catalytic triad is regenerated: His399 is deprotonated and Tyr408 is protonated by a water molecule.

This mechanism could be strongly supported by elucidation of 3D structures of the native enzyme hylSpn in complex with hyaluronan-based fragments of various lengths.[58] Furthermore, both hyaluronidases also cleave chondroitin and chondroitin sulfate (specific sulfation pattern provided)[19] which could also be analysed in detail by a X-ray structure of hylSpn in complex with chondroitin and chondroitin sulfate disaccharides.[59]

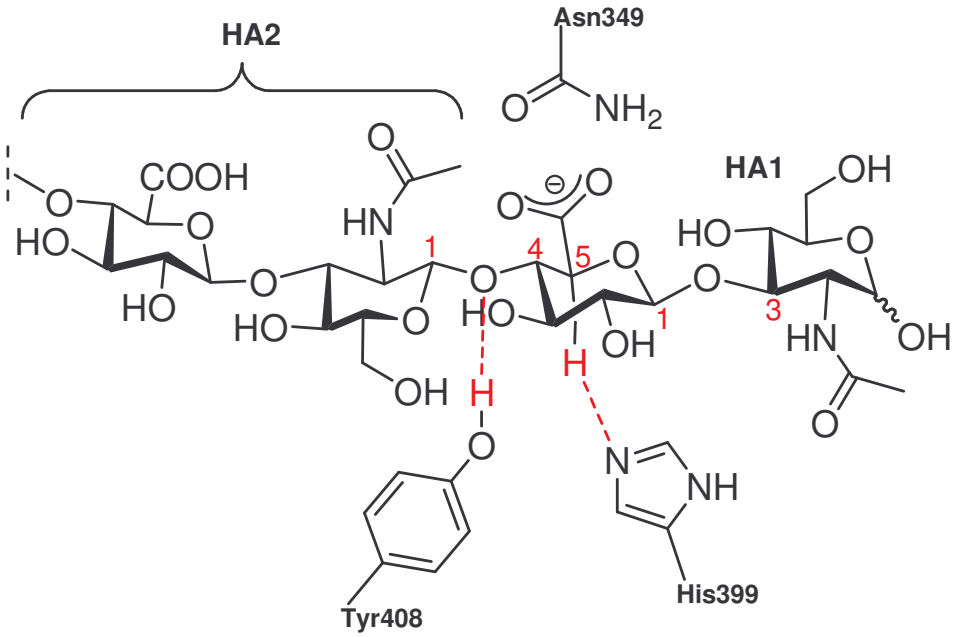

Figure 1.4. Mechanism of hyaluronan degradation by *S. pneumoniae* hyaluronate lyase according to Li et al.[56] Schematic representation of hyaluronic acid with HA1 and HA2 as disaccharide units and the position of the side chains of Tyr408, His399 and Asn349 relative to the substrate.

The *S. agalactiae* strain 4755 hyaluronate lyase ($hylB_{4755}$) shows sequence identities of 98 % with the homologous enzyme of *S. agalactiae* strain 3502 ($hylB_{3502}$)[60,61] and of 53 % with *S. pneumoniae* hyaluronidase. In contrast to the crystal structure of hylSpn,[56] the $hylB_{3502}$ structure consists of three instead of two distinct structural domains (see Figure 1.5).[55] In particular, it contains an additional βI-domain preceding the α-domain at the N-terminus of the protein. The α-domain, the short 10-residue linker after it, and the following β-domain (βI in hylSpn, βII in $hylB_{3502}$) are present in both lyases.

In general, both hyaluronidases are highly similar with respect to the overall architecture of the structures and to the spatial arrangement of the active site residues, but major differences occur at the end of the α-domain, especially in the region that includes the catalytic cleft. In the $hylB_{3502}$ structure, rotation of the α- with respect to the βII-domain by a small angle leads to a cleft which is about 7.3 Å wider than in the hylSpn structure (Figure 1.5).[55] As a consequence, the spatial positions of the catalytically active amino acids Tyr488, His479 and Asn429 (Tyr408, His399 and Asn349 in hylSpn) are significantly different.[55] Nevertheless, the catalytic mechanisms of $hylB_{3502}$ and hylSpn are probably identical since the observed more open conformation of $hylB_{3502}$ might result from the crystallisation conditions.

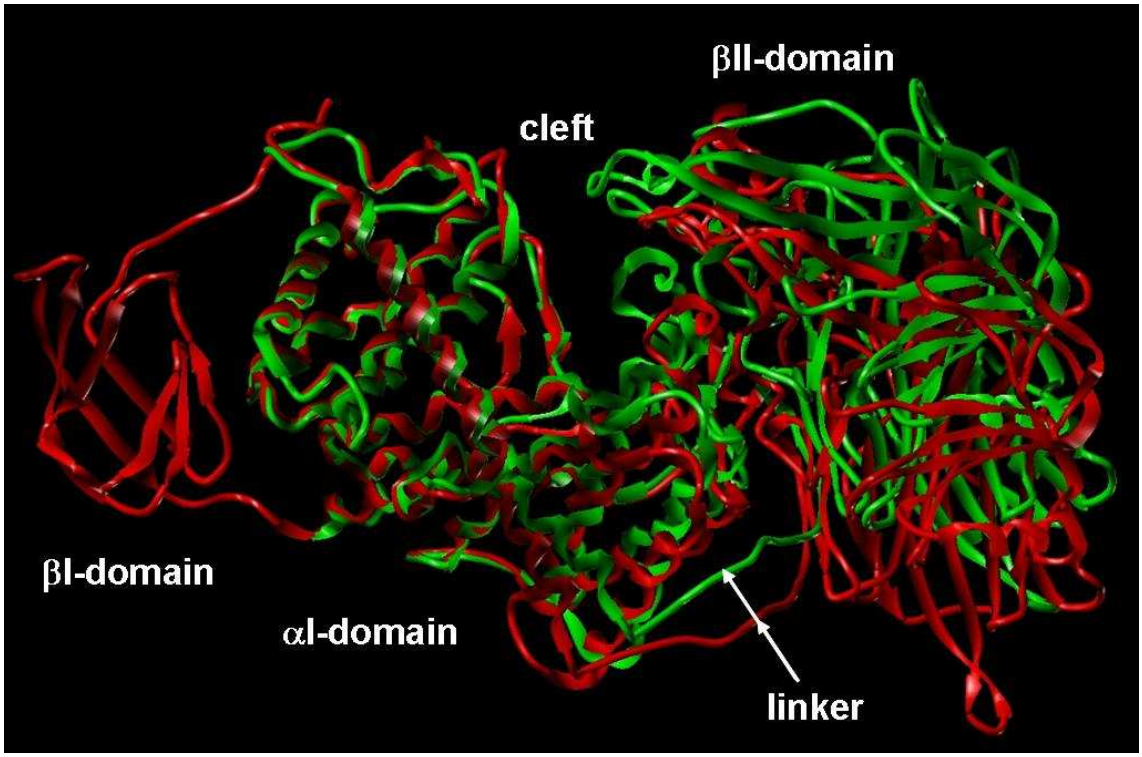

Figure 1.5. Superposition of αI-domains of crystal structures of hylSpn (green) and $hylB_{3502}$ (red).

Bacterial hyaluronate lyase is a virulence factor which facilitates the spreading of the microorganisms by degradation of hyaluronan. Human infection by *S. agalactiae* is one of the major causes of meningitis and septicaemia and many other serious diseases leading to death in neonates.[62,63] To study the role of hyaluronan and hyaluronidases in bacterial infection, the design and development of hyaluronate lyase inhibitors become more and more important.

1.3 Medical applications of hyaluronan and hyaluronidases

Due to the high water-binding capacity of hyaluronan and the viscoelasticity of hyaluronan solutions, it is suitable for various therapeutical purposes. Probably in the late 1950s hyaluronan was applied for the first time to humans, namely as vitreous humour supplement/replacement during eye surgery, an application which has proven of value up to now (e.g., in cataract surgery).[64] Sodium hyaluronate and a covalently cross-linked form of hyaluronan are successfully used for the treatment of osteoarthritis.[65] Anabolic effects of HA on degraded articular cartilages suppress their degeneration.[66] HA normalises the properties of synovial fluids[67] and reduces the

perception of pain.[68,69] Additionally, in many clinical situations, a rapid increase of hyaluronan levels is observed, e.g. in shock incidents, septicaemia and in burn patients.[13,14,25]

By cleaving hyaluronan in tissues, hyaluronidases increase the membrane permeability, reduce the viscosity and promote the diffusion of injected fluids; these phenomena are referred to as spreading effect of hyaluronidases. Thus, these enzymes could be used therapeutically to increase the speed of absorption, to facilitate resorption of excess fluids, to improve the effectiveness of local anaesthesia and to prevent tissue destruction resulting from subcutaneous and intramuscular injection of fluids.[14,32] Hyaluronidases, especially BTH preparations, are indeed widely used in many fields like orthopaedia, surgery, ophthalmology, internal medicine, oncology, dermatology, gynaecology etc.[6,32,70,71] Due to depleted supplies of pharmaceutical BTH preparations, a number of cases of iatrogenic strabismus have been observed after cataract surgeries.[72] With respect to this shortage, pharmaceutical preparations with bacterial[34] or ovine hyaluronidase[73] are suggested as replacement of BTH.

Hyaluronidase has been investigated as an additive to chemotherapeutic drugs for augmentation of the anticancer effect.[33,36,74,75] There is evidence that hyaluronidase may have intrinsic anticancer effects and can suppress tumour progression, however, the findings are rather inconsistent. The specific function of Hyal1 and Hyal2 in different tumours is still contradictory, and also the angiogenic effect of HA fragments must be taken into consideration. Furthermore, it was reported, that treatment with hyaluronidase blocks lymph node invasion by tumour cells in an animal model of T cell lymphoma.[76]

Sperm hyaluronidase plays an important role for successful fertilisation in most mammals, including humans.[77,78]

1.4 Inhibitors of hyaluronidases

To prove and to further investigate the role and the importance of hyaluronan and hyaluronidase in physiological and pathophysiological processes, selective and potent inhibitors are required. The first studies on hyaluronidase inhibitors were published 50 years ago.[79-81] In 1951, Meyer et al. reported on hyaluronidase inhibition by iron, copper and zinc salts, heparin, polyphenols and flavonoids.[79] Due to the struc-

tural similarity of heparin and heparan sulfate to hyaluronic acid, these oligosaccharides were investigated as inhibitors of hyaluronidase, but the inhibition was achieved only at concentrations much higher than physiological levels.[32,82-84] Asada et al. examined the effect of various types of alginic acid consisting of L-glucuronic acids and D-mannuronic acids on the bovine testicular hyaluronidase.[85] The inhibition by sodium alginate was dependent on the molecular weight – the higher the molecular weight, the stronger the inhibition. Based on these results, Toida et al. investigated *O*-sulfated glycosaminoglycans of which the fully sulfated compounds showed the highest inhibitory effect.[86]

Also some flavones and flavone analogues like apigenin and kaempferol inhibit hyaluronidase,[87-90] but not selectively and only at millimolar concentrations.[91] Further compounds with likewise weak inhibitory activity were detected, e.g. aescin, disodium cromoglycate, tranilast, traxanox, hederagenin, norlignane, urolithin B etc.[87,92-95] Recently, vitamin C,[96] L-arginine derivatives[97] and fatty acids[98] were reported to inhibit a streptococcal hyaluronidase with IC_{50} values at (sub)millimolar concentration.

In general, the published data (% inhibition and IC_{50} values) of these compounds are not comparable among each other because of differences in the applied test systems (e.g. incubation condition, enzymes and substrate concentrations). Due to the importance of hyaluronan and hyaluronidase in many clinical applications, selective and potent inhibitors are worthwhile but it is apparent that their systematic development has barely begun. In this respect computer-aided molecular design methods could make a significant contribution.

1.5 Virtual screening and structure-based ligand design

One of the key elements in a drug development project is the discovery of new and innovative lead compounds. In the last years, the pharmaceutical industry has invested much effort to establish compound libraries that can be searched for leads. On the one hand, high-throughput facilities with in-house compound stocks were developed to generate biological activity data for a variety of targets in a very short period of time. Despite the great enthusiasm in the early stage, the use of high-throughput screening (HTS) has often resulted in low success rates for the conversion of apparent HTS hits into lead compounds due to many problems like false posi-

tives, non specific binding, low solubility etc.[99] On the other hand, virtual screening has emerged as an alternative and complementary approach to experimental HTS. This methodology subsumes a large repertory of computational tools for the selection of potentially active and bioavailable compounds from libraries. Fast filter approaches and coarse molecular similarity criteria as well as sophisticated docking and scoring techniques are applied in this field.[100]

Starting point of these theoretical methods is a virtual compound library containing in principle any imaginable molecule. Preferentially, due to fast substance acquisition and easy validation of initial computer hits, compound collections of in-house or commercially available molecules are initially screened. The Available Chemical Directory (ACD),[101] the LeadQuest® libraries,[102] the ChemStar Library[103] are examples of libraries with commercially available compounds. The World Drug Index[104] and the MDL Drug Data Report[105] databases, which are compiled from drugs launched or under development, are frequently used in virtual screening approaches, too. Further libraries are designed by means of building blocks of combinatorial chemistry.

Reasonably, applying fast filter criteria, compounds with undesired physicochemical properties are eliminated at the beginning of a virtual screening approach. Since insufficient pharmacokinetic properties (ADMET: absorption, distribution, metabolism, excretion, and toxicity) of the proposed drug candidates have led or still lead to the termination of many drug development projects,[106] increasing efforts are made to define structural requirements which molecules have to meet for further consideration as potential drug. Apart from filters like molecular weight ranges, the total number of H-bond acceptor and donor groups,[107] neural networks are applied to discriminate between drug-like and non drug-like molecules on basis of structural patterns.[108,109]

Nowadays, the application of virtual screening approaches accelerates the discovery of new lead compounds and their structural optimisation with respect to affinity and pharmacological properties. The general kind of approach depends on the availability of a three-dimensional (3D) structure of the biological target. If present, structure-based virtual screening is possible, otherwise only ligand-based design methods may be applied.[110]

Structure-based approaches are to design compounds which spatially fit to a binding site on the macromolecule by forming electrostatic, steric and hydrophobic interactions. Two general cases of searching for such biologically active molecules may be

discriminated: molecular database mining and *de novo* ligand design combined with fast automated docking. Prerequisite of all virtual screening methods is the detailed knowledge about the localisation and the geometry of the binding site, mostly deduced from X-ray structures with co-crystallised natural substrates or synthetic organic ligands.

Until now, several screening and *de novo* design programmes like CAVEAT,[111] TOPAS,[112] LeapFrog[113] and LUDI[114] have been described enabling the rational design of new ligands based on the 3D structure of a target protein.[100,115] As initial step most of these programmes perform a detailed analysis of the amino acid residues forming the binding pocket and extract the spatial binding features which potential ligands have to meet. These favourable interaction sites are then converted into a complex pharmacophoric model of the active site of the target. Large databases of small molecules can be computationally screened for fit with this model, resulting in the identification of complementary ligands in terms of geometrical and physicochemical properties. Putative screening hits are selected by a scoring function roughly predicting affinity. The scoring of the proposed ligand pose (target-bound conformation and orientation of the screened ligand) approximates the interaction between the ligand and the amino acid residues of the binding pocket.[116,117] Any rational design approach includes several design cycles with appropriate structural modifications, syntheses and testing of the new candidate structures, aiming at ligands with improved binding affinities.

In many cases, these approaches are accompanied by fast automated post-docking.[100] Prerequisites of these automated methods are the knowledge of the 3D coordinates of the target protein and the candidate molecules as well as a scoring function for the accurate prediction of binding affinities. Programmes which vary the relative orientation and the conformation of the ligand in the binding site are classified as flexible docking programmes. However, most methods still neglect protein flexibility by docking into a rigid active site. A variety of protein-ligand docking algorithms have been developed like FlexX,[118] AutoDock,[119] DOCK[120] etc. Exemplarily, the principles of FlexX are outlined very briefly. Its incremental construction algorithm handles the conformational freedom of the ligands by dividing them into smaller fragments at their rotatable bonds and reassembling these fragments within the binding site. First, the base fragment, a rather rigid ligand fragment, is favourably placed into the binding site in terms of directed hydrophobic and/or hydrogen bond

interactions. Subsequently, by creating a set of high-scoring partial placements, the remaining fragments are successively connected to the base fragments. The crucial issue of FlexX and all other flexible docking programmes is a prediction of a native-like binding mode in combination with an accurate scoring of the putative binding affinity. The evaluation of the docking performance of several flexible docking algorithm revealed significant differences in docking and scoring quality and a dependence of the resulting best performing algorithm on the particular polarity of the active site.[121]

Ligand-based methods are applied if no structural information about the target and its ligand binding site, i.e. no crystal structure or no reliable homology model, is available. Based on the analysis of ligands with known biological activity, these methods include the design of pharmacophoric models[122] by, e.g., the active analogue approach,[123] the analysis of quantitative structure-activity relationships (classical QSAR) and 3D-QSAR.[124] Also pseudoreceptor models for screening are employed to discover lead compounds and/or to optimise known ligands.[110]

By now, computer aided drug design has evolved into a substantial part of the drug discovery process. The application of virtual screening approaches accelerates the decision-making process in drug discovery and will become an indispensable part of future medicinal chemistry.[100]

1.6 References

(1) Meyer, K.; Palmer, J. W. The polysaccharide of the vitreous humor. *J Biol Chem* **1934**, *107*, 629-634.

(2) Scott, J. E. Secondary structures in hyaluronan solutions: chemical and biological implications. *The Biology of Hyaluronan.*; Ciba Foundation Symposium, 1989; pp 6-14.

(3) Sheehan, J.; Atkins, E. X-ray fibre diffraction study of conformational changes in hyaluronate induced in the presence of sodium, potassium and calcium ions. *Int J Biol Macromol* **1983**, *5*.

(4) Almond, A.; Brass, A.; Sheehan, J. Oligosaccharides as model systems for understanding water-biopolymer interaction: hydrated dynamics of a hyaluronan decamer. *J Phys Chem B* **2000**, *104*, 5634-5640.

(5) Laurent, T. C.; Laurent, U. B.; Fraser, J. R. The structure and function of hyaluronan: An overview. *Immunol Cell Biol* **1996**, *74*, A1-7.

(6) Glycoforum http://www.glycoforum.gr.jp/, 2003.

(7) Laurent, T.; Fraser, J. Hyaluronan. *FASEB J* **1992**, *6*, 2397-2405.

(8) West, D. C.; Chen, H. Is hyaluronan degradation an angiogenic/metastatic switch? *New Frontiers in Medicinal Sciences: Redefining Hyaluronan*; Elsevier Science, 2000; pp 77-86.

(9) Day, A. J.; Prestwich, G. D. Hyaluronan-binding proteins: tying up the giant. *J Biol Chem* **2002***, 277*, 4585-4588.

(10) Duran-Reynals, F. Exaltation de l'activité du virus vaccinal par les extraits de certains organes. *CR Séances Soc Biol Fil* **1928***, 99*, 6-7.

(11) Meyer, K.; Dubos, R.; Smith, E. M. The hydrolysis of the polysaccharide acids of vitreous humor, of umbilical cord and of streptococcus by the autolytic enzyme of pneumococcus. *Journal of Biological Chemistry* **1937***, 118*, 71-77.

(12) Chain, E.; Duthie, E. S. A mucolytic enzyme in testis extracts. *Nature* **1939***, 144*, 977-978.

(13) Csoka, T. B.; Frost, G. I.; Wong, T.; Stern, R. Purification and microsequencing of hyaluronidase isozymes from human urine. *FEBS Lett* **1997***, 417*, 307-310.

(14) Frost, G.; Csoka, T.; Stern, R. The hyaluronidases: a chemical, biological and clinical overview. *Trends Glycosci Glycotechnol* **1996***, 8*, 419-434.

(15) Kreil, G. Hyaluronidases - A group of neglected enzymes. *Prot Sci* **1995***, 4*, 1666-1669.

(16) Meyer, K. Hyaluronidases. *The Enzymes*; Academic Press: New York, 1971; pp 307-320.

(17) Cramer, J. A.; Bailey, L. C.; Bailey, C. A.; Miller, R. T. Kinetic and mechanistic studies with bovine testicular hyaluronidase. *Biochim Biophys Acta* **1994***, 1200*, 315-321.

(18) Takagaki, K.; Nakamura, T.; Izumi, J.; Saitoh, H.; Endo, M. et al. Characterization of hydrolysis and transglycosylation by testicular hyaluronidase using ion-spray mass spectrometry. *Biochem* **1994***, 33*, 6503-6507.

(19) Pritchard, D.; Trent, J.; Zhang, P.; Egan, M.; Baker, J. Characterization of the Active Site of Group B Streptococcal Hyaluronan Lyase. *Proteins* **2000***, 40*, 126-134.

(20) Csoka, A. B.; Frost, G. I.; Stern, R. The six hyaluronidase-like genes in the human and mouse genomes. *Matrix Biol* **2001***, 20*, 499-508.

(21) Gmachl, M.; Sagan, S.; Ketter, S.; Kreil, G. The human sperm protein PH-20 has hyaluronidase activity. *FEBS* **1993***, 336*, 545-548.

(22) Cherr, G. N.; Yudin, A. I.; Overstreet, J. W. The dual functions of GPI-anchored PH-20: hyaluronidase and intracellular signaling. *Matrix Biol* **2001***, 20*, 515-525.

(23) Myles, D. G.; Primakoff, P. Why did the sperm cross the cumulus? To get to the oocyte. Functions of the sperm surface proteins PH-20 and fertilin in arriving at, and fusing with, the egg. *Biol Reprod* **1997***, 56*, 320-327.

(24) Triggs-Raine, B.; Salo, T. J.; Zhang, H.; Wicklow, B. A.; Natowicz, M. R. Mutations in HYAL1, a member of a tandemly distributed multigene family encoding disparate hyaluronidase activities, cause a newly described lysosomal disorder, mucopolysaccharidosis IX. *Proc Natl Acad Sci U S A* **1999***, 96*, 6296-6300.

(25) Natowicz, M. R.; Short, M. P.; Wang, Y.; Dickersin, G. R.; Gebhardt, M. C. et al. Clinical and biochemical manifestations of hyaluronidase deficiency. *N Engl J Med* **1996***, 335*, 1029-1033.

(26) Frost, G. I.; Mohapatra, G.; Wong, T. M.; Csoka, A. B.; Gray, J. W. et al. HYAL1LUCA-1, a candidate tumor suppressor gene on chromosome 3p21.3, is inactivated in head and neck squamous cell carcinomas by aberrant splicing of pre-mRNA. *Oncogene* **2000***, 19*, 870-877.

(27) Csoka, T. B.; Frost, G. I.; Heng, H. H.; Scherer, S. W.; Mohapatra, G. et al. The hyaluronidase gene HYAL1 maps to chromosome 3p21.2-p21.3 in human and 9F1-F2 in mouse, a conserved candidate tumor suppressor locus. *Genomics* **1998***, 48*, 63-70.

(28) Novak, U.; Stylli, S. S.; Kaye, A. H.; Lepperdinger, G. Hyaluronidase-2 overexpression accelerates intracerebral but not subcutaneous tumor formation of murine astrocytoma cells. *Cancer Res* **1999***, 59*, 6246-6250.

(29) Chang, N. S. Transforming growth factor-beta1 blocks the enhancement of tumor necrosis factor cytotoxicity by hyaluronidase Hyal-2 in L929 fibroblasts. *BMC Cell Biol* **2002***, 3*, 8.

(30) West, D. C.; Hampson, I. N.; Arnold, F.; Kumar, S. Angiogenesis induced by degradation products of hyaluronic acid. *Science* **1985***, 228*, 1324-1326.

(31) Stern, R. Devising a pathway for hyaluronan catabolism: are we there yet? *Glycobiology* **2003***, 13*, 105R-115R.

(32) Menzel, E.; Farr, C. Hyaluronidase and its Substrate Hyaluronan: Biochemistry, Biological Activities and Therapeutic Uses. *Cancer Lett* **1998***, 131*, 3-11.

(33) Baumgartner, G.; Gomar-Hoss, C.; Sakr, L.; Ulsperger, E.; Wogritsch, C. The impact of extracellular matrix on the chemoresistance of solid tumors--experimental and clinical results of hyaluronidase as additive to cytostatic chemotherapy. *Cancer Lett* **1998***, 131*, 85-99.

(34) Oettl, M.; Hoechstetter, J.; Asen, I.; Bernhardt, G.; Buschauer, A. Comparative characterization of bovine testicular hyaluronidase and a hyaluronate lyase from *Streptococcus agalactiae* in pharmaceutical preparations. *Eur J Pharm Sci* **2003***, 18*, 267-277.

(35) Meyer, M. F.; Kreil, G.; Aschauer, H. The soluble hyaluronidase from bull testes is a fragment of the membrane-bound PH-20 enzyme. *FEBS Lett* **1997***, 413*, 385-388.

(36) Muckenschnabel, I.; Bernhardt, G.; Spruss, T.; Buschauer, A. Pharmacokinetics and tissue distribution of bovine testicular hyaluronidase and vinblastine in mice: an attempt to optimize the mode of adjuvant hyaluronidase administration in cancer chemotherapy. *Cancer Lett* **1998***, 131*, 71-84.

(37) Gorham, S. D.; Olavesen, A. H.; Dodgson, K. S. Effect of ionic strength and pH on the properties of purified bovine testicular hyaluronidase. *Connective Tissue Research* **1975***, 3*, 17-25.

(38) Saitoh, H.; Takagaki, K.; Majima, M.; Nakamura, T.; Matsuki, A. et al. Enzymic reconstruction of glycosaminoglycan oligosaccharide chains using the transglycosylation reaction of bovine testicular hyaluronidase. *J Biol Chem* **1995***, 270*, 3741-3747.

(39) Gmachl, M.; Kreil, G. Bee venom hyaluronidase is homologous to a membrane protein of mammalian sperm. *Proc Natl Acad Sci* **1993***, 90*, 3569-3573.

(40) Markovic-Housley, Z.; Miglinerini, G.; Soldatova, L.; Rizkallah, P.; Müller, U. et al. Crystal Structure of Hyaluronidase, a Major Allergen of Bee Venom. *Structure* **2000***, 8*, 1025-1035.

(41) Mikami, B.; Degano, M.; Hehre, E. J.; Sacchettini, J. C. Crystal structures of soybean beta-amylase reacted with beta-maltose and maltal: active site components and their apparent roles in catalysis. *Biochemistry* **1994***, 33*, 7779-7787.

(42) Jain, S.; Drendel, W. B.; Chen, Z. W.; Mathews, F. S.; Sly, W. S. et al. Structure of human beta-glucuronidase reveals candidate lysosomal targeting and active-site motifs. *Nat Struct Biol* **1996***, 3*, 375-381.

(43) Perrakis, A.; Tews, I.; Dauter, Z.; Oppenheim, A.; Chet, I. et al. Crystal structure of bacterial chitinase at 2.3 A resolution. *Structure* **1994***, 2*, 1169-1180.

(44) Markovic-Housley, Z.; Schirmer, T. Structural Evidence for substrate assisted catalytic mechanism of bee venom hyaluronidase, a major allergen of bee venom. *Carbohydrate Bioengineering: Interdisciplinary Approaches*; RCS: London, 2002; pp 19-27.

(45) Withers, S. G.; Aebersold, R. Approaches to labeling and identification of active site residues in glycosidases. *Protein Sci* **1995***, 4*, 361-372.

(46) Davies, G. J.; Wilson, K. S.; Henrissat, B. Nomenclature for sugar-binding subsites in glycosyl hydrolases. *Biochem J* **1997***, 321 (Pt 2)*, 557-559.

(47) White, A.; Rose, D. R. Mechanism of catalysis by retaining beta-glycosyl hydrolases. *Curr Opin Struct Biol* **1997***, 7*, 645-651.

(48) Drouillard, S.; Armand, S.; Davies, G. J.; Vorgias, C. E.; Henrissat, B. Serratia marcescens chitobiase is a retaining glycosidase utilizing substrate acetamido group participation. *Biochem J* **1997***, 328 (Pt 3)*, 945-949.

(49) Tews, I.; Terwisscha van Scheltinga, A. C.; Perrakis, A.; Wilson, K. S.; Dijkstra, B. W. Substrate-Assisted Catalysis Unifies Two Families of Chitinolytic Enzymes. *Journal of the American Chemical Society* **1997***, 119*, 7954-7959.

(50) Brameld, K. A.; Shrader, W. D.; Imperiali, B.; Goddard, W. A., 3rd Substrate assistance in the mechanism of family 18 chitinases: theoretical studies of potential intermediates and inhibitors. *J Mol Biol* **1998***, 280*, 913-923.

(51) Coutinho, P. M.; Henrissat, B. Carbohydrate-Active Enzymes server at URL: http://afmb.cnrs-mrs.fr/CAZY/, 1999.

(52) Jedrzejas, M.; Chantalat, L. Structural studies of *Streptococcus agalactiae* hyaluronate lyase. *Acta Cristallograph D* **2000***, 56*, 460-463.

(53) Jedrzejas, M. J. Three-dimensional structures of hyaluronate lyases from Streptococcus species and their mechanism of hyaluronan degradation. *Science of Hayluronan Today*; Glycoforum www.glycoforum.gr.jp/science/hyaluronan, 2002.

(54) Linker, A.; Meyer, K. *Nature* **1954***, 174*, 1192-1194.

(55) Li, S.; Jedrzejas, M. J. Hyaluronan binding and degradation by *Streptococcus agalactiae* hyaluronate lyase. *J Biol Chem* **2001***, 276*, 41407-41416.

(56) Li, S.; Kelly, S.; Lamani, E.; Ferraroni, M.; Jedrzejas, M. Structural basis of hyaluronan degradation by *Streptococcus pneumoniae* hyaluronate lyase. *EMBO J* **2000***, 19*, 1228-1240.

(57) Kelly, S. J.; Taylor, K. B.; Li, S.; Jedrzejas, M. J. Kinetic properties of *Streptococcus pneumoniae* hyaluronate lyase. *Glycobiology* **2001***, 11*, 297-304.

(58) Nukui, M.; Taylor, K. B.; McPherson, D. T.; Shigenaga, M. K.; Jedrzejas, M. J. The function of hydrophobic residues in the catalytic cleft of *Streptococcus pneumoniae* hyaluronate lyase. Kinetic characterization of mutant enzyme forms. *J Biol Chem* **2003***, 278*, 3079-3088.

(59) Rigden, D. J.; Jedrzejas, M. J. Structures of Streptococcus pneumoniae hyaluronate lyase in complex with chondroitin and chondroitin sulfate disaccharides. Insights into specificity and mechanism of action. *J Biol Chem* **2003***, 278*, 50596-50606.

(60) Baker, J. R.; Pritchard, D. G. Action pattern and substrate specificity of the hyaluronan lyase from group B streptococci. *Biochem J* **2000***, 348 Pt 2*, 465-471.

(61) Ponnuraj, K.; Jedrzejas, M. Mechanism of Hyaluronan Binding and Degradation: Structure of *Streptococcus pneumoniae* Haluronate Lyase in Complex with Hyaluronic Acid Disaccharide at 1.7 A Resolution. *J Mol Biol* **2000***, 299*, 885-895.

(62) Hynes, W.; Walton, S. Hyaluronidases of gram-positive bacteria. *FEMS Microbiol Lett* **2000***, 183*, 201-207.

(63) Dillon, H. C., Jr.; Khare, S.; Gray, B. M. Group B streptococcal carriage and disease: a 6-year prospective study. *J Pediatr* **1987***, 110*, 31-36.

(64) Liesegang, T. J. Viscoelastic substances in ophthalmology. *Surv Ophthalmol* **1990***, 34*, 268-293.

(65) Balazs, E. A.; Denlinger, J. L. Clinical uses of hyaluronan. *Ciba Found Symp* **1989***, 143*, 265-275; discussion 275-280, 281-265.

(66) Fukuda, K.; Dan, H.; Takayama, M.; Kumano, F.; Saitoh, M. et al. Hyaluronic acid increases proteoglycan synthesis in bovine articular cartilage in the presence of interleukin-1. *J Pharmacol Exp Ther* **1996***, 277*, 1672-1675.

(67) Asari, A.; Miyauchi, S.; Matsuzaka, S.; Ito, T.; Kominami, E. et al. Molecular weight-dependent effects of hyaluronate on the arthritic synovium. *Arch Histol Cytol* **1998***, 61*, 125-135.

(68) Iwata, H. Pharmacologic and clinical aspects of intraarticular injection of hyaluronate. *Clin Orthop* **1993**, 285-291.

(69) Gotoh, S.; Onaya, J.; Abe, M.; Miyazaki, K.; Hamai, A. et al. Effects of the molecular weight of hyaluronic acid and its action mechanisms on experimental joint pain in rats. *Ann Rheum Dis* **1993***, 52*, 817-822.

(70) Few, B. J. Hyaluronidase for treating intravenous extravasations. *MCN Am J Matern Child Nurs* **1987***, 12*, 23.

(71) Bertelli, G.; Dini, D.; Forno, G. B.; Gozza, A.; Silvestro, S. et al. Hyaluronidase as an antidote to extravasation of Vinca alkaloids: clinical results. *J Cancer Res Clin Oncol* **1994***, 120*, 505-506.

(72) Brown, S. M.; Coats, D. K.; Collins, M. L.; Underdahl, J. P. Second cluster of strabismus cases after periocular anesthesia without hyaluronidase. *J Cataract Refract Surg* **2001***, 27*, 1872-1875.

(73) Hyaluronidase (Vitrase)--ISTA: hyaluronidase--ISTA pharmaceuticals. *Drugs R D* **2003***, 4*, 194-197.

(74) Muckenschnabel, I.; Bernhardt, G.; Spruss, T.; Buschauer, A. Hyaluronidase Pretreatment Produces Selective Melphalan Enrichment in Malignant Melanoma in Nude Mice. *Cancer Chemother Pharmacol* **1996***, 38*, 88-94.

(75) Spruss, T.; Bernhardt, G.; Schönenberger, H.; Schiess, W. Hyaluronidase significantly enhances the efficacy of regional vinblastine chemotherapy of malignant melanoma. *J Cancer Res Clin Oncol* **1995***, 121*, 193-202.

(76) Zahalka, M. A.; Okon, E.; Gosslar, U.; Holzmann, B.; Naor, D. Lymph node (but not spleen) invasion by murine lymphoma is both CD44- and hyaluronate-dependent. *J Immunol* **1995***, 154*, 5345-5355.

(77) Lin, Y.; Mahan, K.; Lathrop, W. F.; Myles, D. G.; Primakoff, P. A hyaluronidase activity of the sperm plasma membrane protein PH-20 enables sperm to penetrate the cumulus cell layer surrounding the egg. *J Cell Biol* **1994***, 125*, 1157-1163.

(78) Primakoff, P.; Hyatt, H.; Myles, D. G. A role for the migrating sperm surface antigen PH-20 in guinea pig sperm binding to the egg zona pellucida. *J Cell Biol* **1985***, 101*, 2239-2244.

(79) Meyer, K.; Rapport, M. M. The inhibition of testicular hyaluronidase by heavy metals. *J Biol Chem* **1951***, 188*, 485-490.

(80) Haas, E. Invasion. I. Antinvasin I, an enzyme in plasma. *J Biol Chem* **1946***, 163*, 63-88.

(81) Dorfman, A.; Ott, M. L.; Whitney, R. The hyaluronidase inhibitor of human blood. *J Biol Chem* **1948***, 174*, 621-629.

(82) Houck, J. C. The competitive inhibition of hyaluronidase. *Arch Biochem* **1957***, 71*, 336-341.

(83) Mio, K.; Stern, R. Inhibitors of the hyaluronidases. *Matrix Biol* **2002***, 21*, 31-37.

(84) Wolf, R. A.; Glogar, D.; Chaung, L. Y.; Garrett, P. E.; Ertl, G. et al. Heparin inhibits bovine testicular hyaluronidase activity in myocardium of dogs with coronary artery occlusion. *Am J Cardiol* **1984***, 53*, 941-944.

(85) Asada, M.; Sugie, M.; Inoue, M.; Nakagomi, K.; Hongo, S. et al. Inhibitory effect of alginic acids on hyaluronidase and on histamine release from mast cells. *Biosci Biotechnol Biochem* **1997***, 61*, 1030-1032.

(86) Toida, T.; Ogita, Y.; Suzuki, A.; Toyoda, H.; Imanari, T. Inhibition of hyaluronidase by fully *O*-sulfonated glycosaminoglycans. *Arch Biochem Biophys* **1999***, 370*, 176-182.

(87) Kakegawa, H.; Matsumoto, H.; Satoh, T. Inhibitory effects of some natural products on the activation of hyaluronidase and their anti-allergic actions. *Chem Pharm Bull (Tokyo)* **1992***, 40*, 1439-1442.

(88) Kakegawa, H.; Matsumoto, H.; Satoh, T. Inhibitory effects of hydrangenol derivatives on the activation of hyaluronidase and their antiallergic activities. *Planta Med* **1988***, 54*, 385-389.

(89) Kuppusamy, U. R.; Das, N. P. Inhibitory effects of flavonoids on several venom hyaluronidases. *Experientia* **1991***, 47*, 1196-1200.

(90) Kuppusamy, U.; Khoo, H.; Das, N. Structure-activity studies of flavonoids as inhibitors of hyaluronidase. *Biochem Pharmacol* **1990***, 40*, 397-401.

(91) Salmen, S. Inhibitors of bacterial and mammalian hyaluronidases: synthesis and structure-activity relationships; University of Regensburg: Regensburg, 2003.

(92) Facino, R.; Carini, M.; Stefani, R.; Aldini, G.; Saibene, L. Anti-Elastase and Anti-Hyaluronidase Activities of Saponins and Sapogenis from *Hedera helix*, *Aesculus hippocastanum*, and *Ruscus aculeatus*: Factors Contributing to their Efficacy in the Treatment of Venous Insufficiency. *Arch Pharm* **1995***, 328*, 720-724.

(93) Jeong, S.; Kim, N.; Kim, D.; Kang, T.; Ahn, N. et al. Hyaluronidase Inhibitory Active 6*H*-Dibenzo[*b*,*d*]Pyran-6-Ones from the Feces of *Trogopterus xanthipes*. *Planta Med* **2000***, 66*, 76-77.

(94) Jeong, S.-J.; Ahn, N.; Kim, Y.; Inagaki, M.; Miyamato, T. et al. Norlignans with Hyaluronidase Inhibitory Activity from *Anemarrhena asphodeloides*. *Planta Med* **1999***, 65*, 367-368.

(95) Tung, J. S.; Mark, G. E.; Hollis, G. F. A microplate assay for hyaluronidase and hyaluronidase inhibitors. *Anal Biochem* **1994***, 223*, 149-152.

(96) Li, S.; Taylor, K. B.; Kelly, S. J.; Jedrzejas, M. J. Vitamin C inhibits the enzymatic activity of *Streptococcus pneumoniae* hyaluronate lyase. *J Biol Chem* **2001***, 276*, 15125-15130.

(97) Akhtar, M. S.; Bhakuni, V. *Streptococcus pneumoniae* hyaluronate lyase contains two non-cooperative independent folding/unfolding structural domains: characterization of functional domain and inhibitors of enzyme. *J Biol Chem* **2003***, 278*, 25509-25516.

(98) Suzuki, K.; Terasaki, Y.; Uyeda, M. Inhibition of hyaluronidases and chondroitinases by fatty acids. *J Enzyme Inhib Med Chem* **2002***, 17*, 183-186.

(99) Stahl, M.; Rarey, M.; Klebe, G. Screening of databases. *Bioinformatics - From Genomes to Drugs*; VCH-Wiley Verlag GmbH: Weinheim, 2002; pp 137-170.

(100) Schneider, G.; Böhm, H. J. Virtual screening and fast automated docking methods. *Drug Discov Today* **2002***, 7*, 64-70.

(101) www.mdli.com Available Chemical Directory.

(102) LeadQuest Chemical Compounds Libraries; Vol. 1-2 ed.; Tripos, Inc.: St. Louis, MO, 2000.

(103) www.chemstar.ru ChemStar Ltd.

(104) World Drug Index; Thomson Scientific.

(105) MDL® Drug Data Report; MDL Information Systems, Inc., USA.

(106) Lin, J.; Sahakian, D. C.; de Morais, S. M.; Xu, J. J.; Polzer, R. J. et al. The role of absorption, distribution, metabolism, excretion and toxicity in drug discovery. *Curr Top Med Chem* **2003***, 3*, 1125-1154.

(107) Lipinski, C. A.; Lombardo, F.; Dominy, B. W.; Feeney, P. J. Experimental and computational approaches to estimate solubility and permeability in drug discovery and development settings. *Adv Drug Deliv Rev* **1997***, 23*, 3-25.

(108) Ajay, A.; Walters, W. P.; Murcko, M. A. Can we learn to distinguish between "drug-like" and "nondrug-like" molecules? *J Med Chem* **1998***, 41*, 3314-3324.

(109) Sadowski, J.; Kubinyi, H. A scoring scheme for discriminating between drugs and nondrugs. *J Med Chem* **1998***, 41*, 3325-3329.

(110) Veselovsky, A. V.; Ivanov, A. S. Strategy of computer-aided drug design. *Curr Drug Targets Infect Disord* **2003***, 3*, 33-40.

(111) Lauri, G.; Bartlett, P. A. CAVEAT: a program to facilitate the design of organic molecules. *J Comput Aided Mol Des* **1994***, 8*, 51-66.

(112) Schneider, G.; Lee, M. L.; Stahl, M.; Schneider, P. De novo design of molecular architectures by evolutionary assembly of drug-derived building blocks. *J Comput Aided Mol Des* **2000***, 14*, 487-494.

(113) Tripos Inc., St. Louis, Missouri, USA. www.tripos.com.

(114) Böhm, H. J. LUDI: rule-based automatic design of new substituents for enzyme inhibitor leads. *J Comput Aided Mol Des* **1992***, 6*, 593-606.

(115) Böhm, H. J. Current computational tools for *de novo* ligand design. *Curr Opin Biotechnol* **1996***, 7*, 433-436.

(116) Gohlke, H.; Klebe, G. Approaches to the description and prediction of the binding affinity of small-molecule ligands to macromolecular receptors. *Angew Chem Int Ed Engl* **2002***, 41*, 2644-2676.

(117) Klebe, G.; Grädler, U.; Grüneberg, S.; Krämer, O.; Gohlke, H. Understanding receptor-ligand interactions as a prerequisite for virtual screening. *Virtual Screening for Bioactive Molecules*; Wiley-VCH: Weinheim, 2000; pp 207-227.

(118) Rarey, M.; Kramer, B.; Lengauer, T.; Klebe, G. A fast flexible docking method using an incremental construction algorithm. *J Mol Biol* **1996***, 261*, 470-489.

(119) Goodsell, D. S.; Morris, G. M.; Olson, A. J. Automated docking of flexible ligands: applications of AutoDock. *J Mol Recognit* **1996***, 9*, 1-5.

(120) Ewing, T. J.; Makino, S.; Skillman, A. G.; Kuntz, I. D. DOCK 4.0: search strategies for automated molecular docking of flexible molecule databases. *J Comput Aided Mol Des* **2001***, 15*, 411-428.

(121) Kontoyianni, M.; McClellan, L. M.; Sokol, G. S. Evaluation of docking performance: comparative data on docking algorithms. *J Med Chem* **2004***, 47*, 558-565.

(122) Good, A.; Mason, J.; Pickett, S. Pharmacophore pattern application in virtual screening, library design and QSAR. *Virtual Screening for Bioactive Molecules*; Wiley-VCH Verlag: Weinheim, 2000; pp 131-159.

(123) Kettmann, V.; Höltje, H. D. Mapping of the Benzothiazepine Binding Site on the Calcium Channel. *Quantitative Structure-Activity Relationships* **1998***, 17*, 91-101.

(124) Bravi, G.; Gancia, E.; Green, D.; Hann, M. Modelling Structure-Activity Relationships. *Virtual Screening for Bioactive Molecules*; Wiley-VCH Verlag: Weinheim, 2000; pp 81-116.

Chapter 2 Objectives

Potent and selective hyaluronidase inhibitors are required as pharmacological tools to study the physiological and pathophysiological role of hyaluronan and hyaluronidases. Additionally, such compounds are of potential therapeutic value for the treatment of a variety of diseases, e.g. arthroses, cancer, or bacterial infections. Nowadays, the application of computer-aided drug design accelerates the discovery of new lead compounds and their structural optimisation with respect to affinity and pharmacological properties. As potent and selective inhibitors of bacterial and mammalian hyaluronidases are not known to date, the main goal of this thesis was the prediction and selection of lead-like structures by *de novo* ligand design and virtual screening of generated compound libraries. The inhibitory effects of the suggested molecules were investigated on *S. agalactiae* hyaluronate lyase and on the bovine testicular hyaluronidase as main representatives of the bacterial and mammalian enzymes, respectively.

As first project, a *de novo* design approach was intended to discover inhibitors of *S. agalactiae* strain 4755 hyaluronan lyase based on the elucidation of the three-dimensional structures of two other bacterial hyaluronidases.[†] This project comprises the development of a homology model of *S. agalactiae* strain 4755 hyaluronan lyase by means of the programme MODELLER and the subsequent *de novo* ligand generation using the structure-based design software LUDI.

Prerequisites of *de novo* design are databases with three-dimensional (3D), predominantly drug-like structures. In the second project, starting from the ChemACX selection of commercially available compounds, a 3D database should be generated by elimination of putatively non drug-like compounds. In comparison to LeadQuest® libraries of drug-like, synthetically feasible screening compounds, the resulting ChemACXF database should be analysed with respect to suitability for virtual screening purposes.

[†] The synthesis and pharmacological investigations of the proposed molecules have been carried out by Sunnhild Salmen as part of her PhD project, Universität Regensburg, 2003.

The third project aimed at structure-based ligand design for inhibitors of mammalian hyaluronidase. A homology model of the bovine testicular hyaluronidase was generated by means of MODELLER on the basis of crystal structures of the bee venom hyaluronidase. Subsequent LUDI calculations with this enzyme model should result in first lead compounds. Further BTH ligands should be derived by an active analogue-like approach starting from the superposition of the binding site of bovine testicular hyaluronidase with similar sites of related chitinases in complex with their inhibitors.

The X-ray structure of *S. pneumoniae* hyaluronate lyase complexed with L-ascorbic acid was recently elucidated. In the fourth, joint project,[‡] L-ascorbic acid-6-hexadecanoate was investigated as inhibitor of bacterial and bovine hyaluronidase. A crystal structure of a complex of *S. pneumoniae* hyaluronate lyase with the inhibitor should lead to more detailed information about the interaction of L-ascorbic acid-6-hexadecanoate with the amino acids in the active site. In comparison with the bacterial enzyme, flexible docking of L-ascorbic acid-6-hexadecanoate in the bovine testicular hyaluronidase model should help to develop improved binding models for further, more potent and selective hyaluronidase inhibitors.

In the fifth project, following a published strategy of virtual database screening using 3D pharmacophores derived from crystal structure complexes, a 3D pharmacophore model was derived from the X-ray structure of *S. pneumoniae* hyaluronate lyase in complex with a 2-phenylindole-based inhibitor. By comparison of its binding mode and of the 3D pharmacophore with known structure-activity relationships of 2-phenylindole derivatives, conclusions about the putative binding mode of benzoxazole-2-thione derivatives as bacterial hyaluronidase inhibitors should be derived.

[‡] The co-crystallisation experiments have been carried out by *Mark J. Jedrzejas* (Children's Hospital Oakland Research Institute, Oakland, California 94609, USA) and *Daniel J. Rigden* (National Centre of Genetic Resources and Biotechnology, Cenargen/Embrapa, Brasília, D.F. 70770-900, Brazil).

Chapter 3 Structure-based design of hyaluronate lyase inhibitors

3.1 Introduction

Bacterial hyaluronate lyases (EC 4.2.2.1) differ from hyaluronidases from other sources by their mode of action. They cleave the β-1,4-glycosidic bond between *N*-acetyl-β-D-glucosamine and D-glucuronic acid residues by an elimination reaction resulting in unsaturated hexuronic acid residues at the nonreducing ends.[1] The hyaluronan lyases of pathogenic bacteria are putative virulence factors due to the spreading effect in host tissues resulting from the degradation of hyaluronic acid (HA) of the extracellular matrix.[2] Potent inhibitors of hyaluronan lyases are not known to date. Such compounds could be useful in studying the role of hyaluronan and hyaluronidases in bacterial infections and may even be promising with respect to the investigation of a novel, possibly auxiliary antibacterial therapy.

Some small compounds like arginine and guanidine derivatives[3] and vitamin C[4] with IC_{50} values in the range of 150 to 0.150 mM *vs.* bacterial hyaluronidases have been described. For the development of a new class of bacterial hyaluronidase inhibitors, the primary goal of the present study was the identification of simple compounds as possible lead structures. A crucial issue for improving binding affinity, selectivity or bioavailability is the quick synthetic accessibility of relatively simple structures by derivatisation of the lead compound. Until now, several computational methods like GROW,[5] LEGEND[6] and LUDI[7,8] have been described enabling the rational design of new ligands based on the three-dimensional (3D) structure of a target protein.[9,10] As initial step most of these programmes perform a detailed analysis of the amino acid residues constituting the binding pocket and extract the spatial binding features which potential ligands have to meet. These favourable interaction sites are then converted into a complex pharmacophoric model of the active site of the enzyme. Large databases of small molecules can be computationally screened for fit with this model, resulting in the identification of complementary ligands in terms of geometrical and physicochemical properties. Putative screening hits are selected *via* a rough af-

finity prediction estimated by a scoring function. The scoring of the proposed ligand pose (target-bound conformation and orientation of screened ligand) reflects the interaction between the functional moieties on the ligand and the amino acid residues of the binding pocket.[11,12] Rational design includes several design cycles with appropriate structural modifications, synthesis and testing of the new candidate structures, aiming at ligands with improved binding affinities.

As a pilot scheme for hyaluronidase inhibitor design in general, we launched a structure-based design programme of *S. agalactiae* strain 4755 hyaluronate lyase ($hylB_{4755}$) inhibitors using the *de novo* design software LUDI.[7,8] A homology model of $hylB_{4755}$ was derived from the crystal structures of two streptococcal lyases. The $hylB_{4755}$ hyaluronidase shows extensive sequence identity with the homologous template enzymes encoded by genes from group B *Streptococcus* (*S. agalactiae*) strain 3502 ($hylB_{3502}$) and *S. pneumoniae* (hylSpn). Recently, the X-ray structures of hylSpn and $hylB_{3502}$ were determined.[13,14] Additionally, a complex of $hylB_{3502}$ with a substrate-based HA hexasaccharide could be elucidated by means of X-ray crystallography.[15] These results reveal the catalytic mode of action, including the identification of specific residues involved in the degradation of hyaluronan by $hylB_{3502}$.[15]

In this chapter, the design and identification of first promising leads as micromolar inhibitors of *S. agalactiae* strain 4755 hyaluronate lyase are reported.

3.2 Results and discussion

3.2.1 $HylB_{4755}$ model construction

Necessary conditions for homology modelling of protein structures are a significant similarity of the target and the template sequences and a sequence alignment close to reality.[16] The sequence identity of the crystallised hyaluronate lyases hylSpn (pdb code 1egu)[13] and $hylB_{3502}$ (pdb code 1f1s)[14] is 53 % whereas it is even 98 % between the streptococcal enzymes $hylB_{3502}$ and $hylB_{4755}$. With respect to the active sites, identities amount to 85 % ($hylB_{4755}$ *vs.* hylSpn) and 99 % ($hylB_{4755}$ *vs.* $hylB_{3502}$), respectively. Thus, the crystal structures of the streptococcal hyaluronidases hylSpn and $hylB_{3502}$ have provided the first possibility to construct a reliable model of the parent bacterial enzyme group B streptococcal hyaluronidase $hylB_{4755}$.

As a first step, a multiple sequence alignment of $hylB_{4755}$, $hylB_{3502}$ and hylSpn (see Figure 3.1) was generated using ClustalW.[17,18] The structurally conserved regions (SCR) of both crystal structures could easily be extracted since almost all insertions in the $hylB_{3502}$ sequence occur in the βII-domain surface loop areas.[14] Given that the primary structures of $hylB_{3502}$ and $hylB_{4755}$ are almost identical, the question arose whether the X-ray structure of *S. agalactiae* strain 3502 hyaluronan lyase may be directly used as starting point for the structure-based ligand design instead of constructing a homology model of the strain 4755 enzyme.

A detailed analysis after superposition of both available X-ray structures of hyaluronate lyases revealed that the conformation of $hylB_{3502}$ does not represent a catalytically active state. In contrast to the crystal structure of hylSpn, the $hylB_{3502}$ structure consists of three instead of two distinct structural domains (see chapter 1, Figure 1.5).[14] In particular, it contains an additional βI-domain preceding the α-domain at the N-terminus of the protein. The α-domain, the short 10-residue linker in-between, and the following β-domain (βI in hylSpn, βII in $hylB_{3502}$) are present in both lyases. Despite of a high similarity of the whole architecture of the structures and of the spatial arrangement of the active site residues, the root mean square (rms) deviation of the Cα-atom positions for the whole structures is 2.47 Å. The major difference is observed at the end of the α-domain, especially in the region that includes the catalytic cleft. The rotation of the α- with respect to the βII-domain by a small angle around the linker in the $hylB_{3502}$ structure leads to a cleft which is about 7.3 Å wider than in the hylSpn structure.[14] As a consequence, the spatial positions of the catalytically active amino acids Tyr488, His479 and Asn429 (Tyr408, His399 and Asn349 in hylSpn) are significantly different.[14]

```
hylB4755 316 KISDKSGKIIKEVPLSVTASTEDKFTKLLDKWNDVTIGNHVYDTNDSNMQKINQKLDETNAKNIKTIKLD
hylB3502 228 KISDKSGKIIKEVPLSVTGSPEDNFTKLLDKWNDVTIGNYVYDTNDSNMQKLTQKLDETNGKNIEAIKLD
hylSpn   150 VIVSKDGKEVKKIPLKILASVKDTYTDRLDDWNGIIAGNQYYDSKNDQMAKLNQELEGKVADSLSSISSQ
                 |         |         |         |         |         |
hylB4755 386 SNHTFLWKDLDNLNNSAQLTATYRRLEDLAKQITNPHSTIYKNEKAIRTVKESLAWLHQNFYNVNKDIEG
hylB3502 298 SNRTFLWKDLDNLNNSAQLTATYRRLEDLAKQITNPHSTIYKNEKAIRTVKESLAWLHQNFYNVNKDIEG
hylSpn   220 ADRIYLWEKFSNYKTSANLTATYRKLEEMAKQVTNPSSRYYQDETVVRTVRDSMEWMHKHVYNSEKSIVG
                 |         |         |         |         |         |
hylB4755 456 SANWWDFEIGVPRSITATLALMNNYFTDAEIKTYTDPIEHFVPDAGYFRKTLDNPFKALGGNLVDMGRVK
hylB3502 368 SANWWDFEIGVPRSITGTLSLMNNYFTDAEIKTYTDPIEHFVPDAEYFRKTLVNPFKALGGNLVDMGRVK
hylSpn   290 --NWWDYEIGTPRAINNTLSLMKEYFSDEEIKKYTDVIEKFVPDPEHFRKTTDNPFKALGGNLVDMGRVK
                 |         |         |         |         |         |
hylB4755 526 IIEGLLRKDNTIIEKTSHSLKNLFTTATKAEGFYADGSYIDHTNVAYTGAYGNVLIDGLTQLLPIIQETD
hylB3502 438 IIEGLLRKDNTIIEKTSHSLKNLFTTATKAEGFYADGSYIDHTNVAYTGAYGNVLIDGLTQLLPIIQETD
hylSpn   358 VIAGLLRKDDQEISSTIRSIEQVFKLVDQGEGFYQDGSYIDHTNVAYTGAYGNVLIDGLSQLLPVIQKTK
                 |         |         |         |         |         |
hylB4755 596 YKISNQELDMVYKWINQSFLPLIVKGELMDMSRGRSISREAASSHAAAVEVLRGFLRLANMSNEERNLDL
hylB3502 508 YKISNQELDMVYKWINQSFLPLIVKGELMDMSRGRSISREAASSHAAAVEVLRGFLRLANMSNEERNLDL
hylSpn   428 NPIDKDKMQTMYHWIDKSFAPLLVNGELMDMSRGRSISRANSEGHVAAVEVLRGIHRIADMSEGETKQRL
                 |         |         |         |         |         |
hylB4755 666 KSTIKTIITSNKFYNVFNNLKSYSDIANMNKMLNDSTVATKPLKSNLSTFNSMDRLAYYNAEKDFGFALS
hylB3502 578 KSTIKAIITSNKFYNVFNNLKSYSDIANMNKLLNDSTVATKPLKSNLSTFNSMDRLAYYNAKKDFGFALS
hylSpn   498 QSLVKTIVQSDSYYDVFKNLKTYKDISLMQSLLSDAGVASVPRTSYLSAFNKMDKTAMYNAEKGFGFGLS
                 |         |         |         |         |         |
hylB4755 736 LHSKRTLNYEGMNDENTRGWYTGDGMFYLYNSDQSHYSNHFWPTVNPYKMAGTTEKDAKREDTTKEFMSK
hylB3502 648 LHSKRTLNYEGMNDENTRGWYTGDGMFYIYNSDQSHYSNHLGPTVNPYKMAGTTEKDAKREDTTKEFMSK
hylSpn   568 LFSSRTLNYEHMNKENKRGWYTSDGMFYLYNGDLSHYSDGYWPTVNPYKMPGTTETDAKRADS-------
                 |         |         |         |         |         |
hylB4755 806 HSKDAKEKTGQVTGTSDFVGSVKLNDHFALAAMDFTNWDRTLTAQKGWVILNDKIVFLGSNIKNTNGIGN
hylB3502 718 HSKDAKEKTGQVTGTSDFVGSVKLNDHFALAAMDFTNWDRTLTAQKGWVILNDKIVFLGSNIKNTNGIGN
hylSpn   631 D-------TGKVLP-SAFVGTSKLDDANATATMDFTNWNQTLTAHKSWFMLKDKIAFLGSNIQNTS-TDT
                 |         |         |         |         |         |
hylB4755 876 VSTTIDQRKDDSKTPYTTYVNGKTIDLKQASSQQFTDTKSVFLESKEPGRNIGYIFFKNSTIDIERKEQT
hylB3502 788 VSTTIDQRKDDSKTPYTTYVNGKTIDLKQASSQQFTDTKSVFLESKEPGRNIGYIFFKNSTIDIERKEQT
hylSpn   692 AATTIDQRKLESSNPYKVYVNDKEASLTEQE-KDYPETQSVFLESSDSKKNIGYFFFKKSSISMSKALQK
                 |         |         |         |         |         |
hylB4755 946 GTWNSINRTSKNTSIVSNPFITISQKHDNKGDSYGYMMVPNIDRTSFDKLANSKEVELLENSSKQQVIYD
hylB3502 858 GTWNSINRTSKNTSIVSNPFITISQKHDNKGDSYGYMMVPNIDRTSFDKLANSKEVELLENSSKQQVIYD
hylSpn   761 GAWKDIN-EGQSDKEVENEFLTISQAHKQNGDSYGYMLIPNVDRATFNQMIKELESSLIENNETLQSVYD
                 |         |         |         |         |         |
hylB47551016 KNSQTWAVIKHDNQESLINNQFKMNKAGLYLVQKVGNDYQNVYYQPQTMTKTDQLAI-----
hylB3502 928 KNSQTWAVIKHDNQESLINNQFKMNKAGLYLVQKVGNDYQNVYYQPQTMTKTDQLAI-----
hylSpn   830 AKQGVWGIVKYDDSVSTISNQFQVLKRGVYTIRKEGDEYKIAYYNPETQESAPDQEVFKKQH
```

Figure 3.1. Sequence alignment of $hylB_{4755}$, $hylB_{3502}$ and hylSpn as the basis of homology modelling. The SCRs α-helices 1-7 (blue), α-helices 8-13 (green) and β-strands (purple) are highlighted. All 26 amino acids of the active sites are coloured in red.

(For a detailed description of the postulated mechanism of HA degradation see chapter 1, Figure 1.4.) This fact can be illustrated by measuring the distances between specific atoms of the side chains of these residues and the complexed substrate-based HA hexasaccharide inside the active site of hylSpn[19] and $hylB_{3502}$ after superposition of the α-domains of both hyaluronidases. The distances between the oxygen atom of the Tyr408/Tyr488 sidechains and the oxygen atom O4 of the glycosidic bond to be cleaved are 2.97 Å and 6.64 Å for hylSpn and $hylB_{3502}$, respectively. A comparable result is obtained for the distances between the ε-nitrogen atom of His399/His479 and the carbon atom C5 of the glucuronic acid in subsite[§] +1 with 3.78 Å and 7.0 Å for hylSpn and $hylB_{3502}$, respectively. Mello et al. obtained similar results by analysing the complex of a substrate-based HA hexasaccharide and $hylB_{3502}$ with distances of 6.14 Å for O4 – Tyr488 OH and 5.68 Å for C5 – His479 Nε, respectively.[15] As a consequence, with respect to the substrate HA, the spatial arrangement of the catalytic residues Tyr488 and His479 in the $hylB_{3502}$ structure is not optimal for catalysis. Therefore, a homology model of $hylB_{4755}$ based on the X-ray structures of hylSpn in terms of optimal geometry and $hylB_{3502}$ in terms of structural similarity was envisaged.

To extract the SCRs from both X-ray structures, a superposition of all secondary structure elements was performed for the α- and βII-domains separately since the within-domain similarities are very high.[14] The α-domains of both lyases were fragmented into two parts; the first one comprises the α-helices 1 to 7 and the second one the α-helices 8 to 13 because visual inspection of the superimposed structures revealed a slight rotation of both parts within the α-domain of $hylB_{3502}$ compared to hylSpn. The rms deviation for all backbone atoms of the α-helices 1 to 7 is 0.59 Å whereas it is 1.08 Å for the α-helices 8 to 13. Both values indicate a very high similarity of both α-domains. The superposition of all β-sheets of the βII-domains also resulted in an excellent overlap with a rms deviation of 0.65 Å.

[§] By convention, the sugar residue subsites are labelled from *-n* to *+n*, with *-n* at the non-reducing end and *+n* at the reducing end of the substrate. Cleavage occurs between the -1 and +1 subsites.[20]

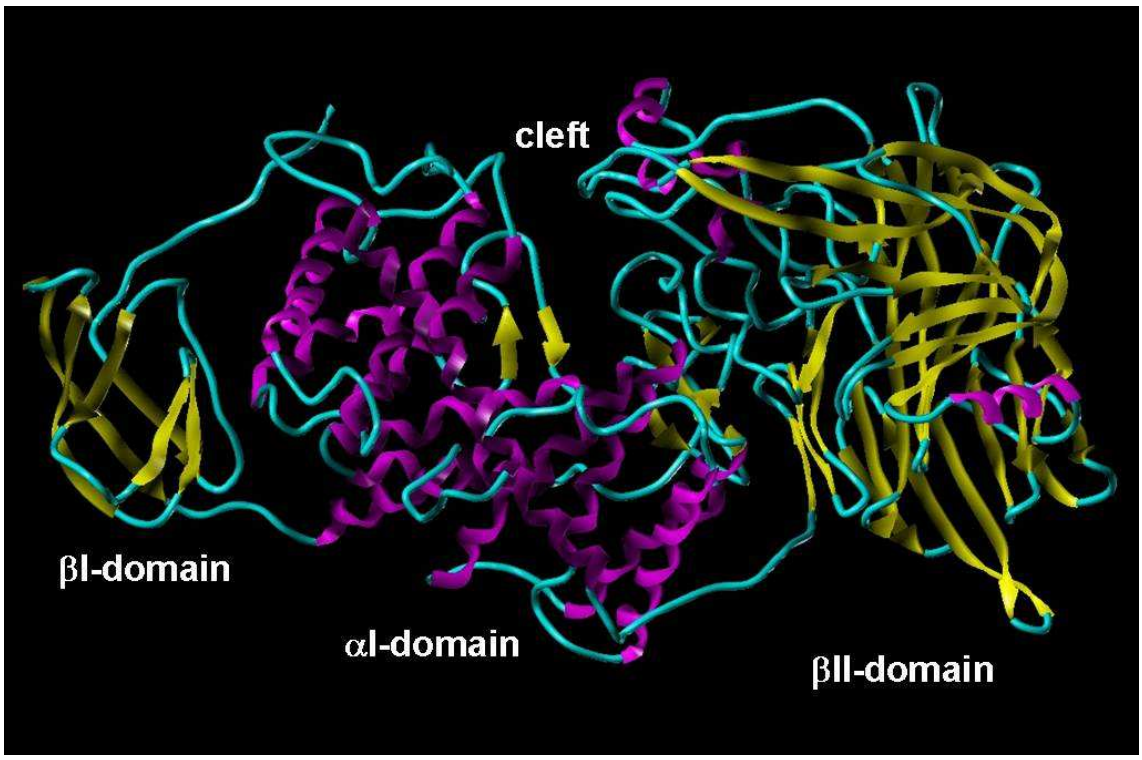

Figure 3.2. Schematic representation of $hylB_{4755}$ model. α-helices, β-sheets and loop regions are coloured in purple, yellow and cyan, respectively.

Hence, the α- and βII-domains of $hylB_{3502}$ separately superimposed with the respective domains of hylSpn were extracted to form the framework of the SCRs of the $hylB_{4755}$ model. The missing linker was inserted from the $hylB_{3502}$ structure and fitted onto the anchor residues at the end of the α-domain and at the beginning of the βII-domain of the framework model. Subsequently, the fifteen different amino acids of the $hylB_{3502}$ primary structure were mutated into the respective amino acids of $hylB_{4755}$. Due to the very high homology of the amino acid sequences, the overall model closely resembles the structure of the templates. The calculated rms deviation of all Cα atoms amounts to 1.02 Å for the $hylB_{4755}$ model *vs.* the hylSpn crystal structure. The energy minimised model of $hylB_{4755}$ is shown in Figure 3.2.

3.2.2 Search for molecular fragments as ligands of bacterial hyaluronidase using the computer programme LUDI

Using the *de novo* design programme LUDI, small and fairly rigid molecules were retrieved from a 3D structure database by positioning them into the protein-binding site. For each successfully docked ligand, LUDI estimates the expected binding affin-

ity by an empirical scoring function.[20] Based on the homology model of $hylB_{4755}$, we screened entries from the LeadQuest® databases Vol. 1&2[21] with LUDI. Prior to the search, the molecules from the LeadQuest® databases were processed using CONVERTER[22] to generate reasonable 3D structures. Using standard parameters for LUDI calculations, all 3D structures are treated as rigid bodies independent of the existence of rotatable bonds.

This 3D database was reprocessed by GENFRA, a module of the LUDI programme suite, to classify all molecules in terms of their hydrogen bonding and lipophilic properties and to calculate the fraction of solvent-accessible surface of their functional groups. Appropriate fit centres were assigned to all functional moieties of the ligands to be screened and saved in a supplementary database by GENFRA. Subsequently, for all functional groups exposed to the active site of the enzyme, putative interaction sites in space were generated by LUDI according to rules which have been derived from composite crystal-field environments compiled with appropriate crystal data of small molecules (Cambridge Structural Database).[7] The programme tries to fit each database molecule onto these interaction sites in the pre-defined binding pocket. The centre of this pocket was defined as the arithmetic mean of all atom positions of the active site amino acids Arg409, Trp460, Tyr576, Val579 and Arg634. All residues within a sphere of 5 Å around this centre were included into the LUDI calculation. This active site of $hylB_{4755}$ is shown together with the pre-calculated interaction sites in Figure 3.3.

After four days calculation time, 122 hits were retrieved by the described procedure and were ranked on a relative scale in terms of their expected binding affinity using the scoring function described by Böhm.[20] Since neither ligand nor protein flexibility is taken into account when using the parameters described above, a subsequent LUDI run with slightly altered parameters was accomplished. To allow for a larger search space and for more interaction possibilities, the radius of the sphere was enlarged to 8 Å and one rotatable bond at a time was treated flexible. In order to retrieve new compounds, the hit database was combined with the original LUDI database as supplied by Accelrys.

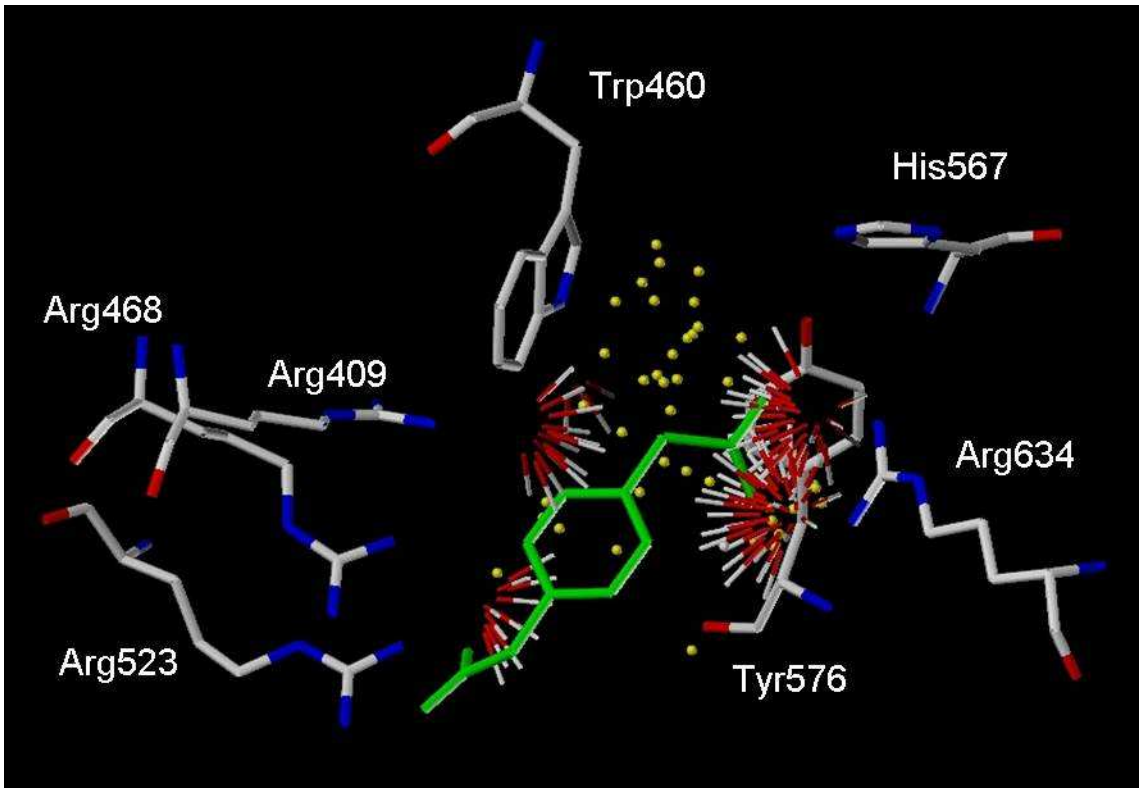

Figure 3.3. Interaction sites generated by LUDI with sphere radius of 5 Å (yellow, lipophilic sites; red, hydrogen bond acceptors) inside the active site of the $hylB_{4755}$ model. Compound **2** (green) retrieved from the combined databases with the highest scoring value is fitted onto these interaction sites.

A LUDI run with these adapted parameters on the whole LeadQuest® database would have taken far too long to be completed in a reasonable time. 212 structures from the combined database were retrieved by LUDI and ranked in terms of their expected binding affinity if the predicted K_i value was lower than 1 mM (LUDI score higher than 300).

In parallel to these investigations, an additional database with commercially available compounds has been constructed starting from the ChemACX database Version 5.5 from CambridgeSoft Corp. (see chapter 4). For the sake of reasonable calculation time, the applied parameters were altered with respect to the sphere radius (6 Å instead of 5 Å) and the number of lipophilic and polar interaction sites per protein atom (25 each instead of 35 before). Around 197000 compounds were screened in 5.5 days with LUDI resulting in 1063 hits. The final selection of compounds for purchase, synthesis and enzyme testing included the following criteria: (a) a high LUDI score larger than 325, (b) commercial availability and (c) efficient synthetic feasibility.

A majority of the selected compounds were carboxylic acids or derivatives thereof (Table 3.1, compounds **2**, **3**, **7**, **9**, **11**, **15** and **19**) since the active site of $hylB_{4755}$ is composed of several arginine residues. All other compounds also bear polar functional groups which may favourably interact with these positively charged guanidino groups. For example, the proposed binding mode of compound **2** is shown in Figure 3.3 as fit onto the calculated interactions sites. It shows favourable ionic interactions between its two carboxylic groups and the arginine residues Arg468 and Arg634 bridging both 'walls' at the narrowest site of the HA binding cleft. Additionally, the proposed binding mode suggests a lipophilic interaction between the phenyl moiety of the ligand and Val579 constituting the bottom of the crevice (Val579 not shown in Figure 3.3 for the sake of clarity). Compound **17** from the LeadQuest® database was similarly docked** into the active site of $hylB_{4755}$ bridging the binding site with its both acetyl groups. Additionally, the sulfur substituent points towards the Trp460 residue of the aromatic patch (see Figure 3.4, purple structure). Such a lipophilic interaction can be frequently observed in protein-ligand crystal structures.

Based on the LUDI search, we assayed nineteen compounds for their abilities to inhibit the degradation of hyaluronic acid by the hyaluronan lyase from *S. agalactiae* strain 4755 (see Table 3.1).[23] With respect to selectivity, the inhibitory activities of all compounds on the bovine testicular hyaluronidase (BTH) were determined, too (see chapter 5 and PhD thesis of Sunnhild Salmen[23]).

Despite moderate LUDI scores, six (compounds **5**, **6**, **8**, **10**, **13** and **18**) out of nineteen compounds induced no inhibition of the hyaluronate lyase up to the maximal test concentration. In contrast to these results, compound **1** of the adapted ChemACX database with the highest LUDI score moderately inhibited the activity of $hylB_{4755}$ with IC_{50} values of 310 µM at catalytically optimal pH and 160 µM at physiological pH.

** For the discussion of an alternative binding mode of compound **17** as suggested by additional LUDI calculations see section 3.2.3.

Table 3.1. Selected compounds with calculated LUDI scores, database source (A = Accelrys, C = ChemACX and LQ = LeadQuest® Database) and IC_{50} value determined on $hylB_{4755}$ (n=3; SEM not larger than 1 %)[23]

No.	Structure	LUDI Score Database	IC_{50} / µM	
			pH 5.0	pH 7.4
1	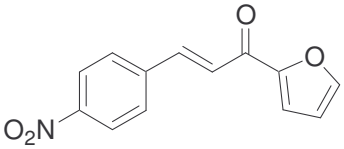	687 C	310	160
2	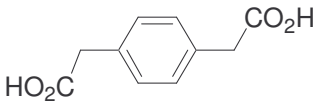	579 A	3710	900
3	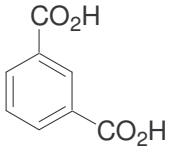	555 A	2680	inactive (≤ 20 mM)
4	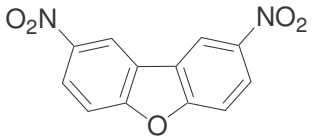	505 C	2900	inactive (≤ 5 mM)
5	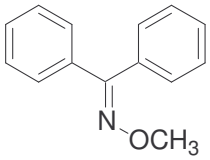	452 A	inactive (≤ 20 mM)	inactive (≤ 20 mM)
6	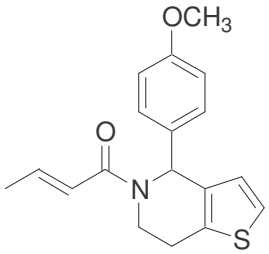	441 LQ	inactive (≤ 5.25 mM)	n.d.
7	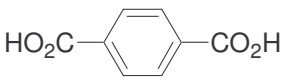	436 A	2500	inactive (≤ 20 mM)
8	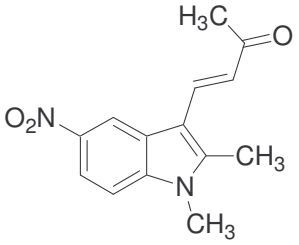	429 LQ	inactive (≤ 2.5 mM)	n.d.

9	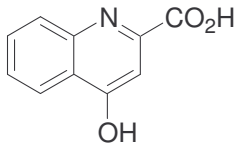	426 A	4470	inactive (≤ 10 mM)
10	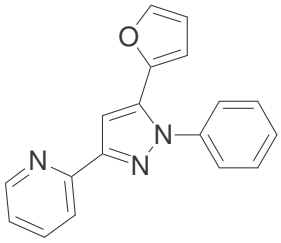	407 C	inactive (≤ 0.1 mM)	inactive (≤ 0.1 mM)
11	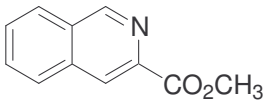	405 A	11000	5000
12	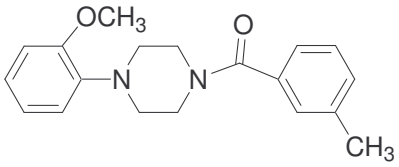	392 LQ	38 % (20 mM) [a]	83 % (15 mM) [a]
13	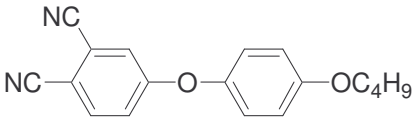	391 LQ	inactive (≤ 5 mM)	n.d.
14	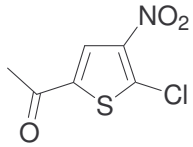	384 LQ	20 % (20 mM) [a]	50 % (20 mM) [a]
15	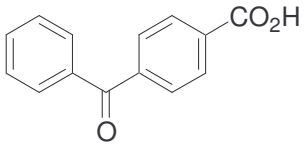	382 A	50 % (20 mM) [a]	35 % (20 mM) [a]
16	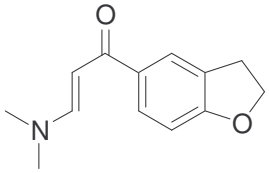	364 LQ	610	46 % (2 mM) [a]
17	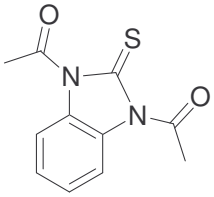	363 LQ	160	5
18	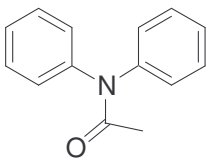	357 LQ	inactive (≤ 20 mM)	inactive (≤ 20 mM)
19	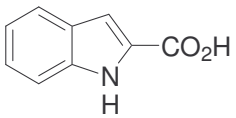	328 A	3550	44 % (20 mM)[a]

[a] % inhibition at concentration given in parenthesis

Although the inhibitory activities of the compounds were determined at two different pH values, the predicted K_i value is only comparable with the measured IC_{50} value for pH 7.4 since the protonation states of the amino acid residues exposed to the active site were defined for a neutral pH. For compound **1**, the predicted inhibition constant of ca. 1 µM and the measured IC_{50} value differ by a factor of around two orders of magnitude. Since other studies have shown predicted affinities by LUDI to be accurate to about 1.3-1.5 lg units,[20,24] this prediction is in accordance with the prediction accuracy of today's scoring functions.

The IC_{50} values for the aromatic dicarboxylic acids determined on the hyaluronate lyase at pH 5.0 were 3.7 mM (**2**), 2.7 mM (**3**) and 2.5 mM (**5**) and were lower than anticipated from the LUDI score. Presumably, the LUDI scoring function did not perform well due to inaccurately predicted hydrogen bonding contribution.[25] Additionally, the LUDI scores just tend to overestimate binding of these compounds at a highly charged (pH-dependent) active site due to several ionic interactions (see discrete contributions to Böhm's LUDI score, data not shown). For benzene-1,4-diacetic acid (**2**), an IC_{50} value of 0.9 mM was determined at physiological pH, whereas isophthalic acid (**3**) and terephthalic acid (**7**) showed no inhibition of the enzyme at neutral pH. It may be speculated about the factors accounting for the varying activity differences of the enzyme inhibitors at pH 5.0 and 7.4. In particular, the protonation state of the tested compounds depends on the pH value of the incubation mixture just like the protonation of amino acid residues inside the active site of the enzyme.

Compounds **4** and **9** weakly inhibited the activity of $hylB_{4755}$ at its catalytic pH optimum with IC_{50} values of 2.9 mM (**4**) and 4.5 mM (**9**) whereas at physiological pH, no inhibition could be detected up to a concentration of 5 mM and 10 mM, respectively. Like in the other cases, the prediction of inhibitory activity based on the LUDI score differed significantly. Compounds **12**, **14** and **15** only showed partial inhibition at the maximal test concentration for both pH values. At pH 5.0, compound **16** from the LeadQuest® database and indole-2-carboxylic acid (**19**) inhibited $hylB_{4755}$ with IC_{50} values of 0.6 mM and 3.6 mM, respectively, but did not approach 50 % inhibition at physiological pH. Inspired by the inhibitory effect of compound **19**, substitution patterns at the indole scaffold were explored leading to potent indole-based hyaluronate lyase inhibitors in the micromolar range.[23] An enzyme-inhibitor complex of

hylSpn with one of these potent inhibitors could be elucidated by means of X-ray crystallography.[23]

Surprisingly, despite a predicted inhibition concentration of only around 1 mM, 1,3-diacetylbenzimidazole-2-thione (**17**) potently inhibited the activity of $hylB_{4755}$ with IC_{50} values of 5 µM at physiological pH and 160 µM at pH 5.0. Since for further modifications and optimisation of the lead 1,3-diacetylbenzimidazole-2-thione (**17**) a determination of the binding mode by analysing an enzyme-inhibitor complex would be beneficial, soaking experiments[††] were accomplished. Probably due to instability against moisture and poor solubility, no X-ray structure of hylSpn complexed with compound **17** could be determined.[27] Nonetheless, prompted by its promising inhibitory activity, structural modifications of the mother substance are the subject of ongoing studies.

3.2.3 Dependence of results on applied LUDI parameters – Comparison with Consensus Scoring methods and FlexX docking

Since any virtual screening method has to face docking and scoring as two critical issues, the calculated LUDI results were firstly analysed for their dependence on the applied docking parameters. For developing a more efficient selection strategy, all nineteen compounds were investigated.

In a first step, the calculated LUDI scores of selected compounds from the LeadQuest® database run were compared with the results of the combined database run with respect to the sphere radius and the flexibility of docked ligands. Additionally, the observed differences were related to the rms deviation of the docked poses[‡‡] in each LUDI run. Results for five selected compounds are presented in Table 3.2.

Compounds **2** and **3** from the Accelrys database were only included in searches using a sphere radius of 8 Å. Their calculated scores were compared with respect to rotating bonds present or not (irot = 1 or 0). For compound **2**, LUDI suggested a rather similar spatial position in both calculations, but the predicted inhibition constants differed by a factor of 35 (60 µM and 1.6 µM for the first and the second calculation, respectively). This may result from a probably high overestimation of ionic

[††] In cooperation, soaking experiments for 1,3-diacetylbenzimidazole-2-thione (**17**) with hylSpn were accomplished by M. J. Jedrzejas, Children's Hospital Oakland Research Institute, Oakland, USA.
[‡‡] target-bound conformation and orientation of each screened ligand

interactions (six instead of four) between the molecule's carboxylic moieties and the amino acid residues Arg468 and Arg634 of the enzyme (data not shown, see Figure 3.3). Additionally, these ionic interactions as well as hydrogen bonds are directional,[28] i.e. they significantly depend on the spatial arrangement of the ligand and the interacting groups of the protein. By contrast, the results for compound **3** did not vary upon alteration of flexibility parameters. But also in this case, the LUDI score seems to be largely overestimated because of ionic interactions.

This problem might be tackled by changing the protonation states of the carboxylic functions on both molecules. During the automated generation of the GENFRA databases, the protonation states of the processed compounds may be defined by applying a special parameter. This parameter could not be altered due to an error in the LUDI programme supplied by Accelrys. Unfortunalely, despite of intensive efforts to solve this issue, the Accelrys hot line could not provide a fix for this crucial error. Alternatively, both compounds were treated as uncharged carboxylic acids after manually altering the protonation states, but then they were not retrieved by LUDI (data not shown).

Although compound **6** was docked in an identical position by LUDI (rmsd = 0.00 Å), the calculated LUDI scores were slightly dependent on the sphere radius, but not on the allowed flexibility of the ligand. Probably, a larger sphere with more and/or additional, differently typed interaction sites (in this case hydrogen donor sites) led to this observed change because the LUDI scoring function is cumulative with respect to the free energy contribution from hydrogen bonds, ionic, and lipophilic interactions.[28] The LUDI scores of compound **12** vary in similar manner as in the case of compound **6**. The slight difference of the docking positions (rms deviation of 0.89 Å) might reflect the dependence of the scores on the absolute position of the interacting functional groups of the ligand and the protein. For compound **17**, a significantly different effect can be observed. Despite a fairly similar LUDI score for all four settings, the respective docking pose is strikingly different with a rms distance of 4.65 Å as depicted in Figure 3.4. This result underlines that alternative poses of the ligand might lead to similar LUDI scores and, thus, similar predicted inhibition constants. An identification of the native binding mode, either manual or by means of the docking programme, is therefore a basic requisite for the reliable prediction of binding affinities.[11]

Table 3.2. Overview of the calculated LUDI Score in dependence of the applied parameter and of the resulted docking accuracy

Compound No.	LUDI Score[a]				rmsd
	r = 5 Å irot = 0	r = 5 Å irot = 1	r = 8 Å irot = 0	r = 8 Å irot = 1	in Å
2	—	—	422	579	1.44[b]
3	—-	—	555	555	0.00[b]
6	400	400	441	441	0.00[c]
12	421	421	392	392	0.89[c]
17	343	343	363	363	4.65[c]

[a] Calculated LUDI score with indicated parameters for sphere radius r and rotatable bonds on or off (irot = 1 or 0)
[b] rms deviation between the pose positions calculated with parameters r = 8 Å, rotatable bonds off (irot = 0) and parameters r = 8 Å, rotatable bonds on (irot = 1)
[c] rms deviation between the pose positions calculated with parameters r = 5 Å, rotatable bonds off (irot = 0) and parameters r = 8 Å, rotatable bonds on (irot = 1)

Several methods were described in the literature for slightly differing scenarios like 1) structure-based inhibitor design,[29,30] 2) virtual screening by pharmacophore filters,[24] and 3) validation of scoring functions.[31,32] In the first scenario, Grädler et al. calibrated the LUDI score starting from a protein-ligand complex of a substrate-like inhibitor with known K_i value by adjusting the LUDI parameters so that the calculated pose resembles the detected binding mode of the co-crystallised ligand and that the predicted score corresponds to the measured K_i value. Following this approach, the X-ray structure of hylSpn complexed with L-ascorbic acid[4] could suit as reference. After superposition of the hylSpn-vitamin C structure with the $hylB_{4755}$ model, vitamin C was merged into the model, and a very low LUDI score of 64 corresponding to a predicted K_i value of 230 mM was calculated (For comparison, the measured IC_{50} value of L-ascorbic acid on $hylB_{4755}$ is 5 mM, see chapter 6.). Therefore, vitamin C could not serve as a reference since its LUDI score falls below the threshold of 300 for acceptable values and, moreover, since it could not be retrieved in several LUDI calculation attempts.

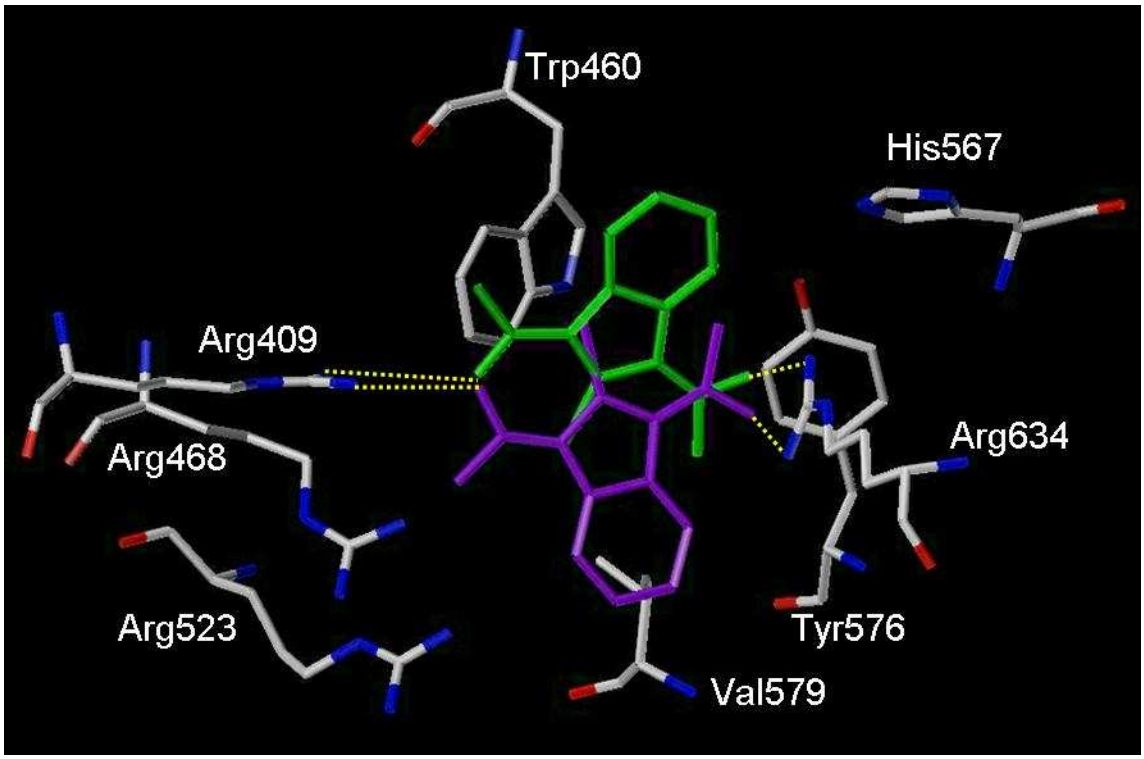

Figure 3.4. Two putative binding modes of compound **17** dependent on the LUDI sphere radius (5 Å, purple, 8 Å, green) encompassing the active site of the $hylB_{4755}$ model. Hydrogen bonds (yellow) between both acetyl substitutents of the molecule and Arg409 and Arg634 are depicted in dashed style.

A pilot project for virtual screening of human carboanhydrase II inhibitors published by Grüneberg et al.[24,33] represents the second scenario. In their work, a hierarchical filtering strategy was applied using a 2D query for essential functional groups, subsequently a 3D pharmacophore query and finally a similarity scoring with FlexS[34] based on known potent inhibitors resulting in around 3300 of 90000 compounds at the beginning. The 100 best scoring molecules were then flexibly docked with FlexX[35] and ranked by FlexX score and DrugScore.[36]

The third scenario was described by Stahl et al. who presented a detailed analysis of scoring functions for virtual screening using the programme FlexX as docking engine.[32] A well-chosen combination of two tested scoring functions led to a new, robust scoring scheme called ScreenScore, which is implemented in the latest versions of FlexX. The results obtained with ScreenScore were compared with those from the combination of other scoring functions, a method called 'consensus scoring'.[37] It was suggested that consensus scoring offered more robust results than individual scoring functions.[38]

In the present work, we attempted to combine approaches from the second and the third scenario in order to obtain a more reliable selection of compounds. In the first step, a consensus scoring of all hits from the calculation with the combined databases was envisaged. To date, several consensus scoring approaches like the CScore modul implemented in SYBYL[39] and X-Score[40] have been described in literature. Since X-Score was readily available from the authors, all hits from the combined databases run were re-scored using standard parameters. The $hylB_{4755}$ model and the poses of all hits were taken as calculated by LUDI in the combined database run. The results of this re-scoring approach with X-Score are summarised in Table 3.3.

The comparison of the ranking order of both scoring functions revealed that the selected compounds were all resorted by the X-Score scoring function. But, in general, the predicted K_i and K_d values of most investigated compounds are rather similar, e.g. for compound **2** with K_i = 1.6 µM as LUDI and K_d = 4.4 µM as X-Score prediction. Only compounds **11**, **18** and **19** differ in their predicted K_i and K_d values, respectively, by more than one order of magnitude. Such discrepancies are certainly due to the different 'basis sets' of the scoring functions. On the one hand, no standardised data set of protein-ligand complexes exists for calibration and, on the other hand, the number and type of appropriate biological systems is rather limited.[11] Nevertheless, Table 3.3 shows that the selection of compounds by their X-Score is as effective as using the LUDI score with respect to picking of potentially active inhibitors.

Table 3.3. Comparison of calculated LUDI score and X-Score for selection of proposed compounds

Compound No.	LUDI score[a]		X-Score[b]		Inhibitory activity[c]
	rank	score	rank	score	
2	1	579	2	5.36	+
3	2	555	15	5.10	+
5	6	452	32	4.78	–
7	10	436	127	3.96	+
9	17	426	141	3.78	+
11	32	403	1	5.41	+
12	46	392	146	3.65	+
13	49	391	90	4.30	–
14	57	384	75	4.43	+
16	79	364	53	4.60	+
17	80	363	116	4.04	+
18	89	357	32	4.78	–
19	131	328	15	5.10	+

[a] $K_i = 10^{\frac{-score}{100}}$

[b] $K_d = 10^{-score}$

[c] ligand with inhibitory activity on $hylB_{4755}$: +; ligand without inhibitory activity on $hylB_{4755}$: –

In general, active compounds are more reliably predicted if a docking engine like LUDI reproduces crystallographically observed (native-like) binding modes within a certain accuracy reflected by a rms deviation below 2.0 Å.[24,32,41]

Recently, in order to cover the entire conformational space of the candidate molecules as well as possible and then to retrieve their native-like binding geometries, flexible docking of the selected compound set followed by – at best – a consensus scoring scheme was proposed.[24,41,42] In our study, we tried to adapt a similar strategy to investigate whether it would facilitate the selection of compounds.

Table 3.4. Overview of FlexX results with respect to docking score and docking accuracy compared to poses calculated by LUDI

Compound No.	LUDI-like pose[a]		FlexX best pose[b]		Inhibitory activity[c]
	score	rmsd/Å	score	rmsd/Å	
5	-22.59	0.97	-26.57	2.05	–
12	-14.84	3.78	-15.88	4.88	–
19	-12.87	0.41	-14.20	4.93	+
7	-12.59	1.34	-22.72	5.34	+
2	-12.06	1.61	-18.70	5.89	+
11	-12.02	0.91	-14.20	4.74	+
13	-11.77	5.32	-17.46	6.82	–
3	-11.45	1.53	-13.56	3.09	+
17	-10.08	0.95	-16.83	5.31	+
16	-9.37	1.57	-18.52	8.42	+
9	-8.72	1.14	-15.41	7.89	+
14	-7.68	1.13	-19.43	5.62	–
18	-3.56	1.85	-10.68	14.46	–

[a] FlexX-Score of the FlexX pose with the lowest rmsd compared to the LUDI pose from the combined database run

[b] FlexX pose with the best FlexX-Score among all poses, rmsd compared to the LUDI pose from the combined database run

[c] ligand with inhibitory activity on $hylB_{4755}$: +; ligand without inhibitory activity on $hylB_{4755}$: –

Therefore, all proposed hits of the combined database run were subjected to an automated flexible docking procedure using FlexX with standard parameters. The results of the FlexX calculations are summarised in Table 3.4. For comparison, the poses calculated by LUDI were taken as reference since LUDI is supposed to be able to predict reliable binding modes.[30,43] A rms deviation smaller than 2 Å between FlexX and LUDI poses was taken as a criterion for the prediction of a LUDI-like binding mode.

For each of the investigated hits, the pose with the best FlexX score and the LUDI pose are very different (column FlexX best pose). There is no correlation between the FlexX scores and inhibitory activity so that a compound selection uniquely based upon this score is not more efficient than a selection based on any other scoring function. However, when the most LUDI-like FlexX poses are considered, the prediction is improved. Apart from two inactive compounds (**12** and **13**) where FlexX did not find a LUDI-like pose and one outlier (compound **5**) with no inhibitory activity but high FlexX score, this double-docking-double-scoring procedure may be able to privilege active ligands (e.g. compounds **7** and **19** *vs.* compounds **14** and **18**) and should therefore be applied for the selection of new compounds in future work.

3.3 Summary and future perspectives

Starting from two crystal structures of streptococcal hyaluronate lyases hylSpn and $hylB_{3502}$, a homology model of *S. agalactiae* strain 4755 hyaluronate lyase $hylB_{4755}$ was constructed. This homology model was applied to structure-based ligand design with the *de novo* design programme LUDI. The three databases LeadQuest® Vol. 1&2, Accelrys and an adapted ChemACX database containing 228000 compounds were screened resulting in 1275 hits. Based on high LUDI scores, synthetic feasibility and commercial availability, nineteen of these putative ligands were selected, subsequently purchased or synthesised and investigated for their abilities to inhibit the degradation of hyaluronic acid by the hyaluronan lyase from S. *agalactiae* strain 4755. Thirteen compounds were active on $hylB_{4755}$ in the milli- and submillimolar range, six did not inhibit the enzyme up to the highest concentration tested. 1,3-Diacetylbenzimidazole-2-thione (**17**) with IC_{50} values of 5 µM and 160 µM at physiological pH and optimum pH, respectively, is one of the most potent inhibitors of hyaluronate lyases known to date. Prompted by this promising result, structural modifications of the compound **17** are the subject of ongoing studies.

Based on the results of the investigated compounds, theoretical investigations were carried out. Using the re-scoring scheme with X-Score and subsequently the automated flexible docking programme FlexX, a double-docking-double-scoring strategy was derived which seems to improve the selection and lead optimisation of hyaluronate lyase inhibitors.

Besides the programmes DrugScore[36] and GRID,[44] LUDI is capable to extract H-donor, H-acceptor and lipophilic interaction sites which can be converted into a complex pharmacophore refined by the analysis of known hyaluronate lyase-inhibitor complexes (see chapter 7 and reference [23]). Subsequently, based on this pharmacophore, databases like ChemACX could be screened using INSIGHT or CATALYST. Such a strategy was shown to be successful in several drug design scenarios[33,42] and could be complemented by the FlexX-Pharm programme, a flexible docking procedure using pharmacophore-type constraints.[45]

3.4 Experimental section

3.4.1 Theoretical methods

3.4.1.1 $HylB_{4755}$ model construction

The coordinates for the bacterial hyaluronan lyase from *S. pneumoniae* (pdb code: 1c82)[46] and the lyase from S. *agalactiae* strain 3502 (pdb code: 1f1s)[4] were obtained prior to publication from M. J. Jedrzejas, Children's Hospital Oakland Research Institute, Oakland, USA. The sequence identity between hylSpn and $hylB_{4755}$ is 53 %, between $hylB_{4755}$ and $hylB_{3502}$ even 98 %. For a homology modelling approach the crystal structure of hylSpn was used as template, since its conformation is supposed to be catalytically active whereas the crystallised state of $hylB_{3502}$ is not optimal for catalysis.[14] Compared to hylSpn, the α-domain of $hylB_{3502}$ is rotated by a small angle around the linker II with respect to the β-II-domain.[14] As a result, the $hylB_{3502}$ structure is more open than the hylSpn conformation. Consequently, corresponding subdomains of hylSpn and $hylB_{3502}$ were superimposed using SYBYL 6.8 (Tripos Inc., St. Louis, USA) on an Indigo² workstation running IRIX 6.5. The superposition of all α-helices of the corresponding α-domains (Asn251-Leu610 and Thr173-Leu530 for $hylB_{3502}$ and hylSpn, respectively) resulted in a rms distance of 0.8 Å, whereas the corresponding β-II-domains (Asn623-Asn972 for $hylB_{3502}$ and Tyr543-Asn874 for $hylB_{3502}$ and hylSpn, respectively) are even more similar with a rms distance of 0.65 Å. A full model of $hylB_{4755}$ was constructed by starting from the $hylB_{3502}$ α- and β-II-domains with lowest rms distance to hylSpn, inserting joining loops from $hylB_{3502}$, and mutating eight amino acids to achieve the $hylB_{4755}$ amino acid sequence. The

resulting model with hydrogens added was energetically minimised using the Amber4.1 force field.

The LeadQuest® databases Vol. 1&2 (May 1998, 23341 molecules[21]) and the adapted ChemACX database (see chapter 4) were converted into 3D using the CONVERTER module from Insight 2000 (Accelrys Inc., San Diego, USA). All-trans conformations of chains and chair conformations of 6-membered rings consisting of only sp^3 atoms were adjusted to allow for energy minimum conformations of the resulting 3D structures. For each molecule of the original 2D databases two stereoisomeres (if possible) were generated, yielding 28717 structures for the LeadQuest® databases and 196908 structures for the ChemACX database. The resulting databases were prepared for use with the LUDI programme (Accelrys Inc.) by means of the LUDI module GENFRA 5[7,48] constructing a structure and a target database with types of each target site (e.g. H-acceptor or H-donor atom) in the fragments.

3.4.1.2 LUDI calculations with the hylB$_{4755}$ model

A LUDI approach was set up with a sphere of 5 Å radius within the active site of hylB$_{4755}$. The centre of this sphere was determined as the arithmetic mean of five amino acid residues belonging to the active site (Arg409, Trp460, Tyr576, Val579 and Arg634). The values of the most important LUDI parameters for the design of hylB$_{4755}$ ligands were as follows: the maximal rms distance of the fit between the fragment and the interaction sites was 0.45 Å, the number of lipophilic and polar interaction sites per protein atom was set to 35 and the minimal contact surface between ligand and protein was set to 30 %. The retrieved candidate molecules were ranked with respect to their expected binding affinity using the empirical scoring function developed by Böhm[43] with a minimal scoring value of 300 (predicted K_i value of 1 mM). All other parameters were set to default values. Performing a LUDI run with the constructed LeadQuest® database resulted in 122 hits. To enable a larger sphere (r = 8 Å) and to consider rotatable bonds in reasonable CPU time, these hits were combined with 1020 compounds from the Accelrys database supplied with the LUDI module. Recalculation with this combined hit database led to the extraction of 212 new hits. Sixteen of these hits were selected for testing hyaluronidase inhibition according to high LUDI scores, availability and efficient synthetic feasibility. Additionally, for the sake of shorter calculation time, the adapted ChemACX database (see chapter 4) was filtered by LUDI using more restricted conditions (sphere radius of 6 Å in-

stead of 5 Å and a density of lipophilic and polar interaction sites of 25 instead of 35 sites per protein atom). Three out of 1063 compounds were selected for testing hyaluronidase inhibition.

3.4.1.3 Re-scoring of LUDI poses with X-Score

For re-scoring using the X-Score programme,[40] all LUDI poses from the combined database run were converted into a multi-mol2 file by the SYBYL module DBTRANSLATE. Polar hydrogen atoms were added to the $hylB_{4755}$ model, and it was saved in pdb format. Subsequently, the X-Score run was set up for all hits and the results were analysed in comparison to the calculated LUDI scores.

3.4.1.4 Re-docking of LUDI poses with FlexX Version 1.11

All LUDI poses of the combined database run were converted into a multi-mol2 file using the SYBYL module DBTRANSLATE and splitted into single mol2 files for use with FlexX Version 1.11.[35,49,50] Protonation states of the molecules were adjusted to generate the structure predominating at neutral pH. The binding site was manually defined by means of the interactive modelling programme SYBYL 6.8. For flexible docking, the binding pocket from the LUDI run with a sphere of 5 Å was selected. The hit set was docked into the target active site using the default FlexX parameter settings contained in the FlexX distribution. For each entity of the hit set, the LUDI pose was taken as reference for further analysis. Final scores were calculated for all FlexX poses (up to 800) per compound.

3.4.2 Test compounds

The test compounds were either purchased from Acros Organics BVBA (Belgium), Lancaster Synthesis GmbH (Germany), Maybridge Chemical Company (United Kingdom), Sigma-Aldrich Chemie GmbH (Germany) and Tripos Receptor Research Ltd. (United Kingdom) or synthesised according to literature procedures by Sunnhild Salmen.[23]

3.4.3 Pharmacological methods

The inhibitory effect of the compounds on the activity hyaluronidases were determined[23] by the method of Reissig[51] based on the Morgan-Elson reaction and by a turbidimetric assay according to the description of Di Ferrante.[52]

3.5 References

(1) Glycoforum http://www.glycoforum.gr.jp/, 2003.

(2) Hynes, W.; Walton, S. Hyaluronidases of gram-positive bacteria. *FEMS Microbiol Lett* **2000**, *183*, 201-207.

(3) Akhtar, M. S.; Bhakuni, V. *Streptococcus pneumoniae* hyaluronate lyase contains two non-cooperative independent folding/unfolding structural domains: characterization of functional domain and inhibitors of enzyme. *J Biol Chem* **2003**, *278*, 25509-25516.

(4) Li, S.; Taylor, K. B.; Kelly, S. J.; Jedrzejas, M. J. Vitamin C inhibits the enzymatic activity of *Streptococcus pneumoniae* hyaluronate lyase. *J Biol Chem* **2001**, *276*, 15125-15130.

(5) Moon, J. B.; Howe, W. J. Computer design of bioactive molecules: a method for receptor-based de novo ligand design. *Proteins* **1991**, *11*, 314-328.

(6) Nishibata, Y.; Itai, A. Automatic creation of drug candidate structures based on receptor structure. Starting point for artificial lead generation. *Tetrahedron* **1991**, *47*, 8985-8990.

(7) Böhm, H. J. The computer program LUDI: a new method for the de novo design of enzyme inhibitors. *J Comput Aided Mol Des* **1992**, *6*, 61-78.

(8) Böhm, H. J. LUDI: rule-based automatic design of new substituents for enzyme inhibitor leads. *J Comput Aided Mol Des* **1992**, *6*, 593-606.

(9) Schneider, G.; Böhm, H. J. Virtual screening and fast automated docking methods. *Drug Discov Today* **2002**, *7*, 64-70.

(10) Böhm, H. J. Current computational tools for *de novo* ligand design. *Curr Opin Biotechnol* **1996**, *7*, 433-436.

(11) Gohlke, H.; Klebe, G. Approaches to the description and prediction of the binding affinity of small-molecule ligands to macromolecular receptors. *Angew Chem Int Ed Engl* **2002**, *41*, 2644-2676.

(12) Klebe, G.; Grädler, U.; Grüneberg, S.; Krämer, O.; Gohlke, H. Understanding receptor-ligand interactions as a prerequisite for virtual screening. *Virtual Screening for Bioactive Molecules*; Wiley-VCH: Weinheim, 2000; pp 207-227.

(13) Li, S.; Kelly, S.; Lamani, E.; Ferraroni, M.; Jedrzejas, M. Structural basis of hyaluronan degradation by *Streptococcus pneumoniae* hyaluronate lyase. *EMBO J* **2000**, *19*, 1228-1240.

(14) Li, S.; Jedrzejas, M. J. Hyaluronan binding and degradation by *Streptococcus agalactiae* hyaluronate lyase. *J Biol Chem* **2001**, *276*, 41407-41416.

(15) Mello, L. V.; De Groot, B. L.; Li, S.; Jedrzejas, M. J. Structure and flexibility of *Streptococcus agalactiae* hyaluronate lyase complex with its substrate. Insights into the mechanism of processive degradation of hyaluronan. *J Biol Chem* **2002***, 277*, 36678-36688.

(16) Sanchez, R.; Sali, A. Comparative protein structure modeling. Introduction and practical examples with modeller. *Methods Mol Biol* **2000***, 143*, 97-129.

(17) Thompson, J. D.; Higgins, D. G.; Gibson, T. J. CLUSTAL W: improving the sensitivity of progressive multiple sequence alignment through sequence weighting, position-specific gap penalties and weight matrix choice. *Nucleic Acids Res* **1994***, 22*, 4673-4680.

(18) Higgins, D. G.; Sharp, P. M. CLUSTAL: a package for performing multiple sequence alignment on a microcomputer. *Gene* **1988***, 73*, 237-244.

(19) Jedrzejas, M. J.; Mello, L. V.; De Groot, B. L.; Li, S. Mechanism of hyaluronan degradation by *Streptococcus pneumoniae* hyaluronate lyase: Structures of complexes with the substrate. *J Biol Chem* **2002**.

(20) Böhm, H. J. Prediction of binding constants of protein ligands: a fast method for the prioritization of hits obtained from *de novo* design or 3D database search programs. *J Comput Aided Mol Des* **1998***, 12*, 309-323.

(21) LeadQuest Chemical Compounds Libraries; Vol. 1-2 ed.; Tripos, Inc.: St. Louis, USA, 2000.

(22) Accelrys, Inc. *CONVERTER in Insight2000*.

(23) Salmen, S. Inhibitors of bacterial and mammalian hyaluronidases: synthesis and structure-activity relationships; University of Regensburg: Regensburg, 2003.

(24) Grüneberg, S.; Wendt, B.; Klebe, G. Subnanomolar Inhibitors from Computer Screening: A Model Study Using Human Carbonic Anhydrase II. *Angew Chem Int Ed Engl* **2001***, 40*, 389-393.

(25) Ajay; Murcko, M. A. Computational methods to predict binding free energy in ligand-receptor complexes. *J Med Chem* **1995***, 38*, 4953-4967.

(26) Kelly, S. J.; Taylor, K. B.; Li, S.; Jedrzejas, M. J. Kinetic properties of *Streptococcus pneumoniae* hyaluronate lyase. *Glycobiology* **2001***, 11*, 297-304.

(27) Jedrzejas, M. personal communication, 2003.

(28) Böhm, H. J. The development of a simple empirical scoring function to estimate the binding constant for a protein-ligand complex of known three- dimensional structure. *J Comput Aided Mol Des* **1994***, 8*, 243-256.

(29) Grädler, U. De Novo-Design und Strukturbestimmung von Inhibitoren der tRNA-Guanin Transglykosylase aus Zymomonas mobilis als neues Target der Bakterienruhr. Institut für Pharmazeutische Chemie und Biochemie; Philipps-Universität Marburg: Marburg, 2000.

(30) Grädler, U.; Gerber, H. D.; Goodenough-Lashua, D. M.; Garcia, G. A.; Ficner, R. et al. A new target for shigellosis: rational design and crystallographic studies of inhibitors of tRNA-guanine transglycosylase. *J Mol Biol* **2001***, 306*, 455-467.

(31) Schulz-Gasch, T.; Stahl, M. Binding site characteristics in structure-based virtual screening: evaluation of current docking tools. *J Mol Model (Online)* **2003***, 9*, 47-57.

(32) Stahl, M.; Rarey, M. Detailed analysis of scoring functions for virtual screening. *J Med Chem* **2001***, 44*, 1035-1042.

(33) Grüneberg, S.; Stubbs, M. T.; Klebe, G. Successful virtual screening for novel inhibitors of human carbonic anhydrase: strategy and experimental confirmation. *J Med Chem* **2002***, 45*, 3588-3602.

(34) Lemmen, C.; Lengauer, T.; Klebe, G. FLEXS: a method for fast flexible ligand superposition. *J Med Chem* **1998***, 41*, 4502-4520.

(35) Rarey, M.; Kramer, B.; Lengauer, T.; Klebe, G. A fast flexible docking method using an incremental construction algorithm. *J Mol Biol* **1996***, 261*, 470-489.

(36) Gohlke, H.; Hendlich, M.; Klebe, G. Knowledge-based scoring function to predict protein-ligand interactions. *J Mol Biol* **2000***, 295*, 337-356.

(37) Charifson, P. S.; Corkery, J. J.; Murcko, M. A.; Walters, W. P. Consensus scoring: A method for obtaining improved hit rates from docking databases of three-dimensional structures into proteins. *J Med Chem* **1999***, 42*, 5100-5109.

(38) Stahl, M.; Böhm, H. J. Development of filter functions for protein-ligand docking. *J Mol Graph Model* **1998***, 16*, 121-132.

(39) Clark, R. D.; Strizhev, A.; Leonard, J. M.; Blake, J. F.; Matthew, J. B. Consensus scoring for ligand/protein interactions. *J Mol Graph Model* **2002***, 20*, 281-295.

(40) Wang, R.; Lai, L.; Wang, S. Further development and validation of empirical scoring functions for structure-based binding affinity prediction. *J Comput Aided Mol Des* **2002***, 16*, 11-26.

(41) Wang, R.; Lu, Y.; Wang, S. Comparative evaluation of 11 scoring functions for molecular docking. *J Med Chem* **2003***, 46*, 2287-2303.

(42) Brenk, R.; Naerum, L.; Grädler, U.; Gerber, H. D.; Garcia, G. A. et al. Virtual screening for submicromolar leads of tRNA-guanine transglycosylase based on a new unexpected binding mode detected by crystal structure analysis. *J Med Chem* **2003***, 46*, 1133-1143.

(43) Böhm, H. J. On the use of LUDI to search the Fine Chemicals Directory for ligands of proteins of known three-dimensional structure. *J Comput Aided Mol Des* **1994***, 8*, 623-632.

(44) Goodford, P. J. A computational procedure for determining energetically favorable binding sites on biologically important macromolecules. *J Med Chem* **1985***, 28*, 849-857.

(45) Hindle, S. A.; Rarey, M.; Buning, C.; Lengauer, T. Flexible docking under pharmacophore type constraints. *J Comput Aided Mol Des* **2002***, 16*, 129-149.

(46) Ponnuraj, K.; Jedrzejas, M. Mechanism of Hyaluronan Binding and Degradation: Structure of *Streptococcus pneumoniae* Haluronate Lyase in Complex with Hyaluronic Acid Disaccharide at 1.7 A Resolution. *J Mol Biol* **2000***, 299*, 885-895.

(47) Tripos LEADQUEST Chemical Compounds Libraries Vol. 1 & 2. *http://www.tripos.com* **1998**.

(48) Böhm, H. J. A novel computational tool for automated structure-based drug design. *J Mol Recognit* **1993***, 6*, 131-137.

(49) Rarey, M.; Kramer, B.; Lengauer, T. Docking of hydrophobic ligands with interaction-based matching algorithms. *Bioinformatics* **1999***, 15*, 243-250.

(50) Rarey, M.; Kramer, B.; Lengauer, T. Multiple automatic base selection: protein-ligand docking based on incremental construction without manual intervention. *J Comput Aided Mol Des* **1997***, 11*, 369-384.

(51) Reissig, J.; Strominger, J.; Leloir, L. A modified colorimetric method for the estimation of *N*-Acetylamino sugars. *J Biol Chem* **1955***, 217*, 959-966.

(52) Di Ferrante, N. Turbidimetric measurement of acid mucopolysaccharides and hyaluronidase activity. *J Biol Chem* **1956**, *220*, 303-306.

Chapter 4 Generation and property analysis of virtual screening databases

4.1 Introduction

Over decades, strategies for drug discovery have not changed much. Natural products isolated from plants and microorganisms or leads resulting from a biochemical concept or just from serendipitous findings were structurally modified to obtain analogues with improved activity, selectivity, bioavailability and/or less toxicity.[1] Regarding the physicochemical properties of these leads, compounds with poor solubility and/or chemical instability in a congeneric series were discarded and most often the starting lead was in a range of physicochemical properties consistent with the historical record of discovering orally active compounds.[2]

In recent years, the sources of drug leads in the pharmaceutical industry have changed significantly. Apart from experimental high-throughput screening (HTS) of large compound libraries, increasingly provided by combinatorial chemistry, computational methods for virtual screening and *de novo* design have emerged due to the immense enhancement of computational power. Compound libraries with 10^2 to 10^6 structures contain virtual and/or preferentially existing compounds that can either be synthesised in-house or in principle purchased from external sources. The Available Chemical Directory (ACD),[3] the LeadQuest® libraries,[4] and the ChemStar Library[5] etc. have recently been used for *de novo* design and virtual screening approaches.[6-9] Furthermore, diverse and focused library design (for lead optimisation) were applied to improve hit rates from experimental HTS and virtual screening.[10]

Due to low 'drugability' with respect to poor ADMET properties (absorption, distribution, metabolism, excretion, toxicity), not all compounds which can be synthesised or are in present compound libraries are worthy of screening on the targets of interest. Thus, pre-filtering of databases to remove compounds with non drug-like characteristics is frequently accomplished. It has been found that physicochemical and chemical parameters of most drugs fall into certain ranges indicating favourable ADMET behaviour. Lipinski's empirical 'rules of 5' use simple, fast calculable (physico)chemical properties like the molecular weight range, log P range, numbers of H-bond donors,

and numbers of H-bond acceptors to predict the drug-likeness.[2] Thus, filtering of databases with respect to Lipinski's rules should lead to collections of 'drugable' compounds.

In this chapter, based on 'Lipinski-like' filters, we describe the compilation of a library suitable for virtual screening starting from the commercially available ChemACX[11] compound collection. Furthermore, the resulting ChemACXF database, the LeadQuest® libraries Vol. 1&2 and Vol. 1-3 as well as the Accelrys[12] database, all used for *de novo* ligand design approaches (see chapters 3 and 5), were analysed according to a description of property distribution of drug-related databases by Oprea.[13] Additionally, the property analysis for all *de novo* design hits from the LeadQuest® and ChemACXF databases (chapter 3) in comparison to the distribution of the original databases should give insights into the capability of the programme LUDI to extract molecules meeting the LUDI-derived pharmacophore features with similar (physico)chemical properties.

4.2 Results and discussion

4.2.1 Analysis of databases suitable for virtual screening

In principle, molecular databases which are virtually screened for structure-based ligand design should contain commercially available compounds or compounds which are readily synthetically feasible. Additionally, hits from these computational approaches should have physicochemical properties that allow favourable pharmacokinetics as postulated by Lipinski's 'rules of 5'.[2] Therefore, we compiled a virtual screening database starting from the ChemACX collection of commercially available compounds. All entities with a molecular weight between 100 g/mol and 500 g/mol were retained. Additionally, compounds with reactive functional groups were discarded (Figure 4.6). The resulting ChemACXF database (196908 molecules), along with the LeadQuest® libraries Vol. 1&2 (28717 molecules) and Vol. 1-3 (87095 molecules), and the Accelrys database (1063 molecules) were used for virtual screening purposes (see chapter 3). LeadQuest® is a library of drug-like, synthetically feasible screening compounds, which provides an ideal source for the discovery of novel leads in terms of both structural diversity and chemical purity.[6] The aforementioned

databases were analysed with respect to 'Lipinski-like' rules[2,13] to investigate the drug-likeness of screened compounds.

4.2.1.1 Molecular weight

The molecular weight (MW) distribution of all databases is shown in Figure 4.1A. The LeadQuest® and the ChemACXF databases follow a Gaussian distribution, whereas about 60 % of all compounds from the Accelrys database are small molecules with a MW below 150 g/mol, and nearly 97 % below 250 g/mol. In contrast to ChemACXF with a median[§§] around 200 g/mol and about 92 % of the molecular weights below 350 g/mol, the medians of the LeadQuest® databases show a tendency towards increased MW of ca. 320 g/mol for database volumes 1&2 and ca. 400 g/mol for volumes 1-3. In general, the LeadQuest® libraries Vol.1-3 contain larger molecules than libraries Vol. 1&2 and thus, upgrades of LeadQuest® include more compounds with higher molecular weight.

4.2.1.2 Partition coefficient

The distribution of the calculated partition coefficient XLOGP[14] of all database entries is shown in Figure 4.1B. All databases follow a Gaussian-like distribution which is relatively narrow in the case of the Accelrys and the LeadQuest® databases and less steep for LeadQuest® Vol. 1&2 compared to Vol. 1-3 and Accelrys. The ChemACXF database has a broad and shallow distribution. It is notable that its entities span the whole spectrum from very polar compounds (XLOGP = -4.5) to very hydrophobic compounds (XLOGP = 9.5). In contrast to the Accelrys and ChemACXF databases with medians around 1.2 and 1.5, respectively, the LeadQuest® databases have significantly larger medians at XLOGP values of around 3.0-3.5. Comparing both LeadQuest® databases, Vol. 1-3 shows a symmetric, well-balanced XLOGP distribution, whereas Vol. 1&2 is more asymmetric due to the accumulation of very hydrophobic compounds. The analysis of a collection of pharmaceutical compounds from Comprehensive Medicinal Chemistry (CMC)[13] with measured log P values also displays a Gaussian distribution with a median around 1.8. In a comparative study of 15 log P calculation procedures, the XLOGP programme proved to be among the best performing procedures with respect to acceptably predicted log P values and a correlation coefficient *r* of 0.971 for experimental and calculated data.[14]

[§§] A median is defined as the point where the sum of cumulative percentage values reaches 50 % of all database entries.

Table 4.1. Percentage values of compounds within distinct intervals of calculated partition coefficient for investigated databases

Database	Percentage of Compounds with -0.5 < XLOGP ≤ 4.5	Percentage of Compounds with 0.5 < XLOGP ≤ 3.5
LeadQuest® Vol. 1&2	60.5 %	49.1 %
LeadQuest® Vol. 1-3	85.6 %	73.2 %
Accelrys	84.7 %	58.2 %
ChemACXF	71.0 %	47.9 %
CMC[a]	79.0 %	61.0 %

[a] Measured log P values only. Adapted from Oprea et al.[13]

Comparing the percentage of compounds with XLOGP values between 0.5 and 3.5 (Table 4.1), the investigated databases fall into two classes: the LeadQuest® Vol. 1&2 as well as the ChemACXF databases with about 50 % of compounds and the Accelrys as well as the LeadQuest® Vol. 1-3 databases with about 60 % and more compounds in this interval. The fraction of compounds with XLOGP values between 0.5 and 3.5 of the latter databases is in good agreement with the analysis of the CMC and the NCE (New Chemical Entities) collections by Oprea[13] reporting that databases of pharmaceutically active compounds like NCE and CMC consist of more compounds in the 0 to 3 log P range than non-drug databases.

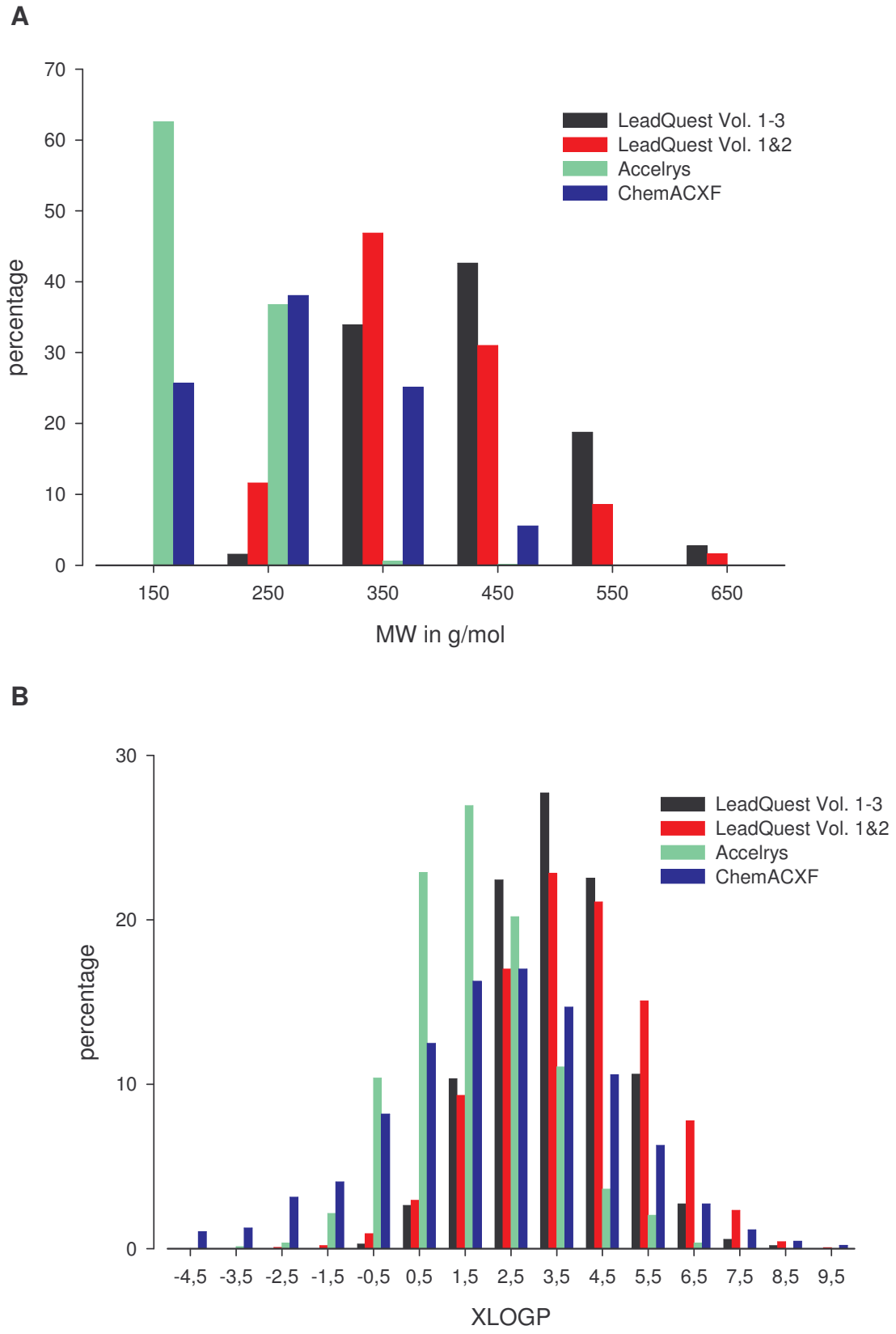

Figure 4.1. Distribution of **A**) molecular weight (MW) and **B**) XLOGP[14] for LeadQuest® libraries Vol. 1&2 and Vol. 1-3, Accelrys, and ChemACXF databases.

4.2.1.3 Number of hydrogen bond acceptors

The distribution of the number of H-bond acceptors n_{acc} is positively skewed in all databases (Figure 4.2A). Both LeadQuest® databases and ChemACXF have similar percentage values. The Accelrys database displays a very steep and narrow distribution with a median between 1 and 2 and with 48 % of the compounds bearing 2 hydrogen bond acceptors. By contrast, the other databases show a broad distribution with up to 12 H-bond acceptors for the ChemACXF database, but all with medians around 3. On average, the entities from the three latter databases have less acceptors than collections of pharmaceutically active compounds or drug collections with averages of 5 or more acceptors.[13,15]

4.2.1.4 Number of hydrogen bond donors

H-bond donors are also asymmetrically distributed with most entries bunched towards low numbers (0 to 2 H-bond donors, Figure 4.2B). All databases show a very similar trend, but only the ChemACXF database contains molecules with up to 9 H-bond donor atoms. Additionally, the ChemACXF database has lower cumulative percentage values than all other databases. Between 60 % (ChemACXF) and almost 80 % (Accelrys, LeadQuest® Vol. 1-3) of the compounds have either 0 or 1 H-bond donors. These results agree well with the analysis of pharmaceutically active compounds or drugs which have up to 3 times more frequently 0 to 2 than 3 to 5 H-bond donor atoms.[13]

4.2.1.5 Number of rotatable bonds

Both LeadQuest® databases follow a positively skewed distribution which is slightly displaced towards higher numbers of rotatable bonds and a median around 5 in the case of Vol. 1-3 whereas the median of Vol. 1&2 is at only 4 rotatable bonds (Figure 4.3A). In principle, the Accelrys and ChemACXF databases are similarly distributed, but they contain more than 50 % and 15 % of all molecules with no rotatable bonds, respectively, and, in comparison to the LeadQuest® databases, also significantly higher percentages of compounds with n_{rot} values of 1 and 2. Thus, molecules of both LeadQuest® databases are more drug-like than entities from the other databases since most drugs and other pharmaceutically active compounds contain more than 5 rotatable bonds.[13]

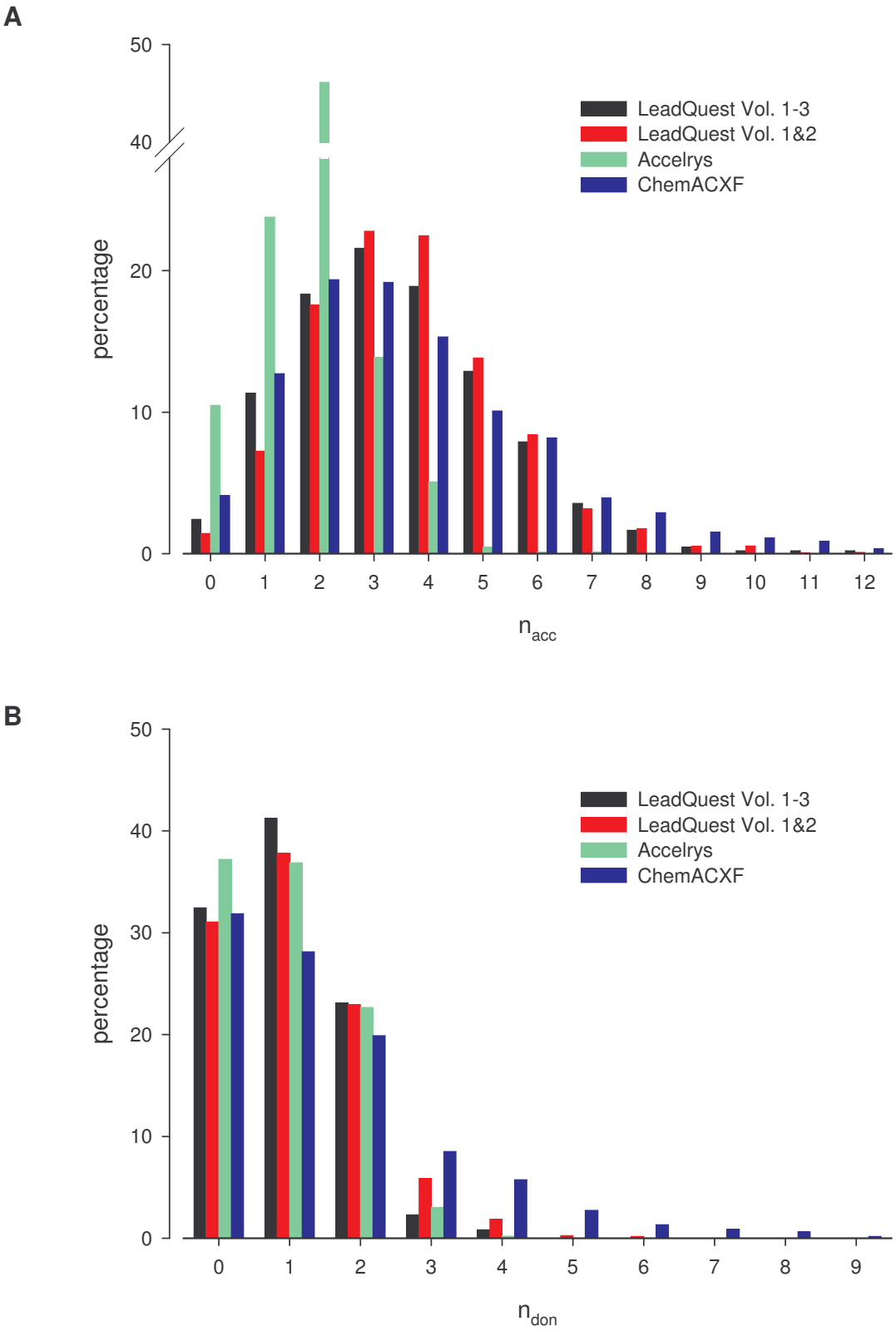

Figure 4.2. Distribution of **A**) number of hydrogen bonding acceptors (n_{acc}) and **B**) number of hydrogen bonding donors (n_{don}) for LeadQuest® libraries Vol. 1&2 and Vol. 1-3, Accelrys, and ChemACXF databases.

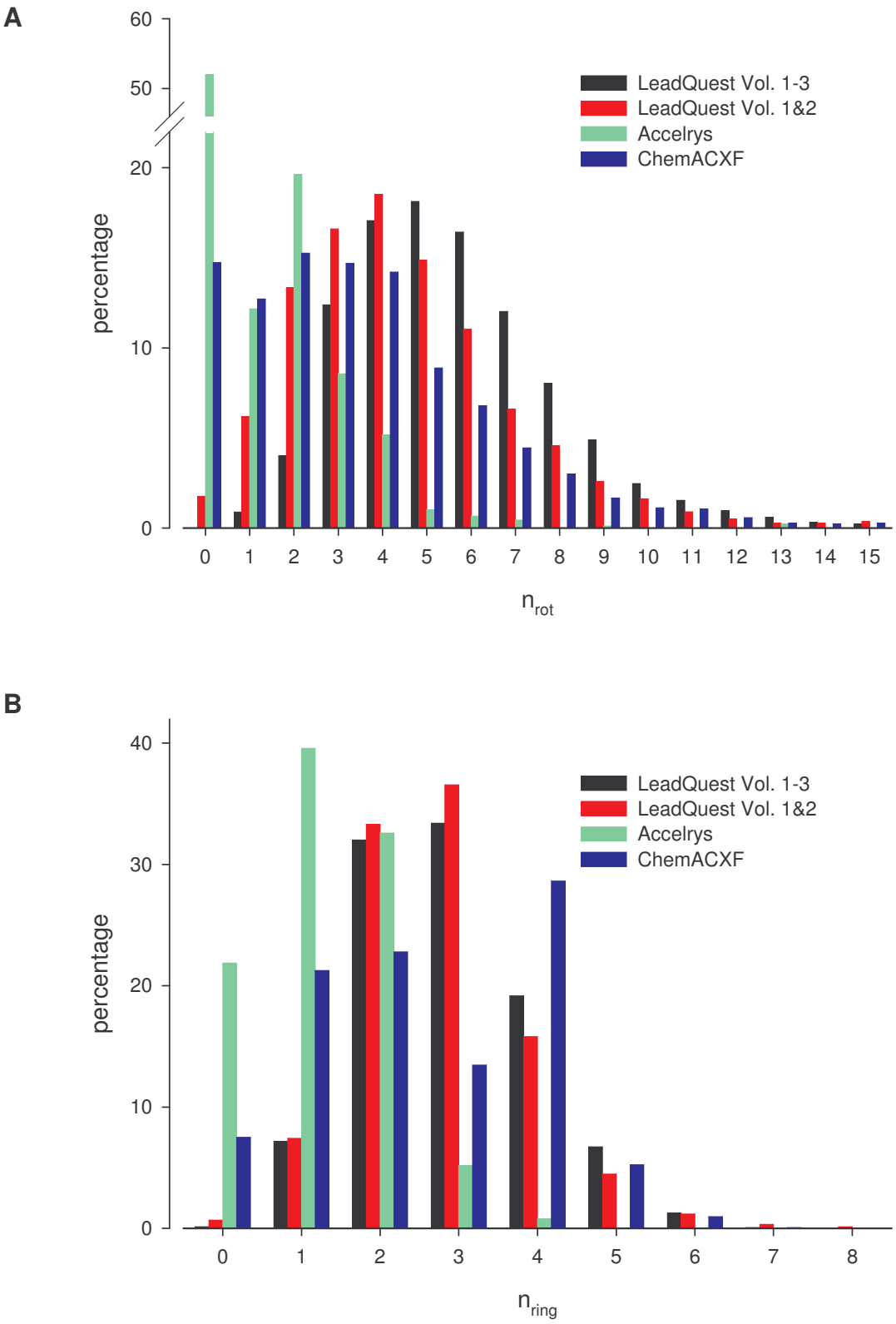

Figure 4.3. Distribution of **A**) number of rotatable bonds (nrot) and **B**) number of rings (nring) for LeadQuest® libraries Vol. 1&2 and Vol. 1-3, Accelrys, and ChemACXF databases.

4.2.1.6 Number of rings

The distribution of the number of rings in the LeadQuest®, Accelrys and ChemACXF databases is illustrated in Figure 4.3B. Both LeadQuest® databases have medians between 2 and 3 rings whereas more than 60 % of the Accelrys entities contain no or just one ring. By contrast, around 80 % of all ChemACXF entities have 1 to 4 rings, nearly uniformly distributed. Drug-like molecules with a medium number of 3 to 5 rings are frequent in the LeadQuest® databases. The ChemACXF database which is partly composed of drug molecules even contains 30 % of compounds with four rings.

4.2.2 Property analysis of hits from LUDI runs

The property analysis of all hits from the LeadQuest® and ChemACXF databases (chapter 3) in comparison to the distribution of the original databases should give insights into the capability of the programme LUDI to accumulate molecules meeting the LUDI-derived pharmacophore with similar (physico)chemical properties including ADMET and 'drugability'. Interestingly, despite significantly different distributions of the original databases, the filtering process of the programme LUDI resulted in very similar distributions. As depicted in Figure 4.4A, the distribution of the molecular weights from both hit lists shows similar fractions of about 50 % for molecules from 150 g/mol to 250 g/mol as well as from 250 g/mol to 350 g/mol, i.e. the distribution of the hit molecules is shifted towards lower molecular weights compared to the medians of the original databases. This result is contrary to other reports where database screening based on 'potential of mean force' (PMF) scoring[16] and DOCK energy scoring[17] has selected compounds with higher molecular weights. Apparently, both scoring schemes are unfavourable in this respect since an advantageous ADMET profile is more likely associated with a lower MW.[18] A probable explanation for our results might be the successive LUDI compound selection procedure. Since energy scoring of the docked compounds is the most time-consuming process, each compound scored has to pass a fast chemo-geometric filter allowing for chemical (H-bond donor/acceptor) as well as geometrical matching which is solely determined by the search radius in the space of the enzyme's active site. Thus, the following rule seems to apply: the smaller the search radius (at best about 5-6 Å, see chapter 3) the lower the molecular weight of the selected compounds.

A similar result was achieved for the XLOGP distribution of both hit lists (Figure 4.4B). They follow a narrower Gaussian-like distribution with slightly higher percentage values compared to the original distributions. Additionally, the median of both distributions is shifted towards 3.5. Apparently, the filtering of the databases by LUDI extracts molecules with relatively similar lipophilicity, i.e. the simple LUDI pharmacophore (H-bond donor/acceptors and lipophilic centres) seems to reflect indispensable properties of the hit molecules leading to a common XLOGP distribution independent of the source of the compounds.

With respect to the number of H-bond donor and acceptor atoms, both hit list distributions are very similar with 80 % of all hits having one donor and around 90 % having one to three acceptors, respectively (data not shown). This result is not surprising since the H-bond donor and H-bond acceptor interaction sites calculated by LUDI are well defined inside the search sphere and are preferentially included in the molecules by the algorithm.

As depicted in Figure 4.5A, even the hit list distributions of the number of rotatable bonds in the molecules show a rather good agreement. Only the percentage of hits with no rotatable bond is significantly higher in the ChemACXF database (ca. 30%). Compared to the original distributions, the entities from both hit lists contain less rotatable bonds. Such more rigid molecules are significantly enriched by the LUDI calculation with cumulative percentage values for up to one rotatable bond of 50 to 55 % for the filtered vs. 9 % (LeadQuest® Vol. 1&2) and 29 % (ChemACXF) for the unfiltered databases. In contrast, the hit list distributions of the number of rings approximately reflect the percentage values of the original databases (Figure 4.5B). It might be suspected that a search sphere of 5-6 Å radius is large enough to ‘accommodate’ molecules with up to four rings which act as spacers bridging the H-bond donor or acceptor functionalities placed at the surface of the search sphere. Thus, the resulting hit list distributions should be directly related to those of the original databases.

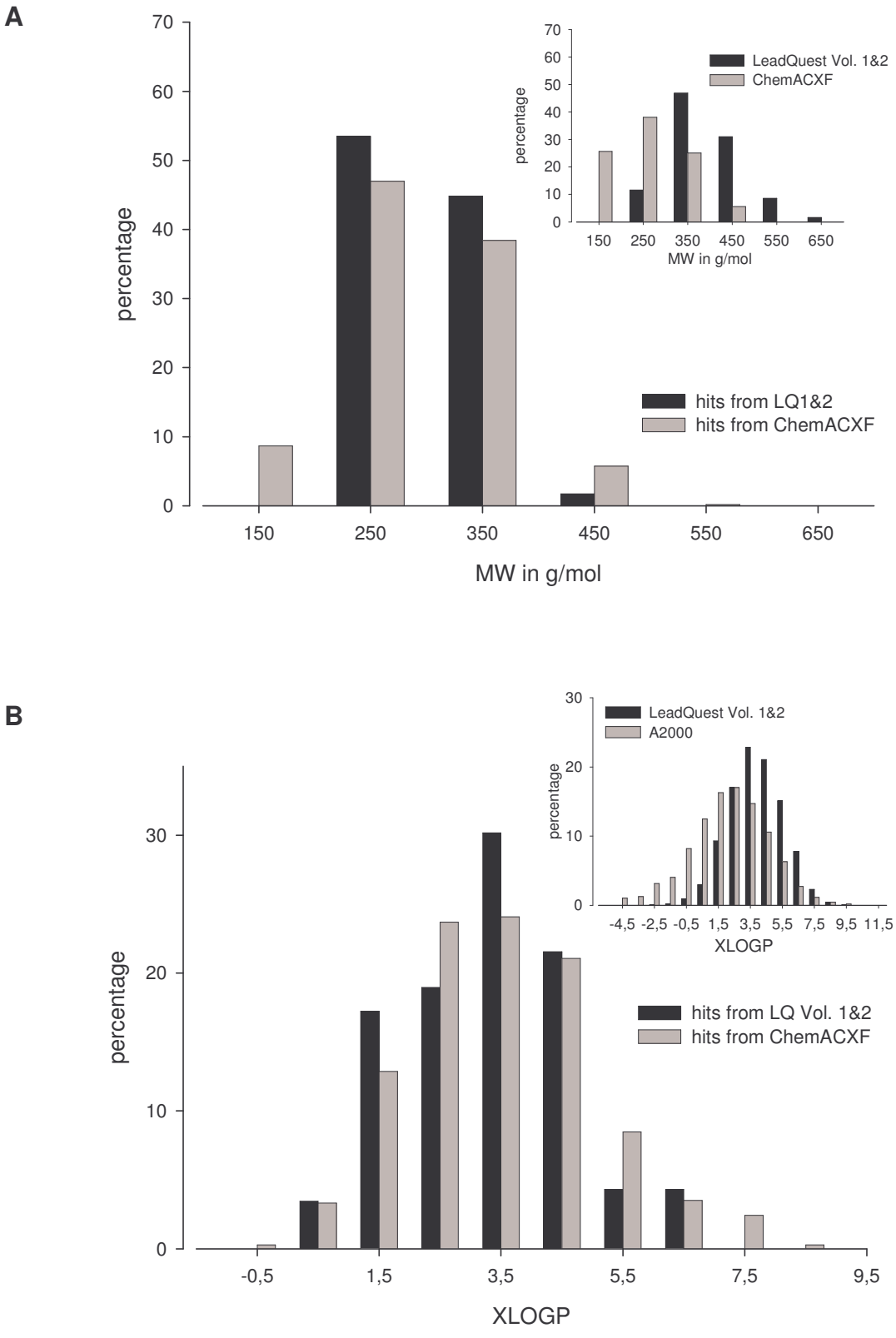

Figure 4.4. Distribution of **A**) molecular weight (MW) and **B**) calculated logP value (XLOGP) for hit lists derived from LeadQuest® database Vol. 1&2 and ChemACXF database. For direct comparison, insets depict the distribution of the unfiltered databases.

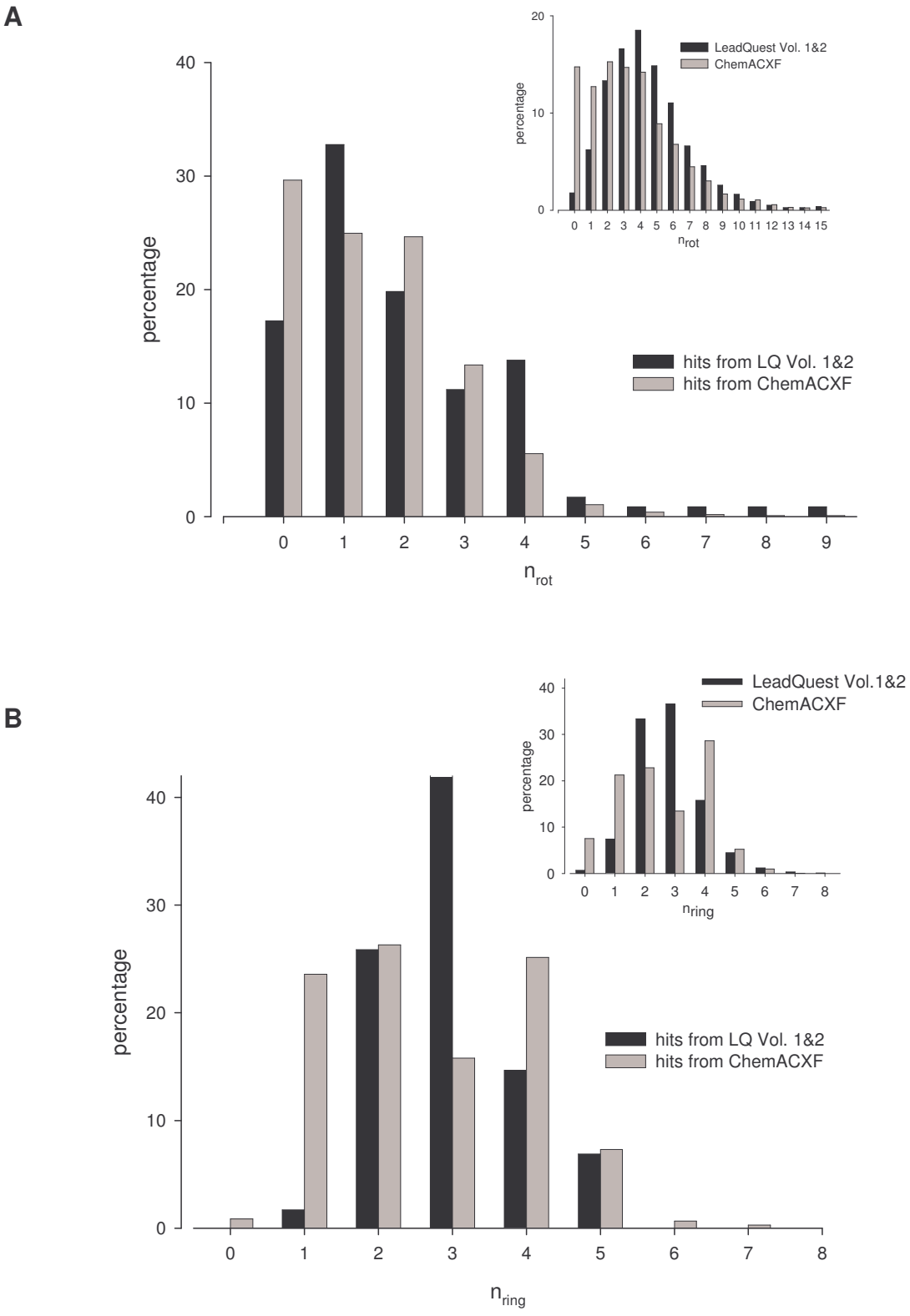

Figure 4.5. Distribution of **A**) number of rotatable bonds (n_{rot}) and **B**) number of rings (n_{ring}) for hit lists derived from LeadQuest® database Vol. 1&2 and ChemACXF database. For direct comparison, insets depict the distribution of the unfiltered databases.

4.3 Conclusions and summary

With respect to drug-likeness, the distribution analysis of six (physico)chemical properties within four different databases revealed that both LeadQuest® databases provide a suitable basis for virtual screening purposes. Obviously, the further development of the LeadQuest® database to Vol. 1-3 led to a compound selection which contains more drug-like molecules than its ancestor with respect to all examined properties except for molecular weight. Furthermore, the rather raw pre-filtering of a compound selection of commercially available molecules, the ChemACX database, by elimination of reactive compounds and of entities outside of a certain molecular weight range resulted in a database with property distributions significantly different from those of the LeadQuest® databases, though the physiochemical space well suited for a virtual screening database is covered. From the perspective of a medicinal chemist this point is of great significance since virtual screening projects may aim at drug molecules or at lead structures. Generally, hits are optimised during the medicinal chemistry phase of a drug development process, but pre-optimisation of leads with respect to 'drugability' is also an appropriate approach.[10] Thus, filtering of screening databases by means of raw (physico)chemical properties adapted from e.g. Lipinski's 'rules of 5´ provides an adequate basis for virtual screening. The property analysis of the hit selections from the LeadQuest® and the ChemACXF database, on the other hand, reflects the screening filter of the programme LUDI (the pharmacophoric properties of the enzyme's binding site), leading to a restricted, allowed pharmacological space represented by typical ranges of molecular weights, log P values, numbers of H-bond donor and acceptor atoms, and numbers of rotatable bonds. These ranges are restricted with respect to the property distributions of the databases which should cover most of the 'potential pharmacological space'.

In conclusion, the property analysis of the databases used for *de novo* design of hyaluronidase inhibitors revealed that the LeadQuest® databases as well as the constructed ChemACXF database are at least comparable to the compound selections of pharmaceutical compounds and provide a robust basis for virtual screening with the programme LUDI.

4.4 Theoretical methods

4.4.1 Preparation of the adapted ChemACX database

The ChemACX database Version 5.5 comprising around 139000 molecules from different compound suppliers was purchased from CambridgeSoft Corporation (Cambridge, MA, USA). It was pre-filtered to remove salts, metals, and isotopes by means of ChemFinder Pro® Version 6.0 (CambridgeSoft Corporation, Cambridge, MA, USA). To eliminate very small molecules, e.g. solvents and rather large compounds, the database was also filtered for molecular weights in the range of 100 g/mol to 500 g/mol. Additionally, compounds with reactive functional groups like acyl halides, sulfonyl halides etc. as adapted from Oprea et al.[13] (see Figure 4.6) were discarded using the substructure search function from ChemDraw Pro® Version 6.0 (CambridgeSoft Corporation, Cambridge, MA, USA). The final adapted ChemACX database consists of around 96000 2D structures. For the sake of clarity, we refer to the adapted ChemACX database as ChemACXF throughout the study.

4.4.2 Processing of databases

The ChemACXF database (96000 structures), the LeadQuest® databases Vol. 1&2 and Vol. 1-3 (ca. 23000 and 60000 molecules, respectively[4]) were converted into 3D using the CONVERTER module from Insight 2000 (Accelrys Inc., San Diego, CA, USA). All-trans conformations of chains and chair conformations of 6-membered rings consisting of only sp^3 atoms were adjusted to allow for energy minimum conformations of the resulting 3D structures. Additionally, two stereoisomers per stereo centre in each molecule were created if existing. By this procedure, 196908, 28717 and 87095 molecules were generated for ChemACXF, LeadQuest® Vol. 1&2 and Vol. 1-3 databases, respectively. The resulting databases were converted into the respective input file formats with the SYBYL module DBTRANSLATE as required by the subsequently used software, e.g. LUDI or X-Score.

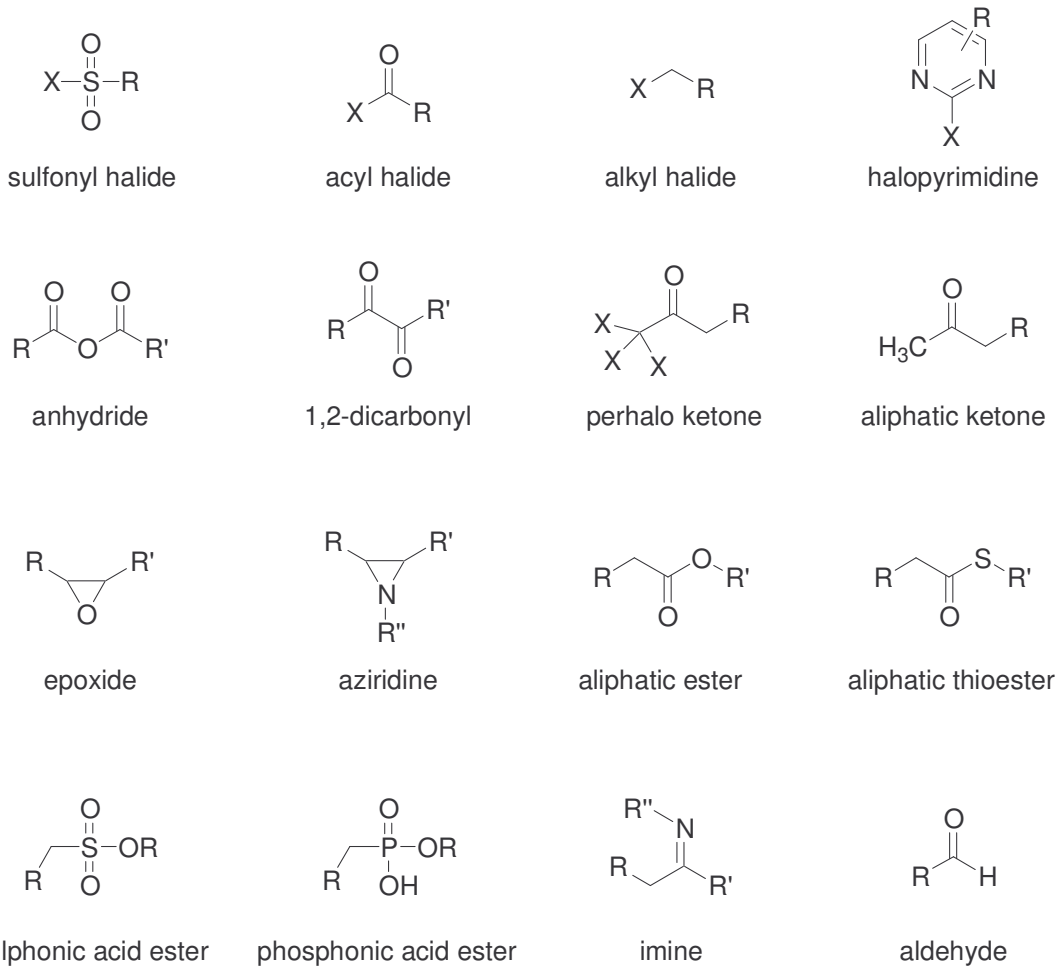

Figure 4.6. Molecules with reactive functional groups removed from the ChemACX Database V5.5. Modified from Oprea et al.[13]

4.4.3 Descriptor analysis of databases

The 3D versions of the ChemACXF database, the LeadQuest® databases Vol. 1&2 and Vol. 1-3, and the Accelrys database as supplied in the LUDI module as well as the hit lists from the LeadQuest® database Vol. 1&2 and the ChemACXF database were analysed with respect to properties described by molecular connectivity following an approach described by Oprea et al.[13] Estimates of molecular weights, XLOGP,[14] number of rings, hydrogen bond donors, hydrogen bond acceptors, and number of rotatable bonds were performed using a personally adapted version of the X-Score[19] programme. The number of rings (n_{ring}) is evaluated using a bond-based algorithm.[19] The numbers of hydrogen bond donors (n_{don}) and acceptors (n_{acc}) are calculated on the basis of a look-up table of adapted Tripos atom types involved in hydrogen bonding that includes only nitrogen and oxygen atoms. Other donors, such as thiols, or acceptor atoms, such as halides, are ignored. Both variables are counted

separately, i.e. an O-H group can be both donor and acceptor. The number of rotors (n_{rot}) implies acyclic sp^3-sp^3 or sp^3-sp^2 single bonds between two non-hydrogen atoms. In contrast to the originally implemented determination of n_{rot}, sp^2-sp^2 rotors were included in the statistical analysis since the original programme neglects these rotors due to its rotor definition.[19]

Property distributions were analysed by adding a module to the original X-Score code. This routine performs a histogram-type of analysis on large numbers of data, in a manner that can be user-defined (with respect to, e.g., the bin size). It counts the number of data points between the current bin and the adjoining higher bin. A value is counted in a particular bin if it is equal to, or less than the bin value down to the last bin limit. For integer variables (e.g., n_{rot}, n_{ring}), results are displayed for the corresponding values (bin counts for that particular integer value). A median is defined as the point where the sum of cumulative percentage values reaches 50 % of all database entries. The data transformation and visualisation was done with Sigma Plot 8.0 (SPSS Inc., Illinois, USA).

4.5 References

(1) Kubinyi, H. Strategies and recent technologies in drug discovery. *Pharmazie* **1995***, 50*, 647-662.

(2) Lipinski, C. A.; Lombardo, F.; Dominy, B. W.; Feeney, P. J. Experimental and computational approaches to estimate solubility and permeability in drug discovery and development settings. *Adv Drug Deliv Rev* **1997***, 23*, 3-25.

(3) www.mdli.com; Available Chemical Directory.

(4) Tripos LEADQUEST Chemical Compounds Libraries. *http://www.tripos.com* **1998**.

(5) www.chemstar.ru; ChemStar Ltd.

(6) Grüneberg, S.; Wendt, B.; Klebe, G. Subnanomolar Inhibitors from Computer Screening: A Model Study Using Human Carbonic Anhydrase II. *Angew Chem Int Ed Engl* **2001***, 40*, 389-393.

(7) Grüneberg, S.; Stubbs, M. T.; Klebe, G. Successful virtual screening for novel inhibitors of human carbonic anhydrase: strategy and experimental confirmation. *J Med Chem* **2002***, 45*, 3588-3602.

(8) Brenk, R.; Naerum, L.; Grädler, U.; Gerber, H. D.; Garcia, G. A. et al. Virtual screening for submicromolar leads of tRNA-guanine transglycosylase based on a new unexpected binding mode detected by crystal structure analysis. *J Med Chem* **2003***, 46*, 1133-1143.

(9) Grädler, U.; Gerber, H. D.; Goodenough-Lashua, D. M.; Garcia, G. A.; Ficner, R. et al. A new target for shigellosis: rational design and crystallographic studies of inhibitors of tRNA-guanine transglycosylase. *J Mol Biol* **2001***, 306*, 455-467.

(10) Charifson, P. S.; Walters, W. P. Filtering databases and chemical libraries. *J Comput Aided Mol Des* **2002***, 16*, 311-323.

(11) www.cambridgesoft.com; CambridgeSoft Cooperation.

(12) www.accelrys.com; Accelrys Inc.

(13) Oprea, T. I. Property distribution of drug-related chemical databases. *J Comput Aided Mol Des* **2000***, 14*, 251-264.

(14) Wang, R.; Gao, Y.; Lai, L. Calculating partition coefficient by atom-additive method. *Perspectives in Drug Discovery and Design* **2000***, 19*, 47-66.

(15) Feher, M.; Schmidt, J. M. Property distributions: differences between drugs, natural products, and molecules from combinatorial chemistry. *J Chem Inf Comput Sci* **2003***, 43*, 218-227.

(16) Muegge, I.; Martin, Y. C.; Hajduk, P. J.; Fesik, S. W. Evaluation of PMF scoring in docking weak ligands to the FK506 binding protein. *J Med Chem* **1999***, 42*, 2498-2503.

(17) Pan, Y.; Huang, N.; Cho, S.; MacKerell, A. D., Jr. Consideration of molecular weight during compound selection in virtual target-based database screening. *J Chem Inf Comput Sci* **2003***, 43*, 267-272.

(18) Lipinski, C. A.; Lombardo, F.; Dominy, B. W.; Feeney, P. J. Experimental and computational approaches to estimate solubility and permeability in drug discovery and development settings. *Adv Drug Deliv Rev* **2001***, 46*, 3-26.

(19) Wang, R.; Lai, L.; Wang, S. Further development and validation of empirical scoring functions for structure-based binding affinity prediction. *J Comput Aided Mol Des* **2002***, 16*, 11-26.

Chapter 5 Homology modelling of bovine testicular hyaluronidase and de novo design of ligands of bovine testicular hyaluronidase

5.1 Introduction

Computer aided drug design (CADD) has evolved into a substantial part of the drug discovery process over the last three decades. Nowadays, the application of CADD approaches accelerates the discovery of new lead compounds and their structural optimisation with respect to affinity and pharmacological properties (see chapter 3). The computer methods are developed to predict interactions between small organic compounds and macromolecular targets, mainly proteins and nucleic acids. In general, the kind of approach depends on the availability of a three-dimensional (3D) structure of the biological target. If present, structure-based design is possible, otherwise only ligand-based design methods may be applied.[1]

Structure-based approaches are to design compounds which spatially fit to a binding site of the macromolecule by forming electrostatic, steric and hydrophobic interactions. Two general cases of searching for such biologically active molecules may be discriminated: virtual screening (molecular database mining) and *de novo* ligand design combined with fast automated docking. Prerequisite of all virtual screening methods is the detailed knowledge about the localisation and the geometry of the binding site, mostly deduced from X-ray structures with co-crystallised natural substrates or synthetic organic ligands. All screening and *de novo* design programmes like CAVEAT,[2] TOPAS,[3] LeapFrog,[4] LUDI[5] etc. derive a complex pharmacophore which accounts for specific steric and electrostatic interactions, hydrogen bond formation and other factors relevant for ligand-protein binding. A large database of small organic, mostly drug-like molecules is screened to retrieve compounds meeting the pharmacophoric features. The predicted binding affinities of suitable candidates are ranked by an integrated scoring function for subsequent compound selection. In many cases, these approaches are accompanied by fast automated post-docking using FlexX,[6] AutoDock,[7] and DOCK[8] etc.[9]

Ligand-based methods are applied if no structural information about the target and its ligand binding site, i.e. no crystal structure or no reliable homology model, is available. Based on the analysis of ligands with known biological activity, these methods include the design of pharmacophoric models[10] by, e.g., the active analogue approach[11], the analysis of quantitative structure-activity relationships (classical QSAR) and 3D-QSAR.[12] Also pseudoreceptor models for screening are employed to discover lead compounds and/or to optimise known ligands.[1]

For the design of mammalian hyaluronidase inhibitors, a structure-based strategy could be applied. A homology model of bovine testicular hyaluronidase (BTH) derived from crystal structures of the bee venom hyaluronidase[13] as templates was accomplished with the help of the programme MODELLER.[14-16] The bovine enzyme shows a satisfying sequence identity of ca. 30 % with respect to the bee hyaluronidase. Subsequently, potential BTH inhibitors were generated by the *de novo* design software LUDI.[5,17] Additionally, an 'active analogue-like' approach was applied for the design of BTH ligands starting from the superposition of the BTH binding site with similar sites of related chitinases in complex with their inhibitors.

5.2 Results and discussion

5.2.1 Homology modelling of bovine testicular hyaluronidase

Homology modelling of BTH was the prerequisite for structure-based ligand design of mammalian hyaluronidase inhibitors. In consideration of the low, but significant amino acid sequence identity between insect and mammalian hyaluronidases, the crystal structure of bee venom hyaluronidase[13] has provided the first possibility to construct reliable homology models of mammalian hyaluronidases like BTH.

The homology modelling of BTH with MODELLER was based on a multiple sequence alignment of BTH and two templates, the human PH-20 protein and the bee venom hyaluronidase (see chapter 6), using ClustalW.[18] Subsequently, a fully automated construction of a template-fitting BTH model was performed by MODELLER version 6.2.[14-16] The resulting structure was evaluated for correct local geometry and completed by addition of hydrogen atoms and energy minimisation (for more details see chapter 6). A schematic representation of the homology model of BTH is presented in Figure 5.1. Both catalytic residues Asp147 and Glu149 are located in the centre of

the wide HA binding crevice crossing the whole enzyme (yellow bow). Thus, both amino acids are rather solvent-exposed.

5.2.2 Search for molecular fragments as bovine hyaluronidase inhibitors using the computer programme LUDI

With the help of the *de novo* design programme LUDI, small and fairly rigid molecules were retrieved from the 3D structure databases LeadQuest® Vol. 1-3[4] and ChemACXF (see chapter 3) by docking into the binding site of the homology model of BTH. LUDI estimates the expected binding affinity for each successfully docked ligand by an empirical scoring function.[19] Using standard parameters for LUDI calculations, all 3D structures are treated as rigid bodies independent of the presence of rotatable bonds.

The ligand-binding region of the enzyme where interactions are considered is represented by a sphere with a selectable radius. Based on a superposition of all Cα-atoms of the BTH homology model with the corresponding atoms of the crystal structure of bee venom hyaluronidase in complex with a hyaluronan (HA) tetrasaccharide fragment, the centre of the search sphere was defined by the coordinates of the carbon C3 of the *N*-acetylglucosamine monomer at the reducing end of the substrate. For all functional groups of the enzyme exposed to the binding region within a sphere radius of 6 Å, putative interaction sites in space were generated by LUDI according to rules which have been derived from composite crystal-field environments compiled with appropriate small molecule crystal data (Cambridge Structural Database).[17] The programme tries to fit each database molecule onto these interaction sites.

The most important amino acids within the search sphere of BTH and the pre-calculated interaction sites are shown in Figure 5.2. Next to both catalytic residues, the HA binding site is rather open and is dominated by several hydrophobic amino acids. The subsite[***] -1 for the *N*-acetylglucosamine residue forms a small pocket defined by the tyrosines Tyr220, Tyr265 and Tyr305 as well as the tryptophan Trp341. The attached subsite -2 for glucuronic acid is constituted by Tyr93 at the bottom as well as by Trp341 and Leu344 on either side. The LUDI H-bond acceptor interaction sites in

[***] By convention, the sugar residue subsites are labelled from *-n* to *+n*, with *-n* at the non-reducing end and *+n* at the reducing end of the substrate. Cleavage occurs between the -1 and +1 subsites.[20]

the upper left part of Figure 5.2 reflect the backbone NH-group of Leu344 which interacts with the carboxylic group of glucuronic acid.

For the LUDI calculations, an accurate treatment of the protonation states of all residues inside the active site is important. Since both catalytic residues Asp147 and Glu149 are solvent-exposed, two different protonation patterns seemed to be possible *a priori*. In the crystal structure of BVH, the corresponding aspartate and glutamate side chains (Asp111 and Glu113) are in close proximity – independent of an acidic or neutral pH used for crystallisation[13] – forming a short hydrogen bond between both carboxylates. Therefore, Asp147 was always protonated in virtual screening runs. Glu149 probably acts as the proton donor during HA hydrolysis.[13] This switching implies that Glu149 must be treated in both protonisation states in different LUDI approaches.

Performing LUDI runs with the constructed LeadQuest® database Vol. 1-3 resulted in 257 and 175 hits with charged and uncharged Glu149, respectively, ranked on a relative scale by their expected binding affinity according to the scoring function described by Böhm.[19] The numbers of hits retrieved from the ChemACXF database were 4030 (Glu149 charged) and 1339 (Glu149 uncharged). Five of the proposed hits were selected for testing hyaluronidase inhibition according to high LUDI scores, availability and efficient synthetic feasibility.

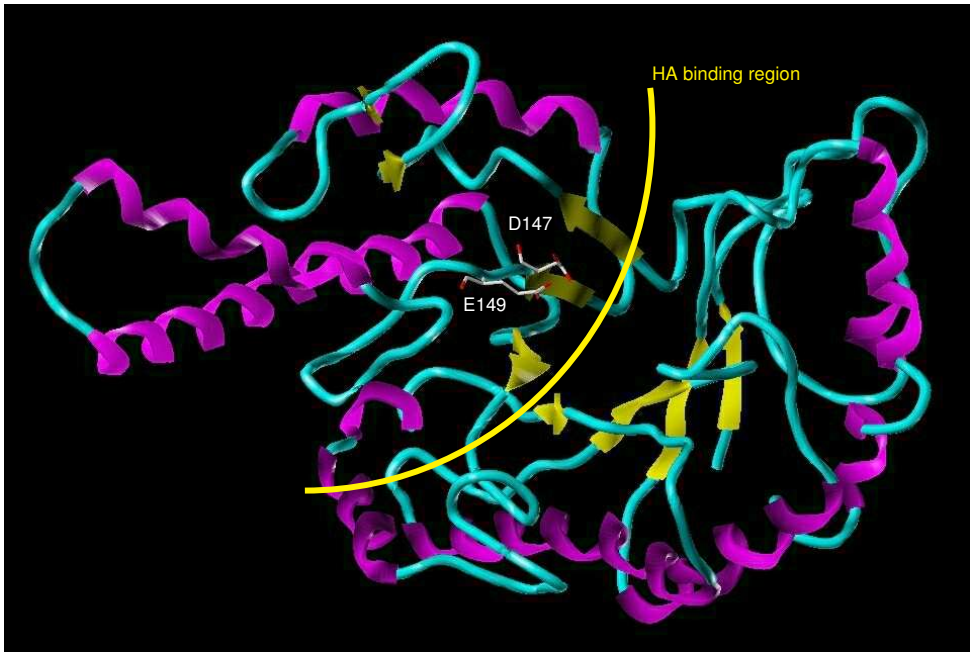

Figure 5.1. Schematic representation of the BTH model. α-helices and β-sheets are depicted in purple and yellow, respectively. The hyaluronan binding region and both catalytic residues are shown explicitly.

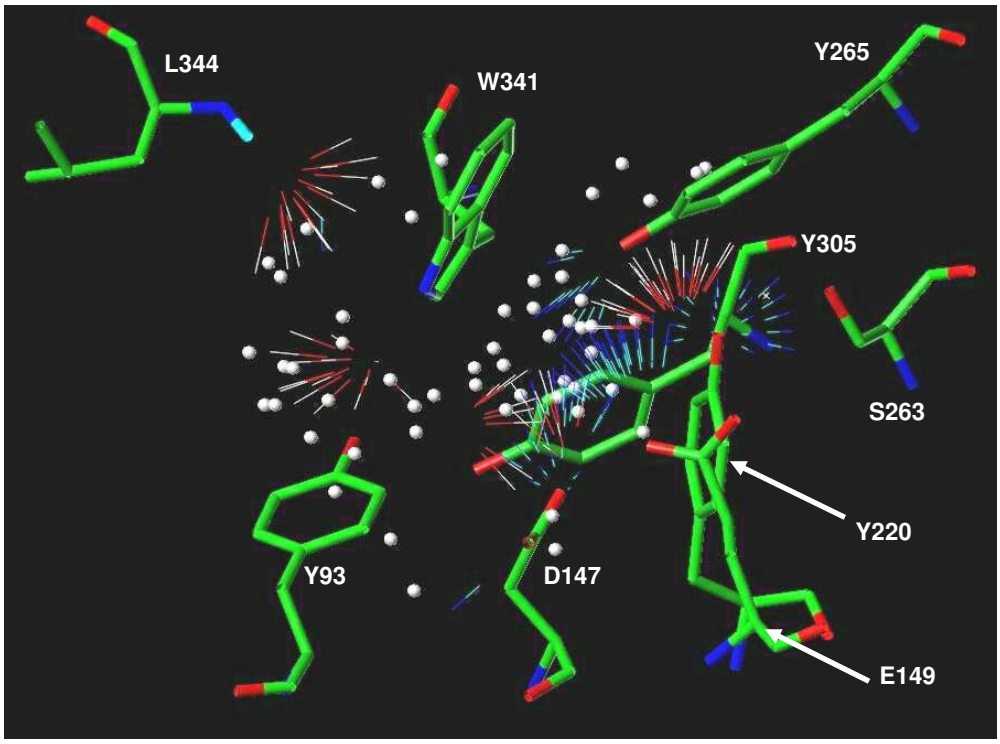

Figure 5.2. Interaction sites generated by LUDI with a sphere radius of 6 Å inside the active site of the BTH model (white, lipophilic sites; red, hydrogen bond acceptors, blue, hydrogen bond donors).

As shown in Table 5.1, none of the investigated compounds induced an inhibition of BTH except compound **4**, which displayed with very weak partial inhibitory activity of the enzyme (by 10 % at maximal test concentration). All compounds were also investigated for their inhibitory potencies on $hylB_{4755}$. Surprisingly, compounds **1**, **2** and **5** partially inhibited the activity of this bacterial hyaluronidase. The results for the first two structures were the starting point of an extended investigation of substituted indoles and indolines as hyaluronate lyase inhibitors which led to the identification of several indole derivatives with inhibitory activities on $hylB_{4755}$ in the lower micromolar concentration range.[21]

In general, most of the investigated compounds were poorly soluble, thus complicating the identification of BTH inhibitors since lead compounds are commonly active only in the submillimolar to millimolar concentration range. Additionally, not all of the potential H-bond acceptor and H-bond donor interaction sites present in the search sphere inside the active site of BTH are adopted by the hits. Most of the compounds selected by LUDI are rather lipophilic, i.e. their lipophilic score fractions clearly dominate their total scores. Also very few of the proposed molecules dunk into the pocket of subsite -1 and, simultaneously, form hydrogen bonds with the catalytic residues as well as with Leu344 (data not shown). Thus, the probably most important and

specific interactions of the amphiphilic HA substrate in the bee venom hyaluronidase complex[13,22] are not reproduced by the majority of the hits. In general, the probablility of finding leads ranges from 1 per mill to 1 % depending on the target of interest. In many cases, the virtual screening approach significantly increases the hit rate, but still a substantial number of compounds has to be screened for biological activtiy. Thus, due to statistical reasons, more than only five compounds should have been investigated for inhibitory activity on BTH.

Therefore, the results from the LUDI calculations will be used only to further optimise compounds for $hylB_{4755}$ inhibition. For BTH inhibitors, an alternative ligand-based approach is presented in the next section.

Table 5.1. Inhibitory activities of selected compounds on BTH and $hylB_{4755}$.

No	Structure	BTH (% inhibition)[a] pH 5.0	$hylB_{4755}$ (% inhibition)[a] pH 5.0
1	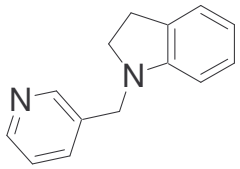	inactive (≤ 3 mM)	37 % (3 mM)
2	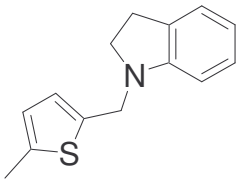	inactive (≤ 200 µM)	30 % (200 µM)
3	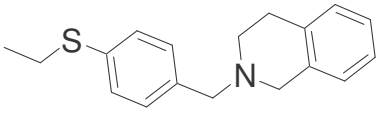	inactive (≤ 4.5 mM)	50 % (4.5 mM)
4	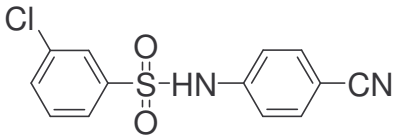	10 % (400 µM)	30 % (400 µM)
5	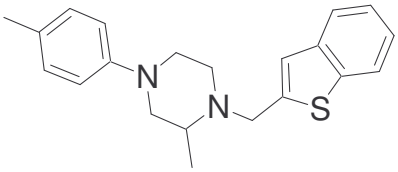	inactive (≤ 1.6 mM)	25 % (1.6 mM)

[a] % inhibition of enzyme at indicated inhibitor concentration (n=3; error not larger than 1 %)

In addition, all compounds which had been selected as inhibitors of *S. agalactiae* strain 4755 hyaluronidase from the LUDI approaches described in chapter 3 were tested for BTH inhibition. Among these $hylB_{4755}$ hits, three compounds proved to be moderate to good inhibitors of the bovine testicular hyaluronidase. 1-Furan-2-yl-3-(4-nitrophenyl)propenone (**6**) and indole-2-carboxylic acid (**7**) induced a concentration-dependent inhibition with an IC_{50} value of 4 mM and 7 mM, respectively. The most active compound of this set was 1,3-diacetylbenzimidazole-2-thione (**8**) which inhibited the BTH activity with an IC_{50} value of 250 µM.[23] This result prompted us to further investigate derivatives of **8**[23] as well as compounds **9** and **10** which were re-

trieved as BTH hits from the ChemACXF database by LUDI. These investigations are part of ongoing work.

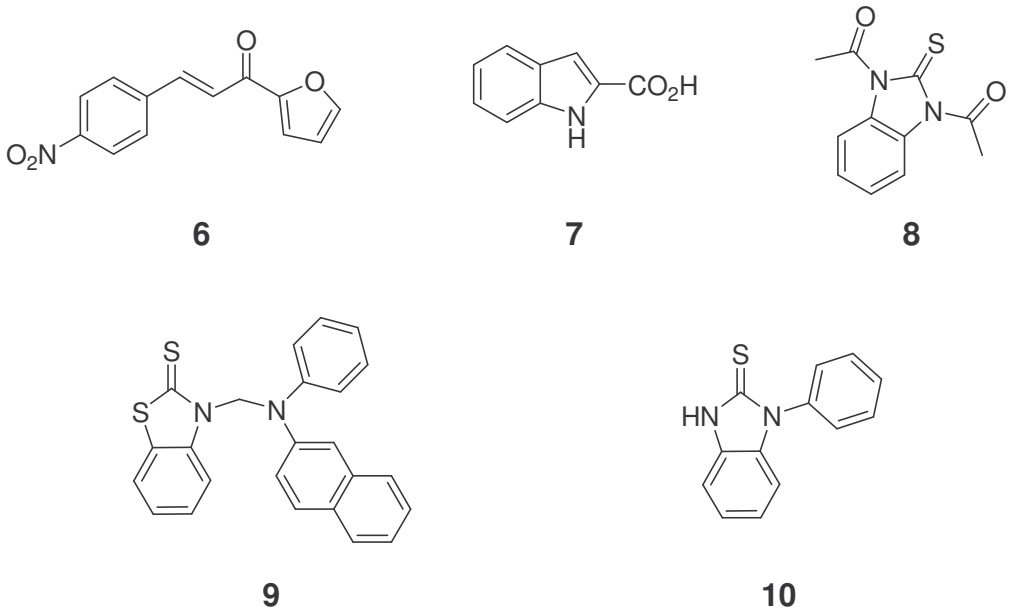

6 **7** **8**

9 **10**

Figure 5.3. Chemical structures of BTH inhibitors **6**-**8** identified by LUDI calculations on $hylB_{4755}$[23] and BTH hits **9** and **10** from the ChemACXF database.

5.2.3 Ligand-based design of inhibitors of bovine testicular hyaluronidase

Elucidation of the crystal structure of bee venom hyaluronidase revealed an unusual fold of an open 7-stranded (β/α)-barrel. By using the DALI server (http://www.ebi.ac.uk/dali/) for the detection of similarly folded proteins, the crystal structure of the bacterial chitinase A (ChiA) from *Serratia marcescens* (pdb code: 1ctn) was identified.[13] The active sites of both enzymes are closely related. Recently, the crystal structure of chitinase A in complex with the inhibitor allosamidin (**11**) could be elucidated.[24] Allosamidin is produced by *Streptomyces sp.*[25] and consists of two β-1,4-linked *N*-acetylallosamine rings and one allosamizoline (an oxazoline derivative). The allosamizoline part of the inhibitor binds to the subsite -1 of the chitin binding site[24] – equivalent to subsite -1 of the hyaluronan binding site at mammalian hyaluronidases – and probably mimics the covalent intermediate **12** of the *N*-acetylglucosamine residue (Figure 5.4) during hydrolysis like suggested for several chitinases.[26-28]

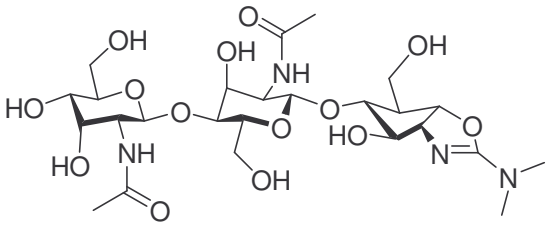

allosamidine (**11**)

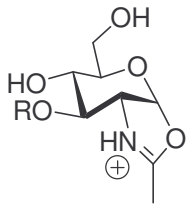

proposed hydrolysis intermediate **12**

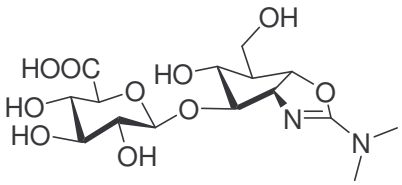

13

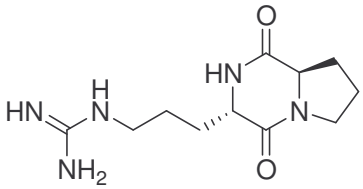

Cl-4 (**14**)

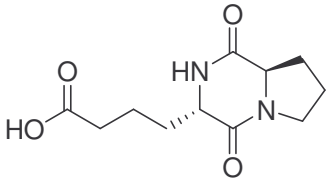

15

Figure 5.4. Chemical structures of chitinase inhibitor allosamidin (**11**), the proposed hydrolysis intermediate of *N*-acetylglucosamine residue **12**, the derived BTH inhibitor **13** and chitinase B (ChiB) inhibitor CI-4 (**14**) as well as the suggested BTH inhibitor **15**.

The five equivalent amino acids of the active sites of the BTH model, the crystal structure of bee venom hyaluronidase in complex with a HA tetrasaccharide fragment (pdb code: 1fcv), and the X-ray structure of chitinase A complexed with allosamidin (pdb code: 1ffq) are closely superimposed (see Figure 5.5A). Surprisingly, the *N*-acetylglucosamine residue of HA also overlaps with the allosamizoline moiety of the chitinase inhibitor. The 3-hydroxy group of allosamizoline aligns with the anomeric oxygen of D-glucuronic acid (Figure 5.5B). Therefore, with respect to hyaluronidase inhibitor design, a substitution in position 3 of allosamizoline with β-D-glucuronic acid (comparable to its position found in the HA tetrasaccharide fragment) is suggested. The topology of compound **13** (Figure 5.4) combining an allosamizoline moiety, proposed to mimic a catalytic intermediate, with glucuronic acid is compatible with binding to bee venom hyaluronidase and probably also to BTH (Figure 5.5B).

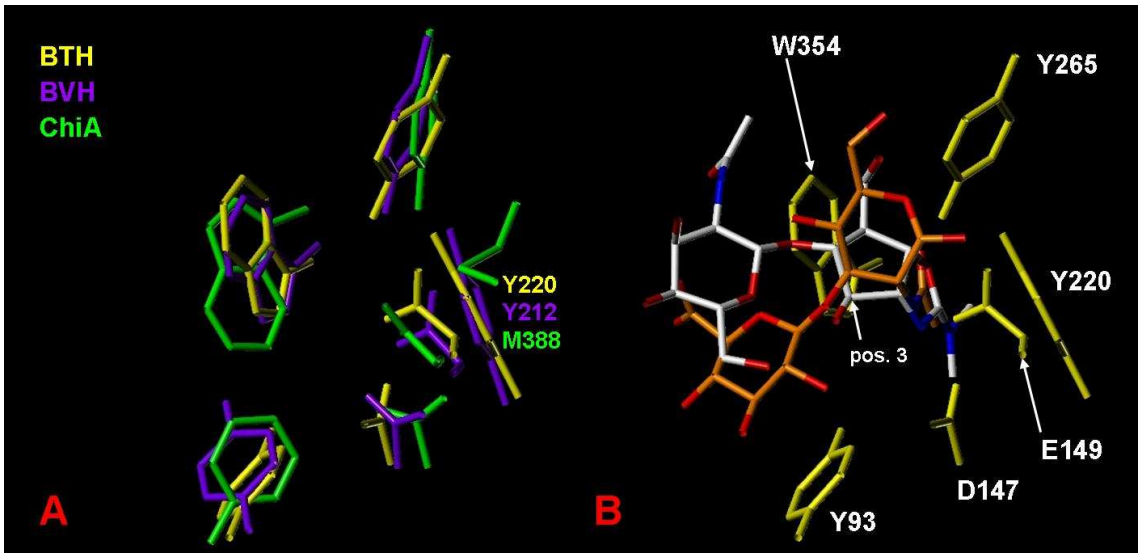

Figure 5.5. A) Superposition of active site residues of BTH model (yellow), BVH crystal structure (purple) and ChiA crystal structure as specified in section 5.4.4. The amino acid Tyr220 (BTH) and its equivalents Tyr184 (BVH) and Met388 (ChiA) are shown additionally but were not included in the superposition procedure. **B)** Overlap of corresponding fragments of HA (C atoms coloured in orange, O atoms coloured in red) and allosamidin (coloured by atom types) as resulting from the superposition in Figure 5.5A. As reference, active site residues of BTH model are shown in yellow. For sake of clarity, not all parts of the co-crystallised ligands are depicted.

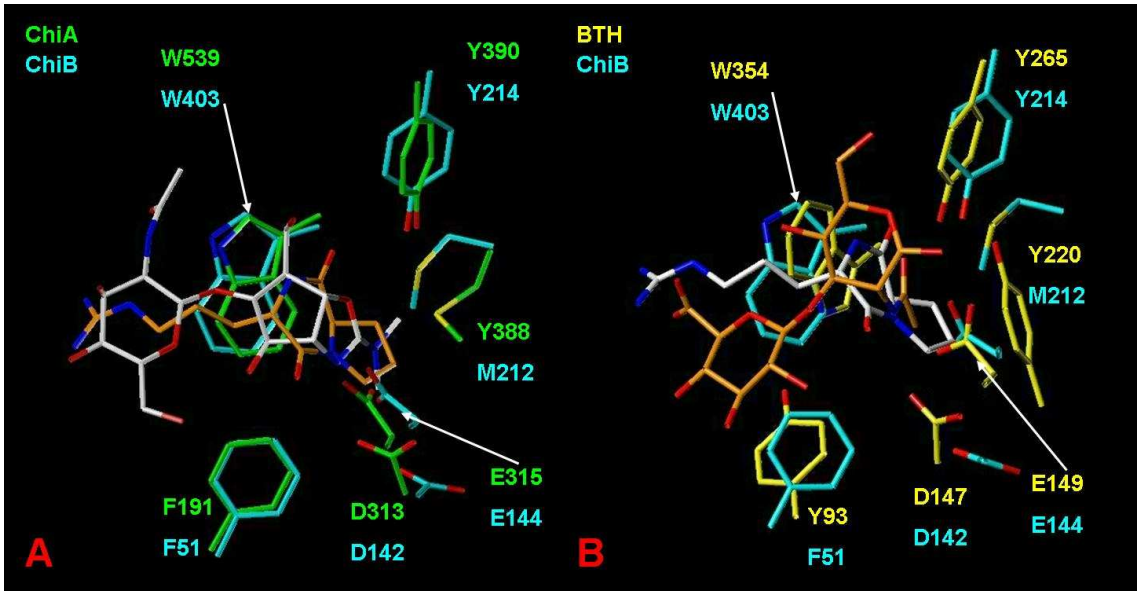

Figure 5.6. A) Superposition of active site residues of ChiA (green) and ChiB (cyan) crystal structures with complexed allosamidin (C atoms grey, other atoms by atom type) and CI-4 (C atoms orange, other atoms by atom type), respectively. **B)** Superposition of active site residues of BTH model (yellow) and ChiB crystal structure with complexed CI-4 (atoms by atom type). HA disaccharide fragment (C atoms orange, O atoms red) was extracted from the BVH-HA complex with coordinates from superposition of the active sites of BTH, BVH and ChiB.

Extensive investigations of various allosamidin derivatives as chitinase A inhibitors revealed that allosamizoline itself is only a moderate inhibitor with an IC_{50} value of ca. 0.2 mM[29] despite its good fit into the pocket of subsite -1 in the complex of ChiA with allosamidin.[24] Additionally, an allosamidin derivative truncated by one sugar unit proved to be almost as potent as allosamidin itself.[29] Due to the highly similar active site, allosamizoline should inhibit BTH too, but also in this case with low potency in the submillimolar concentration range. Consequently, compound **13** might fulfil structural conditions necessary for inhibitory activity on BTH at micromolar concentration.

Recently, the cyclic dipeptide CI-4 [**14**, cyclo-(L-Arg-D-Pro)], identified to weakly inhibit chitinase B (ChiB) from *Serratia marcescens*,[30] has been co-crystallised with this enzyme.[31] After superposition of the active site residues of ChiA and ChiB, the cyclic CI-4 dipeptide backbone is situated in the same hydrophobic pocket (subsite -1) as the allosamizoline moiety of allosamidin (Figure 5.6A). Additionally, the arginine side chain fits to the same region like the *N*-acetylallosamine substructure in ChiA and like the D-glucuronic acid monomer in subsite -2 of BVH (Figure 5.6A,B).

Based on the superposition of CI-4 and the HA disaccharide fragment (Figure 5.6B), compound **15**, a cyclic peptide composed of D-proline and L-2-aminoadipic acid, is proposed. The cyclic dipeptide backbone of **15** might structurally mimic the aforementioned intermediate and might similarly interact with Tyr265 and Glu149 as suggested for CI-4 with the corresponding amino acids Tyr214 and Glu144 of ChiB.[31] The arginine side chain of CI-4 is not involved in direct interactions with amino acids of the active site of ChiB[31] and may therefore be exchanged by other, more suitable moieties. Since the guanidine of CI-4 aligns with the carboxylic group of D-glucuronic acid of the HA disaccharide fragment (Figure 5.6B), arginine may be well replaced by L-2-aminoadipic acid. In conclusion, compound **15** is expected to be a potent inhibitor of BTH due to putative interactions derived from HA.

5.3 Summary

A homology model of bovine testicular hyaluronidase based on crystal structures of bee venom hyaluronidase was constructed with the help of MODELLER and used for *de novo* design of BTH inhibitors with the programme LUDI. Filtering of the Lead-

Quest® databases Vol. 1-3 and the ChemACXF database resulted in more than 5500 hits. According to high LUDI scores, availability and synthetic feasibility, five compounds were selected for testing hyaluronidase inhibition. Unfortunately, none of the compounds inhibited BTH, probably due to their poor solubility.

To possibly overcome this failure a search for less lipophilic compounds was performed by an additional, ligand-based approach. The superposition of the active sites of the BTH model with the crystal structures of bee venom hyaluronidase and the chitinases A and B revealed a very good overlap of the amino acids involved in catalysis and of the co-crystallised ligands (HA tetrasaccharide fragment, allosamidin and CI-4). By considering essential substructures mimicking the proposed intermediate of HA hydrolysis and by introducing suitable substituents suggested to interact with amino acid of the active site, compounds **13** and **15** were proposed as potential BTH inhibitors. The synthesis and biochemical investigations of these compounds are part of ongoing work.

5.4 Theoretical methods

All calculations were done on a SGI OCTANE R10000 workstation.

5.4.1 BTH model construction

The homology modelling of bovine testicular hyaluronidase (BTH) is described in detail in chapter 6.

5.4.2 LUDI calculations with the BTH model

A LUDI approach was set up with a sphere of 6 Å radius in the space of the active site of the BTH model. To determine the centre of this sphere, the BTH model and the crystal structure of bee venom hyaluronidase in complex with a HA fragment (pdb code: 1fcv) were superimposed by using the Cα-atoms of corresponding amino acids. The coordinates of the carbon atom C3 of the sugar monomer *N*-acetylglucosamine in subsite[†††] -1 were taken as centre of the search sphere. The values of the

[†††] By convention, the sugar residue subsites are labelled from *-n* to *+n*, with *-n* at the non-reducing end and *+n* at the reducing end of the substrate. Cleavage occurs between the -1 and +1 subsites.[20]

most important LUDI parameters for design of BTH ligands were as follows: the maximal rms deviation of the fit between the fragments and the interaction sites was 0.45 Å, the density of lipophilic and polar interaction sites per protein atom was set to 25 and the minimal contact surface between ligand and protein was set to 30 %. The retrieved candidate molecules were ranked with respect to their expected binding affinity using the empirical scoring function developed by Böhm[32] with a minimal scoring value of 300 (predicted K_i value of 1 mM). All other parameters were set to default values. The ambiguous protonisation state of the catalytic residue Asp149 is considered by performing two separated LUDI calculations (charged and uncharged Glu149, respectively).

LUDI runs with the constructed LeadQuest® database Vol. 1-3 resulted in 257 and 175 hits for Glu149 and uncharged Glu149, respectively. The number of hits from the ChemACXF database was 4030 and 1339 for Glu149 and uncharged Glu149, respectively. Of the proposed hits five compounds were selected for testing hyaluronidase inhibition according to high LUDI scores, availability and efficient synthetic feasibility.

5.4.3 Determination of the inhibitory effects of the test compounds

The inhibitory effects of the test compounds on the hyaluronidase from bovine testis were measured using a turbidimetric assay according to the description of Di Ferrante.[33] Details are given in chapter 6.

5.4.4 Ligand-based design by superposition of X-ray structures of related enzymes complexed with inhibitors

Putative inhibitors of BTH could be suggested by superimposing the BTH model and the crystal structure of bee venom hyaluronidase with crystal structures of bacterial chitinases sharing similar active site architectures.[13,22] The following corresponding amino acids of the active sites were superimposed (see Table 5.2).

Table 5.2. Active site amino acids selected for superposition of hyaluronidases and chitinases complexed with ligands.

enzyme	superimposed amino acids					pdb code	ligand
BTH[1]	Tyr93	Asp147	Glu149	Tyr265	Trp354	model	none
BVH	Tyr55	Asp111	Glu113	Tyr227	Trp309	1fcv	HA fragment
ChiA[2]	Phe191	Asp313	Glu315	Tyr390	Trp539	1ffq	allos-amidin[3]
ChiB[2]	Phe51	Asp142	Glu144	Tyr214	Trp403	1o6i	CI-4[3]

[1] Amino acid sequence according to Meyer et al.[34]

[2] Chitinase A (ChiA) and chitinase B (ChiB) from *Serratia marcescens*.

[3] Chemical structures are depicted in Figure 5.4.

By superimposing all complexed structures, the HA fragment, allosamidin as well as CI-4 show a common overlap at the binding subsite -1 of the *N*-acetylglucosamine monomer of hyaluronan. Since substructures of allosamidin and CI-4 mimic the postulated intermediate of the *N*-acetylglucosamine moiety (**12**), the combination of these mimicking moieties and the introduction of substituents suggested to interact with amino acids of the active site of BTH led to the prediction of two BTH inhibitors (see Figure 5.4).

5.5 References

(1) Veselovsky, A. V.; Ivanov, A. S. Strategy of computer-aided drug design. *Curr Drug Targets Infect Disord* **2003**, *3*, 33-40.

(2) Lauri, G.; Bartlett, P. A. CAVEAT: a programme to facilitate the design of organic molecules. *J Comput Aided Mol Des* **1994**, *8*, 51-66.

(3) Schneider, G.; Lee, M. L.; Stahl, M.; Schneider, P. De novo design of molecular architectures by evolutionary assembly of drug-derived building blocks. *J Comput Aided Mol Des* **2000**, *14*, 487-494.

(4) Tripos Inc., St. Louis, Missouri, USA. www.tripos.com.

(5) Böhm, H. J. LUDI: rule-based automatic design of new substituents for enzyme inhibitor leads. *J Comput Aided Mol Des* **1992**, *6*, 593-606.

(6) Rarey, M.; Kramer, B.; Lengauer, T.; Klebe, G. A fast flexible docking method using an incremental construction algorithm. *J Mol Biol* **1996***, 261*, 470-489.

(7) Goodsell, D. S.; Morris, G. M.; Olson, A. J. Automated docking of flexible ligands: applications of AutoDock. *J Mol Recognit* **1996***, 9*, 1-5.

(8) Ewing, T. J.; Makino, S.; Skillman, A. G.; Kuntz, I. D. DOCK 4.0: search strategies for automated molecular docking of flexible molecule databases. *J Comput Aided Mol Des* **2001***, 15*, 411-428.

(9) Schneider, G.; Böhm, H. J. Virtual screening and fast automated docking methods. *Drug Discov Today* **2002***, 7*, 64-70.

(10) Good, A.; Mason, J.; Pickett, S. Pharmacophore pattern application in virtual screening, library design and QSAR. *Virtual Screening for Bioactive Molecules*; Wiley-VCH Verlag: Weinheim, 2000; pp 131-159.

(11) Kettmann, V.; Höltje, H. D. Mapping of the Benzothiazepine Binding Site on the Calcium Channel. *Quantitative Structure-Activity Relationships* **1998***, 17*, 91-101.

(12) Bravi, G.; Gancia, E.; Green, D.; Hann, M. Modelling Structure-Activity Relationships. *Virtual Screening for Bioactive Molecules*; Wiley-VCH Verlag: Weinheim, 2000; pp 81-116.

(13) Markovic-Housley, Z.; Miglinerini, G.; Soldatova, L.; Rizkallah, P.; Müller, U. et al. Crystal Structure of Hyaluronidase, a Major Allergen of Bee Venom. *Structure* **2000***, 8*, 1025-1035.

(14) Marti-Renom, M. A.; Stuart, A. C.; Fiser, A.; Sanchez, R.; Melo, F. et al. Comparative protein structure modeling of genes and genomes. *Annu Rev Biophys Biomol Struct* **2000***, 29*, 291-325.

(15) Sali, A.; Blundell, T. L. Comparative protein modelling by satisfaction of spatial restraints. *J Mol Biol* **1993***, 234*, 779-815.

(16) Fiser, A.; Do, R. K.; Sali, A. Modeling of loops in protein structures. *Protein Sci* **2000***, 9*, 1753-1773.

(17) Böhm, H. J. The computer programme LUDI: a new method for the de novo design of enzyme inhibitors. *J Comput Aided Mol Des* **1992***, 6*, 61-78.

(18) Thompson, J. D.; Higgins, D. G.; Gibson, T. J. CLUSTAL W: improving the sensitivity of progressive multiple sequence alignment through sequence weighting, position-specific gap penalties and weight matrix choice. *Nucleic Acids Res* **1994***, 22*, 4673-4680.

(19) Böhm, H. J. Prediction of binding constants of protein ligands: a fast method for the prioritization of hits obtained from *de novo* design or 3D database search programmes. *J Comput Aided Mol Des* **1998***, 12*, 309-323.

(20) Davies, G. J.; Wilson, K. S.; Henrissat, B. Nomenclature for sugar-binding subsites in glycosyl hydrolases. *Biochem J* **1997***, 321 (Pt 2)*, 557-559.

(21) Spickenreither, M. personal communication, 2003.

(22) Markovic-Housley, Z.; Schirmer, T. Structural Evidence for substrate assisted catalytic mechanism of bee venom hyaluronidase, a major allergen of bee venom. *Carbohydrate Bioengineering: Interdisciplinary Approaches*; RCS: London, 2002; pp 19-27.

(23) Salmen, S. Inhibitors of bacterial and mammalian hyaluronidases: synthesis and structure-activity relationships; University of Regensburg: Regensburg, 2003.

(24) Papanikolau, Y.; Tavlas, G.; Vorgias, C. E.; Petratos, K. De novo purification scheme and crystallization conditions yield high-resolution structures of chitinase A and its complex with the inhibitor allosamidin. *Acta Crystallogr D Biol Crystallogr* **2003***, 59*, 400-403.

(25) Sakuda, S.; Isogai, A.; Matsumoto, S.; Suzuki, A. Search for microbial insect growth regulators. II. Allosamidin, a novel insect chitinase inhibitor. *J Antibiot (Tokyo)* **1987***, 40*, 296-300.

(26) Tews, I.; Terwisscha van Scheltinga, A. C.; Perrakis, A.; Wilson, K. S.; Dijkstra, B. W. Substrate-Assisted Catalysis Unifies Two Families of Chitinolytic Enzymes. *Journal of the American Chemical Society* **1997***, 119*, 7954-7959.

(27) van Aalten, D. M.; Komander, D.; Synstad, B.; Gaseidnes, S.; Peter, M. G. et al. Structural insights into the catalytic mechanism of a family 18 exo-chitinase. *Proc Natl Acad Sci U S A* **2001***, 98*, 8979-8984.

(28) Brameld, K. A.; Shrader, W. D.; Imperiali, B.; Goddard, W. A., 3rd Substrate assistance in the mechanism of family 18 chitinases: theoretical studies of potential intermediates and inhibitors. *J Mol Biol* **1998***, 280*, 913-923.

(29) Spindler-Barth, M.; Blattner, R.; Vorgias, C. E.; Spindler, K. D. Inhibition of Two Family 18 Chitinases by Various Allosamidin Derivatives. *Pest Sci* **1998***, 52*, 47-52.

(30) Izumida, H.; Imamura, N.; Sano, H. A novel chitinase inhibitor from a marine bacterium *Pseudomonas sp. J Antibiot* **1996***, 49*, 76-80.

(31) Houston, D. R.; Eggleston, I.; Synstad, B.; Eijsink, V. G.; van Aalten, D. M. The cyclic dipeptide CI-4 [cyclo-(l-Arg-d-Pro)] inhibits family 18 chitinases by structural mimicry of a reaction intermediate. *Biochem J* **2002***, 368*, 23-27.

(32) Böhm, H. J. On the use of LUDI to search the Fine Chemicals Directory for ligands of proteins of known three-dimensional structure. *J Comput Aided Mol Des* **1994***, 8*, 623-632.

(33) Di Ferrante, N. Turbidimetric measurement of acid mucopolysaccharides and hyaluronidase activity. *J Biol Chem* **1956***, 220*, 303-306.

(34) Meyer, M. F.; Kreil, G.; Aschauer, H. The soluble hyaluronidase from bull testes is a fragment of the membrane-bound PH-20 enzyme. *FEBS Lett* **1997***, 413*, 385-388.

Chapter 6 L-ascorbic acid-6-hexadecanoate as potent hyaluronidase inhibitor: structural elucidation and molecular modelling of enzyme-inhibitor complexes

6.1 Introduction

The glycosaminoglycan hyaluronic acid (HA), consisting of repeating disaccharide units of (β-1,4)-D-glucuronic acid-(β-1,3)-*N*-acetyl-D-glucosamine, is a major component of the extracellular matrix of all mammalian tissues. It occurs in significant quantities in the skin (dermis and epidermis), brain, and central nervous system[1] and is also present in some bacteria. HA is the common substrate of a class of enzymes termed hyaluronidases (for a review see http://www.glycoforum.co.jp). The enzymes from bacterial sources are endo-*N*-acetyl-glucosaminidases (hyaluronate lyases, EC 4.2.2.1).[2,3] Their proposed catalytic mechanism[4-7] has been firmly supported by successive structural determinations[4,8-10] and mutagenesis studies.[8,9,11] Main degradation products are unsaturated disaccharides or tetrasaccharides which might be utilised as an additional carbon source.[12] More probably, the degradation of HA decreases the viscoelasticity of the extracellular matrix leading to increased spreading of the bacteria and the toxins in the tissue.[12]

The other group of hyaluronidases, with the bovine testicular hyaluronidase or bovine PH-20 protein as well-known representative, are present in vertebrate tissues as well as in the venom of bees, wasps, etc. and act as endo-*N*-acetyl-glucosaminidases (hyaluronate glycanohydrolases, EC 3.2.1.35 and EC 3.2.1.36).[2,13] In contrast to the bacterial enzymes, the human enzymes PH-20 protein, Hyal1[14] and Hyal2 probably exist in several isoforms. To date, six human hyaluronidases have been cloned[15] and expressed in different cell lines, but no larger amounts of the enzymes could be produced for enzymological investigation. As the only exception, the crystal structure of the distantly related bee venom hyaluronidase could be elucidated.[16] The mammalian enzymes like PH-20 protein, Hyal1 and Hyal2 seem to be involved in physiological and pathophysiological processes like fertilisation,[17] embryonic development,[18] tumour growth and metastasation,[19] but the specific functions of HA and hyaluroni-

dases within these processes remain obscure up to now. Therefore, hyaluronidase inhibitors are needed as pharmacological tools to study the physiological and pathophysiological role of HA and HA degrading enzymes. Moreover, hyaluronidase inhibitors could be useful as drugs, e.g. in the treatment of arthroses or, combined with antibiotics, in antibacterial therapy.

Heparin,[20] flavonoids[21] and fully O-sulfonated glycosaminoglycanes[22,23] were reported to inhibit bovine testicular hyaluronidase (BTH) *in vitro*, but these compounds show only weak or partial inhibitory activity.[24] For the bacterial hyaluronidase from *S. pneumoniae* (hylSpn), guanidine hydrochloride, N^G-nitro-L-arginine methyl ester, L-arginine[25] and vitamin C (**1**, Figure 6.1,[26]) were described as inhibitors with IC_{50} values from 150 mM to 0.15 mM. Thus, no potent and selective hyaluronidase inhibitors have been characterised to date.

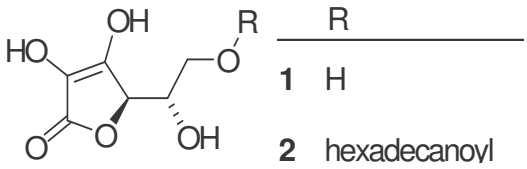

Figure 6.1. Chemical structures of L-ascorbic acid (**1**) and L-ascorbic- acid-6-hexadecanoate (**2**)

Recently, the structural basis of the hylSpn-L-ascorbic acid interaction could be elucidated by means of X-ray crystallography.[26] Most regions of **1** bind inside the active site *via* hydrophobic interactions with two residues, Trp292 and Tyr408. Thus, increased hydrophobicity of vitamin C derivatives might lead to higher inhibitory activity. To prove this hypothesis, L-ascorbic acid-6-hexadecanoate (**2**), a highly effective antioxidant[27] and glutathione-S-transferase inhibitor,[28] was examined as potential inhibitor of two bacterial hyaluronidases from *S. pneumoniae* and *S. agalactiae* strain 4755 and of bovine testicular hyaluronidase as solely available representative of mammalian hyaluronidases. Additionally, the crystal structure of *S. pneumoniae* hyaluronate lyase (hylSpn), co-crystallised with **2**, was determined at 1.65 Å resolution to examine the protein-L-ascorbic acid-6-hexadecanoate interactions at the molecular level. For possible conclusions with respect to the topology of mammalian hyaluronidases, a homology model of BTH based on the crystal structure of bee venom hyaluronidase in complex with a HA tetrasaccharide fragment was constructed. In comparison to the hylSpn-L-ascorbic acid-6-hexadecanoate complex, the potential binding mode of **2** at BTH was predicted by flexible docking. Results and conclusions from these approaches should help to develop improved binding models for further, more potent and selective hyaluronidase inhibitors.

6.2 Results and discussion

6.2.1 Comparison of inhibitory activities of L-ascorbic acid and L-ascorbic acid-6-hexadecanoate on hyaluronidases

Recently, the inhibitory activities of L-ascorbic acid (**1**) on *S. pneumoniae* hyaluronate lyase (hylSpn) and bovine testicular hyaluronidase (BTH) have been investigated. L-Ascorbic acid induced an inhibition of hylSpn with an IC_{50} value of around 6 mM under the reaction conditions used, but no activity could be observed on BTH.[26]
Probably due to the specific HA degradation mechanism of bovine testicular hyaluronidase, the usual colourimetric assay based on the Morgan-Elson reaction results in another pH activity profile than a turbidimetric assay.[29] Therefore, to normalise the experiments among all three enzymes, the turbidimetric assay with equiactive concentrations of all enzymes was applied. In accordance with the aforementioned high IC_{50} value, the bacterial enzymes were weakly inhibited by vitamin C (**1**) with IC_{50} values of 6 mM for $hylB_{4755}$ and 32 mM for hylSpn, respectively, whereas the bovine enzyme was not affected up to 100 mM. Therefore, vitamin C proved to be a weak, but selective inhibitor of streptococcal hyaluronate lyases.

The crystal structure of the bacterial hyaluronate lyase-vitamin C complex[26] suggested which structural variations might lead to stronger inhibitors of the enzyme. Due to the presence and topology of hydrophobic residues in the catalytic cleft,[26] the introduction of lipophilic chains in position 6 of vitamin C like in L-ascorbic acid-6-hexadecanoate (**2**) has promise. Hydrophobic interactions also play an important role for the substrate HA since it has a two-fold helix as secondary structure in aqueous solutions with an extensive hydrophobic patch (about 8 CH units, roughly corresponding in size to octanoic acid). Thus, hyaluronic acid combines hydrophilic regions with hydrophobic patches, both characteristic of lipids.[30]

As a consequence of these suggestions, the effects of compound **2** on the hyaluronate lyases and on the bovine testicular hyaluronidase were determined.

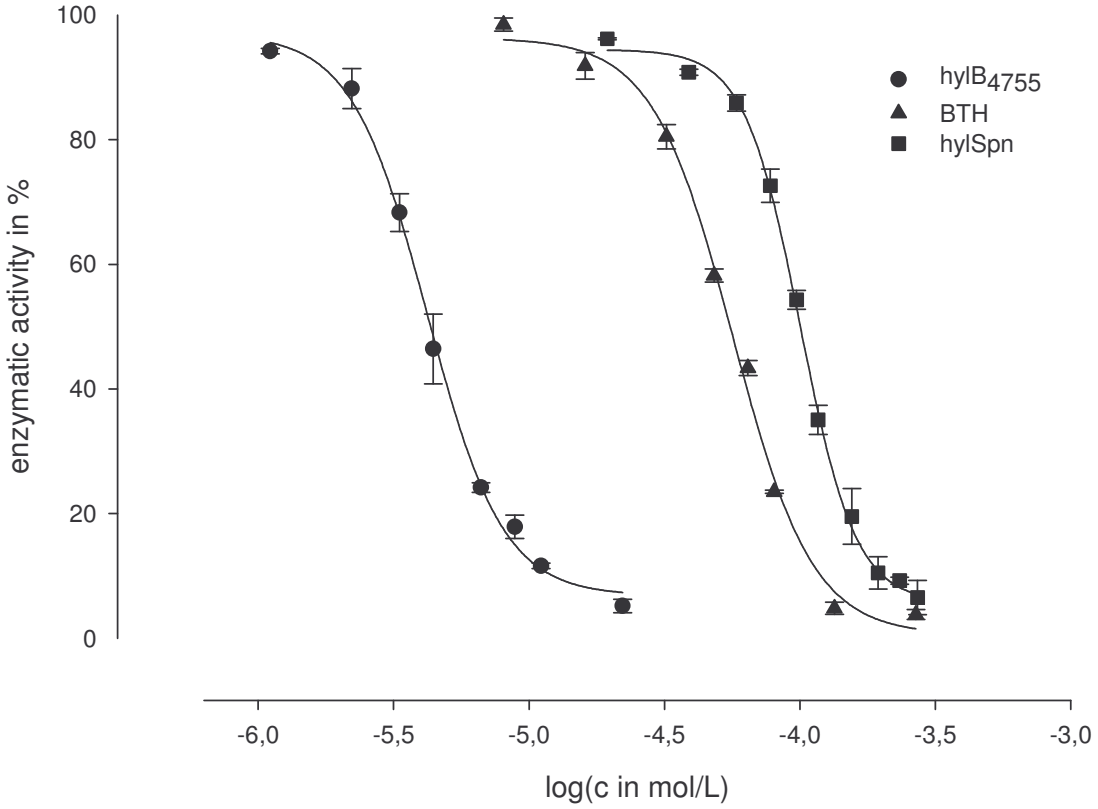

Figure 6.2. Enzyme activity of $hylB_{4755}$, BTH and hylSpn in the presence of L-ascorbic acid-6-hexadecanoate (**2**). The L-ascorbic acid-6-hexadecanoate concentration range was 1.1–300 µM. The inhibition of the enzyme activity by compound **2** is presented in a sigmoidal concentration-dependent manner with 50 % inhibition (IC_{50}) as shown in Table 6.1.

Compound **2** induced a potent inhibition of $hylB_{4755}$ with an IC_{50} value of 4 µM, as illustrated in Figure 6.2. Equiactive concentrations of hylSpn and bovine testicular hyaluronidase resulted in IC_{50} values of 100 µM and 56 µM, respectively. L-Ascorbic acid-6-hexadecanoate is thus up to 1500 times more active than vitamin C (Table 6.1) and proved to be the most potent inhibitor of bacterial and bovine hyaluronidases described to date.

L-Ascorbic acid-6-hexadecanoate exhibits about 25-fold, but vitamin C (**1**) only 6-fold higher inhibitory activity on $hylB_{4755}$ compared to hylSpn. This apparent selectivity of compound **2** for $hylB_{4755}$, which cannot be quantitatively verified without knowledge about the individual K_m values of the HA substrate used, requires further investigations. In contrast to L-ascorbic acid, overall selectivity of L-ascorbic acid-6-hexadecanoate for the bacterial enzymes vs. BTH could not be observed (Table 6.1).

Table 6.1. IC_{50} values (50 % inhibition of equiactive enzyme concentrations) ± SEM (n=4) on *S. pneumoniae* hyaluronate lyase, *S. agalactiae* hyaluronate lyase strain 4755 and BTH for vitamin C (**1**) and L-ascorbic acid-6-hexadecanoate (**2**).

Enzyme \ Inhibitor	Vitamin C IC_{50} (µM)	L-ascorbic acid-6-hexadecanoate IC_{50} (µM)
hylSpn	34800 ± 300	100.0 ± 2.00
$hylB_{4755}$	6100 ± 100	4.2 ± 0.13
BTH	inactive (≤ 100 mM)	56.5 ± 0.13

The strikingly better inhibition of all investigated enzymes by L-ascorbic acid-6-hexadecanoate compared to vitamin C supports the working hypothesis that the long alkyl chain increases the affinity of the molecule by additional hydrophobic interactions with the enzyme.

6.2.2 The binding mode of vitamin C hexadecanoate to *S. pneumoniae* hyaluronidase

X-ray crystallography of the co-crystallised L-ascorbic acid-6-hexadecanoate-hylSpn complex was used for the determination of the binding mode. This information should be useful to deduce a model for the interactions of the inhibitor with amino acid residues inside the active site of the enzyme and should facilitate the further development of more potent inhibitors. In cooperation, crystallisation experiments were accomplished by M. Nukui and M. J. Jedrzejas (Children's Hospital Oakland Research Institute, Oakland, California 94609, USA). The X-ray structure of the complex was solved by D. Rigden (National Center of Genetic Resources and Biotechnology, Cenargen/Embrapa, Brasília, D.F. 70770-900, Brazil).

The density at the binding site allowed for the satisfactory modelling of **2** as shown in Figure 6.3. In the final model, additional difference density and elevated B-factors of the inhibitor (Table 6.2) suggest remaining flexibility and alternative binding modes of **2**. However, despite repeated attempts, only the conformation shown was well supported by density. Surprisingly, no support for a lactone ring was evident from electron density, although the vitamin C moiety of the inhibitor binds to the same region as intact vitamin C.[26] Obviously the vitamin C portion of the inhibitor binds in a ring-

opened form emerging under the terms of crystallisation (Figure 6.3). It is known that oxidation of **1** gives L-dehydroascorbic acid which is rapidly degraded under physiological conditions (pH 7.4) *via* L-diketogulonate to yield L-erythrulose and oxalate.[31] Possibly compound **2** is modified in a similar manner, but only the hydrolysed lactone moiety was modelled into the electron density (Figure 6.3). It is however unlikely that ring-opening also occurs during the enzymatic assay.

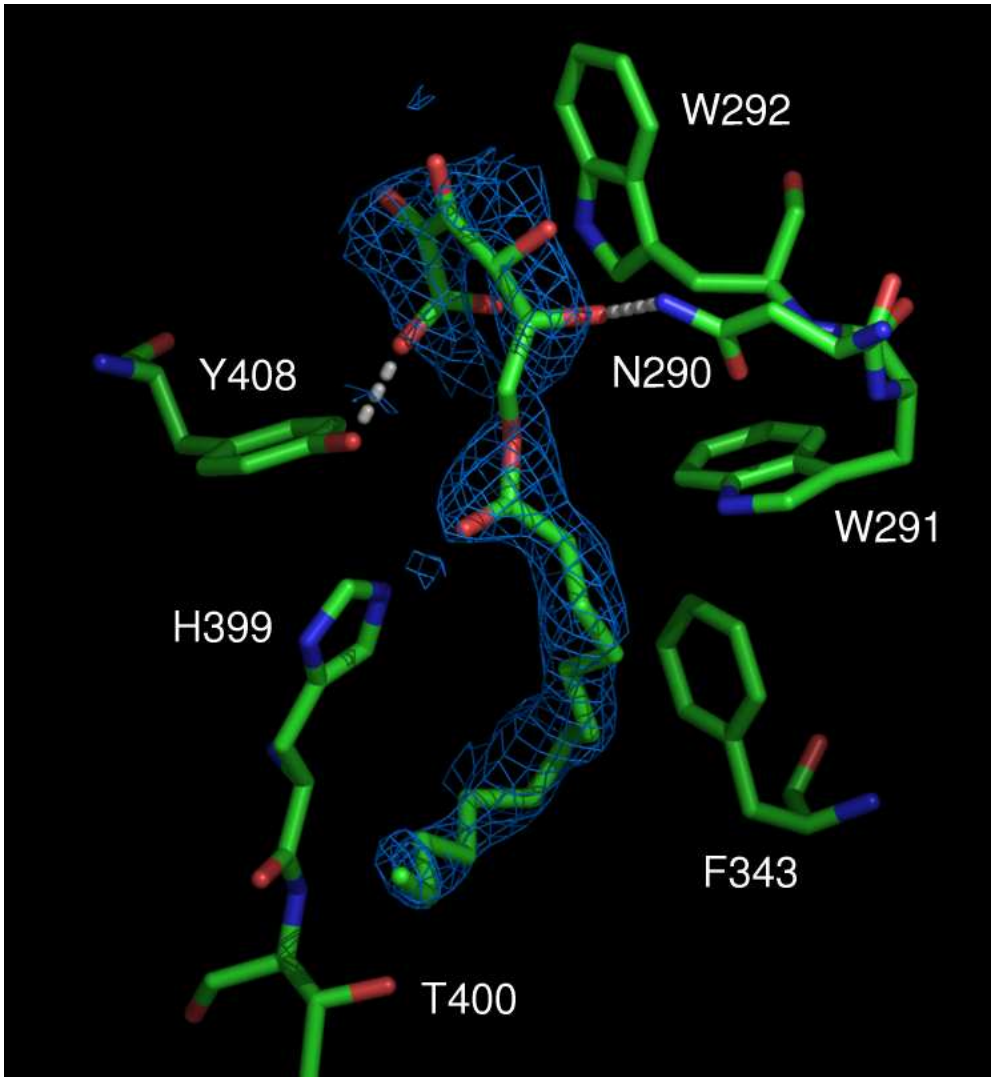

Figure 6.3. The binding site of L-ascorbic acid-6-hexadecanoate**.** Hydrogen bonds are shown as dotted lines and final sigmaA-weighted $|2F_o\text{-}F_c|$ map electron density is shown, contoured at 0.9σ.

The proposed catalytic mechanism of hylSpn[4-7] has been firmly supported by successive structural determinations[4,8-10] and mutagenesis studies.[8,9,11] Catalysis occurs at the most narrow part of the catalytic cleft and involves residues Asn349, His399 and Tyr408. In addition, a hydrophobic patch consisting of Trp291, Trp292 and Phe343 contributes to precise positioning of the substrate. As shown in Figure 6.3, compound **2** binds within the catalytic site explaining the competitive inhibition. Figure 6.3 also

illustrates that the majority of protein-inhibitor interactions are hydrophobic, the only exceptions being a hydrogen bond between the carboxylic group of the inhibitor and the side chain hydroxyl of Tyr408, which acts as catalytic acid on HA cleavage,[6] and another one between the hydroxy group at C5 and Asn290. The hydrophobic face of the vitamin C portion is flatly aligned with the side chain of Trp292 as part of the hydrophobic patch. Such an arrangement is commonly observed in complexes of carbohydrate binding proteins with their ligands.[32] The palmitoyl moiety fits in a mainly hydrophobic surface crevice. The aliphatic chain is well-defined by density with the exception of the three terminal carbon atoms, for which missing density did not permit modelling. Hydrophobic interactions are formed with Trp291 and Phe343, both contributing to the hydrophobic patch along with His399 and Thr400. Figure 6.4A,B compares the binding mode of **2** with that of a substrate-based hexasaccharide (PDB code 1loh;[33]). The binding sites overlap, but the surface which accomodates the palmitoyl group is not directly involved in substrate binding. Interestingly, one of the three well-ordered cryoprotectant xylitol molecules bound to hylSpn fits close to the end of the palmitoyl moiety. The distance between the penultimate visualised carbon of the palmitoyl group and atom O5 of xylitol is only 4.0 Å (Figure 6.4B). This position of the bound xylitol suggests that the affinity of the present inhibitor might be enhanced through addition of matching groups at the aliphatic end of the palmitoyl moiety**.**

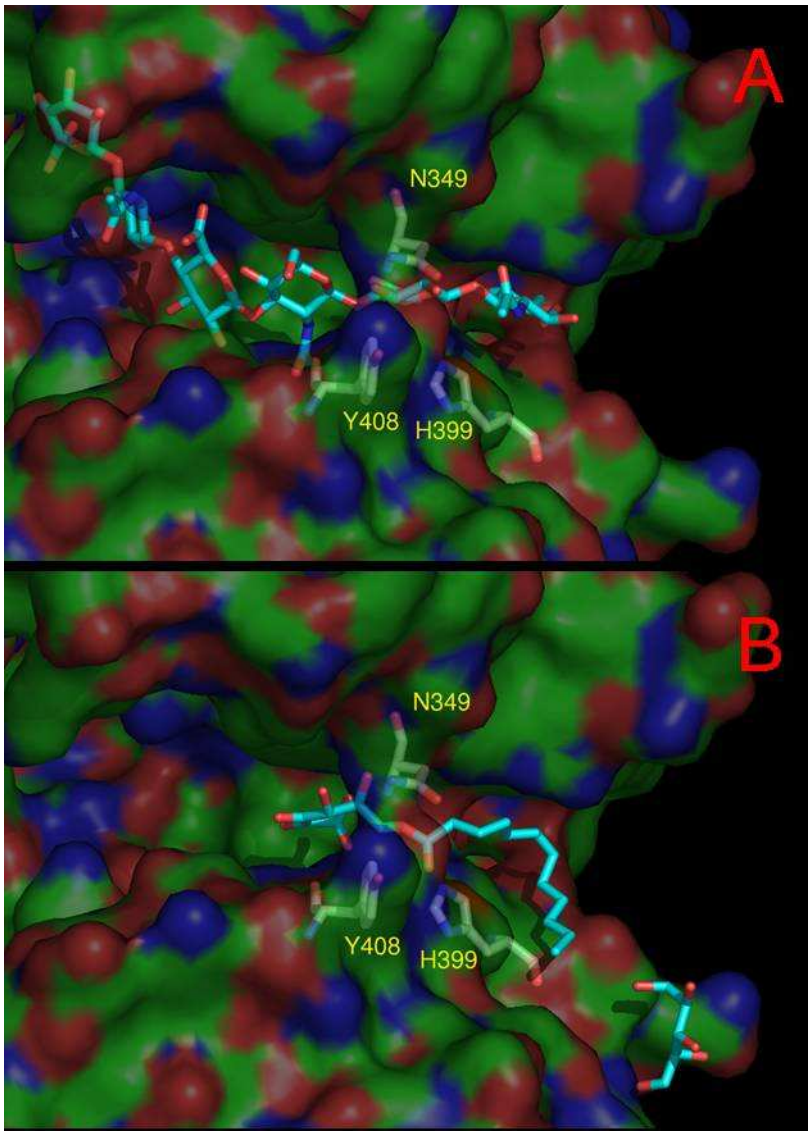

Figure 6.4. Comparison of binding modes of **A**) hexasaccharide substrate and **B**) vitamin C-6-hexadecanoate inhibitor**.** The protein surface is shown semi-transparently in order to enable three key catalytic residues (labelled) to be seen. The nearby cryoprotectant xylitol molecule (see text) is shown towards the lower right of **B**).

6.2.3 Homology model of bovine testicular hyaluronidase as basis for the prediction of inhibitor binding modes

For the prediction of the binding mode of L-ascorbic acid-6-hexadecanoate to BTH by flexible ligand docking, homology modelling was used. In consideration of the low, but significant amino acid sequence identity between insect and mammalian hyaluronidases, the crystal structure of bee venom hyaluronidase[16,34] has provided the first possibility to construct reliable comparative models of mammalian hyaluronidases, like BTH, human PH-20 protein and Hyal1-4. In the case of less than 40 % identity the correct sequence alignment is the most important factor affecting the quality of

the resulting models.[35] Given that the sequence identity between BTH and bee venom hyaluronidase is just 32 % an improvement could be obtained by constructing a multiple – instead of a pairwise – alignment of BTH, human PH-20 protein and the bee venom hyaluronidase using ClustalW.[36]

The functional analysis of mutants of the related human sperm PH-20 protein[37] indicated two catalytic acidic amino acids corresponding to BVH Asp111 and Glu113 which were indeed shown to be involved in catalysis[38] by exploring the binding region of the HA tetrasaccharide co-crystallised with bee venom hyaluronidase (pdb code: 1fcv;[16]). Further analysis of the crystal structures and the multiple sequence alignment clearly show that the residues forming the active site of hyaluronidases are highly conserved (Figure 6.5). Thus, appropriate homology models will be most reliable in regions where competitive inhibitors bind. A fully automated construction of a comparative BTH model was performed using MODELLER version 6.2.[39-41] The resulting structure was evaluated for correct local geometry by PROCHECK,[42,43] by the SYBYL module ProTABLE and by comparison of the Ramachandran plot with that of the template (1fcq), and was completed by addition of hydrogen atoms and energy minimisation.

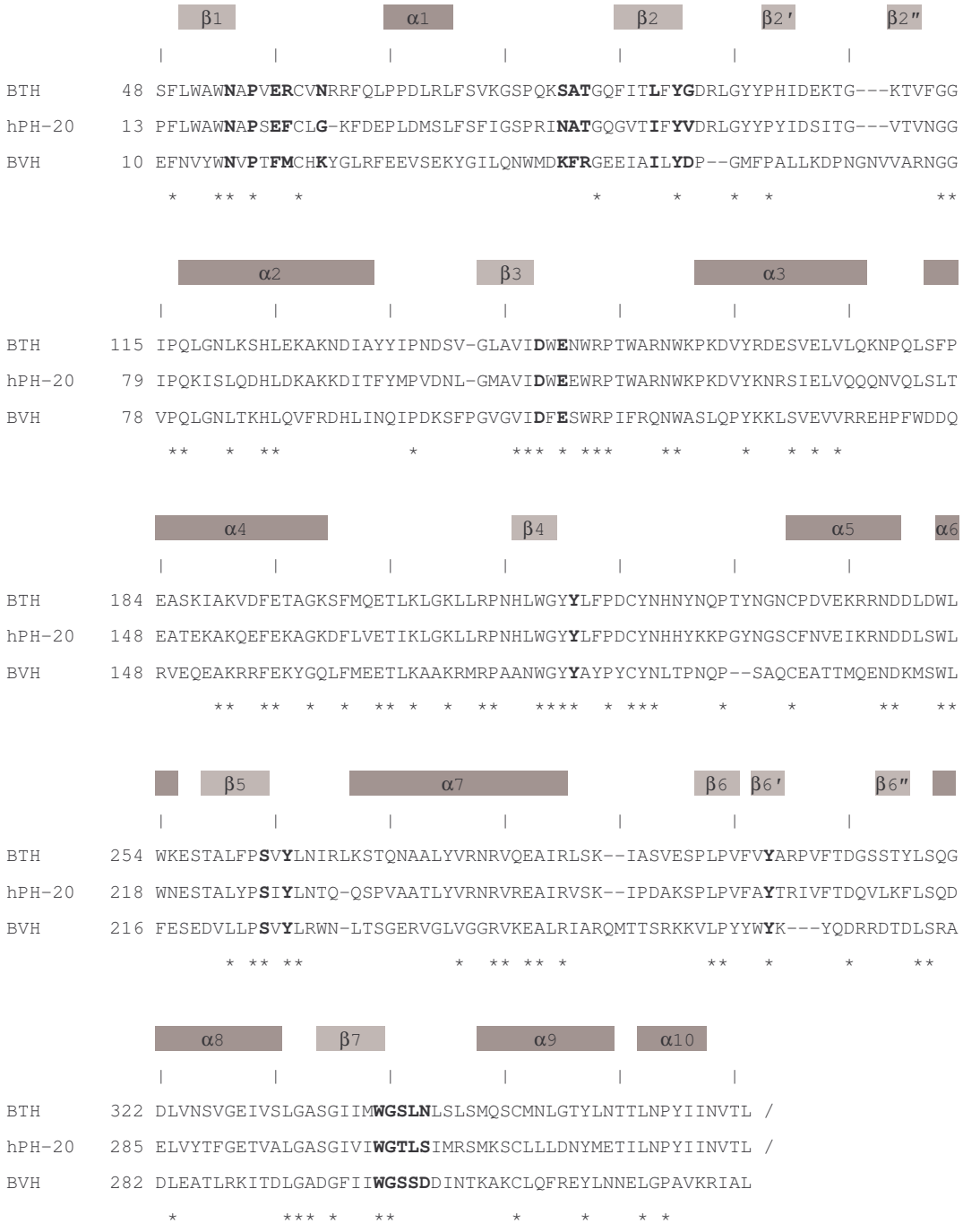

Figure 6.5. Sequence alignment of bovine testicular hyaluronidase (BTH), human PH-20 protein and bee venom hyaluronidase (BVH) as the basis of homology modelling with MODELLER 6.2. α-helices and β-strands are differently shaded. Structurally conserved residues are marked with asterisks, and amino acids residues of BTH and PH-20 protein corresponding to those within the active site of BVH are highlighted in bold type.

6.2.4 Potential binding mode of L-ascorbic acid-6-hexadecanoate at bovine testicular hyaluronidase

In order to identify the binding pocket of BTH the model was superimposed with the crystal structure of bee venom hyaluronidase in complex with a HA tetrasaccharide fragment. The active site of BTH was defined by the set of amino acids within a sphere of 4 Å around residues Tyr220 and Trp341 (BVH: Tyr184 and Trp301), both close to the reducing end of the tetrasaccharide and the amino acids Asp147 and Glu149 (BVH: Asp111 and Glu113) involved in catalysis. In the crystal structure of BVH, the aspartate and glutamate side chains are in close proximity – independent of whether an acidic or a neutral pH was used for crystallisation[16] – and form a short hydrogen bond between both carboxylates. Therefore, Asp147 was treated uncharged on docking simulations of compound **2**.

In analogy to the proposed hydrolysis mechanism of family 18 chitinases[44,45] Glu113 in BVH (equivalent to Glu149 in BTH) was proposed to act as the proton donor while the nucleophile is the acetamido oxygen of the HA substrate probably forming a covalent oxazolinium intermediate (see chapter 1, Figure 1.3). In the next step this intermediate is hydrolysed by a water molecule resulting in the observed retention of the configuration at the anomeric carbon atom.[16,38,45] Like suggested for chitinase B,[45] the protonation of Glu113 in BVH and Glu149 in BTH, respectively, should be simultaneous with substrate binding and the displacement of water molecules from the active site. However, it cannot be ruled out that on inhibitor binding Glu149 will not be protonated. Therefore, the δ-oxygen of Asp147 remains protonated in all flexible docking calculations whereas Glu149 is treated in both forms.

Each of the FlexX calculations was analysed by visual inspection of the suggested docking poses (309 target-bound conformations for both residues uncharged, 237 for only Asp147 uncharged). Each docking series resulted in a preferred binding mode of compound **2** comprising about 70 % of all proposed poses. In both cases, the vitamin C moiety acts as an anchor and is placed in such a way that an optimal hydrogen bonding pattern is achieved. In the case of both residues protonated (mode A), vitamin C interacts with the backbone oxygen atoms of Tyr263 and Tyr265 and with the side chain oxygen of Tyr279. In the other case (mode B), the hydrogen bonding interaction is formed with both amino acids relevant for catalysis, Asp147 and Glu149.

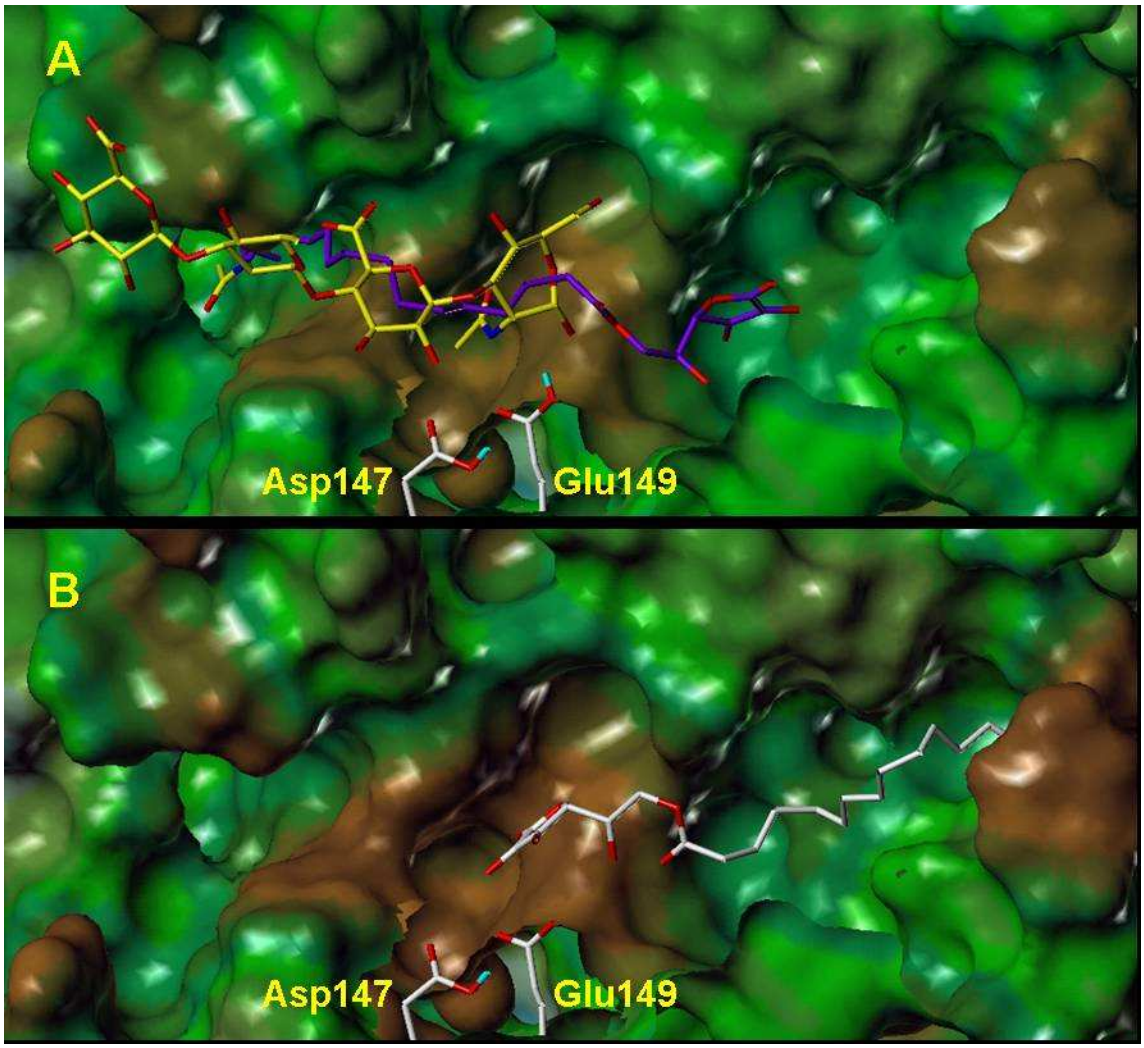

Figure 6.6. Comparison of proposed binding modes of compound **2** within the active site of the BTH models **A**: D147 and E149 uncharged, and **B**: only D147 uncharged. In panel **A**, the HA tetrasaccharide fragment is additionally shown (carbon atoms coloured in yellow) as docked into the binding site of the BTH model according to the binding mode found in the crystal structure of bee venom hyaluronidase (1fcv,[16]). The protein surface is represented by a Connolly surface coloured by lipophilicity (the warmer the colour, the more lipophilic the amino acids). Both catalytically active residues are shown with their protonation states used for the different calculations.

Thus, the specific binding mode seems to depend on the protonation state of the catalytic residues as depicted in Figure 6.6A,B. If Asp147 and Glu149 are both uncharged, the long alkyl chain of **2** occupies the region where the tetrasaccharide was found in the crystal structure of bee venom hyaluronidase (mode A, Figure 6.6A). In the other case the palmitoyl moiety projects to a channel-like region which probably belongs to the binding site of the polymeric HA before being degraded since it is directly attached to the site of the HA tetrasaccharide fragment (mode B, Figure 6.6B). Both of the proposed binding modes suggest a competitive binding mechanism of **2** at BTH. Nevertheless, with respect to potential hydrophobic interactions, binding

mode A seems to be favoured. Depicting the hydrophobic surrounding of **2** by means of hydrophobicity-coloured Connolly surfaces shows that in this binding mode the long alkyl chain favourably interacts with an extended, strongly hydrophobic channel (brown colour) which is formed by mostly conserved amino acids Ala84, Leu91, Tyr93, Tyr220 and Leu344 in BTH (Phe46, Ile53, Tyr55, Tyr184 and Ser304 in BVH). In binding mode B the alkyl chain occupies a less hydrophobic region (green colour) (Figure 6.6A,B).

For a further, more detailed experimental analysis of the mechanism of action of **2** the hexasaccharide fragment of HA should be used. It is the proposed minimal substrate[46] enabling a degradation mechanism that can be evaluated by Michaelis-Menten kinetics. These studies are currently under way.

6.2.5 Comparison of binding modes of L-ascorbic acid and L-ascorbic acid-6-hexadecanoate at hyaluronidases

The binding of L-ascorbic acid (**1**) at *S. pneumoniae* hyaluronate lyase is mainly caused by hydrophobic interactions with the side chain of Trp292, since the indole moiety is stacked with the five-membered ring of **1**. This structural arrangement helps **1** to bind in the narrowest part of the binding site comprising the amino acids Trp292, Arg462 and Arg466.[26] In the L-ascorbic acid-6-hexadecanoate-*S. pneunomiae* hyaluronate lyase structure, the vitamin C moiety of the inhibitor is detected in the same narrow part of the active site, but it is mirrored (at a perpendicular plane through the centre of the 'ring plane'). The alternative binding mode of **2** is probably forced by the long aliphatic side chain which forms strong hydrophobic interactions with residues of the hydrophobic patch. The ring-opened form in the crystal structure is no prerequisite of this mode since the intact vitamin C moiety may be docked in a similar position without changing interactions of the palmitoyl chain.

Multiple binding modes for the vitamin C moiety are observed at the bacterial lyase which might also be principally possible at BTH. A first hint in this respect is given by the docking studies with L-ascorbic acid-6-hexadecanoate (**2**), since the L-ascorbic acid moiety is placed in two different, but adjacent parts of the active site of BTH (Figure 6.6A,B). This result probably follows from the topology of the HA binding site of BTH which is by far more open than that of the streptococcal enzymes. Interactions of vitamin C itself may be too weak and/or immobilisation and orientation effects cannot sufficiently act on the small molecule within this wide crevice so that addi-

tional hydrophobic substituents are needed to impart tight binding on BTH. In conclusion, the observed selectivity of vitamin C for bacterial hyaluronidases *vs.* BTH seems to be due to a closer fit in a narrow binding pocket.

6.3 Summary

Hyaluronidases are enzymes degrading hyaluronan, an important component of the extracellular matrix. The mammalian hyaluronidases, e.g. the testicular PH20 protein and the lysosomal enzyme Hyal1, are considered to be involved in many (patho)physiological processes like fertilisation, tumour growth and metastasis. Bacterial hyaluronidases contribute to the spreading of microorganisms in the tissue. As the role of hyaluronidases is far from being clear, inhibitors are needed as pharmacological tools. Potent and selective inhibitors of hyaluronidases are not known up to now.

Vitamin C (**1**) has been reported as a weak inhibitor of *S. pneumoniae* hyaluronidase. The X-ray structure of this enzyme in complex with vitamin C could be elucidated, suggesting that additional hydrophobic interactions might increase the inhibitory activity. Consequently, we investigated L-ascorbic acid-6-hexadecanoate for its inhibitory activity against streptococcal and bovine testicular hyaluronidase. With an IC_{50} value of 4 µM, L-ascorbic acid-6-hexadecanoate (**2**) strongly inhibited *S. agalactiae* hyaluronidase, whereas. *S. pneumoniae* hyaluronidase and the bovine testicular hyaluronidase were inhibited with IC_{50} values of 100 µM and 56 µM, respectively. Compound **2** is thus up to 1500 times more active than vitamin C and is the most potent inhibitor of bacterial and bovine hyaluronidase described to date.

To determine the binding mode, *S. pneumoniae* hyaluronidase was co-crystallised with **2**. X-ray analysis confirmed the hypothesis that additional hydrophobic interactions with Trp291, Phe343, His399, and Thr400 in the active site result in increased affinity. To predict the potential binding mode of **2** at bovine testicular hyaluronidase, a homology model of bovine testicular hyaluronidase based on the crystal structure of bee venom hyaluronidase was constructed by using MODELLER V6.2. Flexible docking with FlexX suggests two alternative binding modes of compound **2**. With respect to potential hydrophobic interactions, one binding mode seems to be clearly favoured. The long alkyl chain of L-ascorbic acid-6-hexadecanoate favourably inter-

acts with an extended, strongly hydrophobic channel formed by mostly conserved amino acids Ala84, Leu91, Tyr93, Tyr220 and Leu344 in BTH.

6.4 Materials and methods

6.4.1 Materials

Hyaluronic acid from *S. zooepidemicus* was purchased from Aqua Biochem (Dessau, Germany). Bovine serum albumin (BSA) was obtained from Serva (Heidelberg, Germany). The investigated hyaluronidases were enzyme preparations from different sources.

Lyophilised hyaluronidase from bovine testis (Neopermease®), 200 000 IU (according to the declaration of the supplier; 4 mg) plus 25 mg gelatin per vial, was a gift from Sanabo (Vienna, Austria).

Stabilised hyaluronate lyase, i.e., 200 000 IU (according to the declaration of the supplier) of lyophilised hyaluronidase (0.572 mg) from *S. agalactiae* , strain 4755, plus 2.2 mg BSA and 37 mg Tris–HCl per vial was kindly provided by id-Pharma (Jena, Germany).

Streptococcus pneumoniae hyaluronate lyase[5,9,47,48] has been produced as previously described.[49] The enzyme was concentrated to 5 mg/ml in 10 mM Tris-HCl buffer, 150 mM NaCl, 1 mM DTT, (pH 7.4) using centrifugal spin devices with 50 kDa molecular weight cutoff (Millipore, Billerica, USA) and used for the inhibition studies and for crystallisation experiments. The enzyme concentration was determined photometrically at 280 nm using a calculated molar absorption coefficient[49] of 127,090 $L \cdot mol^{-1} \cdot cm^{-1}$ according to Pace et al.[50]

L-ascorbic acid-6-palmitate was purchased from Sigma-Aldrich (Taufkirchen, Germany). All other chemicals were of analytical grade and were obtained either from Merck (Darmstadt, Germany), from Fisher Scientific (Pittsburgh, USA) or Sigma Chemical (St. Louis, USA). Water was purified by a Milli-Q system (Millipore, Eschborn, Germany). Stock solutions of L-ascorbic acid and L-ascorbic acid-6-hexadecanoate in DMSO were prepared.

6.4.2 Activity and inhibition assays

The inhibitory activities of vitamin C and L-ascorbic acid-6-hexadecanoate on the hyaluronidases from *S. pneumoniae* (hylSpn), from *S. agalactiae*, strain 4755 ($hylB_{4755}$), and from bovine testis (BTH) were measured using a turbidimetric assay according to the description of Di Ferrante.[51] Enzyme activity was quantified by determining the turbidity caused by the remaining high molecular weight substrate (molecular weight > 6–8 kDa) precipitated with cetyltrimethylammonium bromide. The incubation mixture was composed of 120 µL of citrate-phosphate buffer (solution A: 0.1 M Na_2HPO_4 / 0.1 M NaCl, solution B: 0.1 M citric acid / 0.1 M NaCl; solution A and B were mixed in appropriate portions to adjust pH 5.0), 30 µl of BSA solution (0.2 mg BSA per mL of water), 30 µL of substrate solution (2 mg hyaluronic acid from *S. zooepidemicus* per mL of water), 50 µL H_2O, 10 µL DMSO and 30 µL of enzyme solution. To normalise the assays due to different enzymatic mechanisms of bacterial and bovine hyaluronidases equiactive concentrations of 54 ng of bovine testicular hyaluronidase, 2.9 ng of hyaluronidase from *S. agalactiae*, strain 4755 and 1.68 ng of hyaluronidase from *S. pneumoniae* in 30 µL of BSA solution were applied. To determine the enzyme activities in presence of the test compounds, instead of 10 µL DMSO, 10 µL of varying concentrations of both inhibitors were used resulting in a final concentration range of 1.1 µM to 300 µM for L-ascorbic acid-6-hexadecanoate and 1 mM to 100 mM for L-ascorbic acid and a final DMSO concentration of 3.8 % (v/v).

After incubation of the assay mixture for 30 min at 37 °C, 720 µL of a 2.5 % (m/v) cetyltrimethylammonium bromide solution (2.5 g CTAB dissolved in 100 mL of 0.5 M sodium hydroxide solution, pH 12.5) were added to precipitate the residual high molecular weight substrate and to stop the enzyme reaction. This mixture was again incubated at 25 °C for 20 min and the turbidity of each sample was determined at 600 nm with an Uvikon 930 UV spectrophotometer (Kontron, Eching, Germany). Experiments were performed in quadruplicate. The turbidity of the sample without any inhibitor was taken as reference for 100 % enzyme activity (absorbance about 0.15), whereas the turbidity of the sample without enzyme (30 µL of BSA solution was used instead) was taken as reference for no degradation of HA (absorbance about 0.83). The activities were plotted against the logarithm of the inhibitor concentration, and

IC_{50} values were calculated by curve fitting of the experimental data with Sigma Plot 8.0 (SPSS Inc., Chicago, USA).

6.4.3 Crystallisation of the complex

The crystallisation experiments were carried out by Masatoshi Nukui and Mark J. Jedrzejas (Children's Hospital Oakland Research Institute, Oakland, California 94609, USA). For crystallisation experiments, L-ascorbic acid-6-hexadecanoate was dissolved in 5 % DMSO (v/v) and 10 mM Tris-HCl buffer, 150 mM NaCl, 1 mM DTT, pH=7.4 to the final concentration of 50 mM. The hanging drop vapour diffusion[52] using Linbro culture plates[53] at room temperature was used to grow the crystals of the enzyme-inhibitor complex. Equal volume of protein, reservoir solution (1µL each) and various amounts of inhibitor solutions (0.1, 0.5, and 1.0 µL) were mixed and equilibrated against 1 mL of the reservoir solution. The reservoir solution contained saturated ammonium sulfate, 0.2 M NaCl, 2 % dioxane, and 0.1 M sodium citrate buffer (pH 6.0) as reported for the native enzyme crystallisation.[49]

6.4.4 X-ray diffraction

The X-ray diffraction experiments were carried out by Masatoshi Nukui and Mark J. Jedrzejas (Children's Hospital Oakland Research Institute, Oakland, California 94609, USA). The crystals of the enzyme-inhibitor complex were cryoprotected using 30 % xylitol (w/v), 3.5 M ammonium sulfate and 0.1 M sodium citrate buffer (pH 6.0) as reported for the native crystals[9] and frozen in liquid nitrogen. Standard fibre loops[53] of a suitable size were used to pick up and mount the frozen crystals under a nitrogen flow at -180 °C. The X-ray diffraction data for the enzyme-inhibitor complex was collected using rotation (oscillation) photography and Quantum 4u CCD detector. The crystallographic setup of beamline 5.0.1 of the Berkeley Center for Structural Biology, Advanced Light Source, Lawrence Berkeley National Laboratory was used. The collected data were analysed, indexed, integrated, and scaled using the HKL2000 software package.[54] The crystals were isomorphous to the native *S. pneumoniae* hyaluronate lyase crystals.[49] The statistics of the native diffraction data were analysed.

6.4.5 Structure solution and refinement

Structure solution and refinement were carried out by Daniel J. Rigden (National Centre of Genetic Resources and Biotechnology, Cenargen/Embrapa, Brasília, D.F. 70770-900, Brazil).

The structure was solved by rigid body refinement in CNS[55] using the 1.56 Å crystal structure of *S. pneumoniae* hyaluronate lyase (PDB code 1egu;[26]) as a search model. Refinement employed alternating cycles of computational refinement with CNS[55] and manual rebuilding using the programme O.[56] All data were used throughout with no intensity or sigma-based cut-offs applied. SigmaA-weighted map coefficients[57] were used throughout.

An R_{free} value,[55] calculated from 5 % of reflections set aside at the outset, was used to monitor the progress of refinement. Water molecules were placed into 3σ positive peaks in $|F_o\text{-}F_c|$ maps when density was also evident in $|2F_o\text{-}F_c|$ maps and suitable hydrogen bonding partners were available. The ligand L-ascorbic acid-6-hexadecanoate was modelled into the catalytic site according to the strong, immediately evident difference density. Sulfate and xylitol molecules, deriving from the crystallisation and cryo-cooling solutions, respectively, were modelled into suitably shaped regions of electron density. Final statistics for the model are shown in Table 6.2.

Programs of the CCP4 package[58] were applied to manipulations and structural superpositions made with LSQMAN.[59] PYMOL[60] was used for illustrations.

Table 6.2. Crystallographic data and refinement statistics

Space group		$P2_12_12_1$
Unit cell	a (Å)	84.13
	b (Å)	102.71
	c (Å)	102.4
Low resolution diffraction limit (Å)		45.9
High resolution diffraction limit (Å)		1.65
Completeness[1]		99.9 (99.0)
$I/\sigma(I)$[1]		22.8 (1.3)
Multiplicity[1] (%)		5.8 (5.7)

R_{merge}[1] (%)		7.3 (87.5)
Non-hydrogen protein atoms		5835
Sulfate atoms		25
Non-hydrogen atoms xylitol		30
Non-hydrogen atoms compound **2**		27
Non-hydrogen atoms solvent		564
Number of reflections[1]		106633 (9620)
R (%)[1]		19.2 (30.5)
R_{free} (%)[1]		21.1 (31.4)
Mean temperature factor B ($Å^2$)	All atoms	23.9
	Protein	22.2
	Protein main chain	21.2
	Protein side chain	22.5
	Sulfate	46.4
	Xylitol	38.1
	Compound **2**	54.9
	vitamin C moiety	56.5
	palmitoyl moiety	46.8
	Solvent	31.1
rms deviation from ideal values	Bond lengths (Å)	0.005
	Bond angles (º)	1.2

[1] Values in brackets are for the highest resolution shell, 1.65 - 1.60 Å.

6.4.6 Construction of bovine testicular hyaluronidase model

All calculations were done on a SGI OCTANE R10000 workstation. For homology modelling of bovine testicular hyaluronidase (BTH) the crystal structures of bee venom hyaluronidase[16] were used as templates (pdb codes: 1fcq, 1fcu and 1fcv). Since the sequence identity between BTH and bee venom hyaluronidase is only 32 %, a multiple sequence alignment including the human PH-20 protein was performed to get more reliable results. The amino acid sequence of BTH[61] was aligned with the sequences of bee venom hyaluronidase extracted from the crystal structures and of the human PH-20 protein (Swiss-Prot Accession Number: p38567) using the

program ClustalW.[36] After manual refinement of the sequence alignment a homology model was generated with the help of MODELLER version 6.2.[39-41] The resulting model was evaluated for correct local geometry using Procheck[42,43] and the SYBYL module ProTABLE. Then the model was protonated using SYBYL 6.8 (Tripos Inc., St. Louis) and energetically minimised with the AMBER all-atom force field[62] with AMBER all-atom charges (distance dependent dielectricity constant 4) up to a root mean square (rms) gradient of 0.1 kcal/mole•Å (Powell conjugate gradient). Surfaces and lipophilic potentials of the model were calculated and visualised by the program MOLCAD implied in SYBYL 6.8.

6.4.7 Flexible docking of L-ascorbic acid-6-hexadecanoate using FlexX

The 3D structure of **2** was generated with the SYBYL SKETCH module and energetically minimised using the Tripos Force Field with Gasteiger-Hückel charges (distance dependent dielectricity constant 1) up to a root mean square (rms) gradient of 0.05 kcal/mole•Å (Powell conjugate gradient). The binding pocket of BTH was defined by the amino acids within a sphere of 4 Å around Tyr220 and Trp341. All docking calculations were performed with FlexX version 1.12.[63-65] Previous versions of FlexX tended to overestimate affinity of hydrogen bonded ligands and performed poor with relatively lipophilic binding sites.[66] Due to the amphiphilic substrate hyaluronan the active site of BTH consists of many polar, mostly ionic amino acids, but contains also some hydrophobic residues (see Figure 6.5). Therefore we used the recently developed scoring function ScreenScore which incorporates hydrophobic[67] and hydrogen bond score contributions with more realistic weights. It was introduced for use in FlexX by Stahl et al. in a detailed analysis of scoring functions for virtual screening.[66] Apart from water particle placement[64] and ScreenScore as fitness and scoring function, standard parameters were applied. The results were analysed and visualised with FlexV version 1.6 and SYBYL 6.8.

6.5 References

(1) Laurent, T.; Fraser, J. Hyaluronan. *FASEB J* **1992**, *6*, 2397-2405.

(2) Kreil, G. Hyaluronidases - A group of neglected enzymes. *Prot Sci* **1995**, *4*, 1666-1669.

(3) Coutinho, P. M.; Henrissat, B. Carbohydrate-Active Enzymes server at URL: http://afmb.cnrs-mrs.fr/CAZY/, 1999.

(4) Jedrzejas, M. J. Three-dimensional structures of hyaluronate lyases from Streptococcus species and their mechanism of hyaluronan degradation. *Science of Hayluronan Today*; Glycoforum www.glycoforum.gr.jp/science/hyaluronan, 2002.

(5) Jedrzejas, M. J. Pneumococcal virulence factors: structure and function. *Microbiol Mol Biol Rev* **2001***, 65*, 187-207.

(6) Jedrzejas, M. J. Mechanisms of polysaccharide degradation by bacterial enzymes: Degradation of hyaluronan. *Recent Research Developments in Biophysics and Biochemistry*; Research Signpost, 2002; pp 197-225.

(7) Jedrzejas, M. J. Extracellular virulence factors of *Streptococcus pneumoniae*. *Encyclopedia, Extracellular Virulence Factors of Gram-positive Bacteria*, 2003.

(8) Nukui, M.; Taylor, K. B.; McPherson, D. T.; Shigenaga, M. K.; Jedrzejas, M. J. The function of hydrophobic residues in the catalytic cleft of *Streptococcus pneumoniae* hyaluronate lyase. Kinetic characterization of mutant enzyme forms. *J Biol Chem* **2003***, 278*, 3079-3088.

(9) Li, S.; Kelly, S.; Lamani, E.; Ferraroni, M.; Jedrzejas, M. Structural basis of hyaluronan degradation by *Streptococcus pneumoniae* hyaluronate lyase. *EMBO J* **2000***, 19*, 1228-1240.

(10) Li, S.; Jedrzejas, M. J. Hyaluronan binding and degradation by *Streptococcus agalactiae* hyaluronate lyase. *J Biol Chem* **2001***, 276*, 41407-41416.

(11) Kelly, S. J.; Taylor, K. B.; Li, S.; Jedrzejas, M. J. Kinetic properties of *Streptococcus pneumoniae* hyaluronate lyase. *Glycobiology* **2001***, 11*, 297-304.

(12) Hynes, W.; Walton, S. Hyaluronidases of gram-positive bacteria. *FEMS Microbiol Lett* **2000***, 183*, 201-207.

(13) Meyer, K. Hyaluronidases. *The Enzymes*; Academic Press: New York, 1971; pp 307-320.

(14) Csoka, T. B.; Frost, G. I.; Wong, T.; Stern, R. Purification and microsequencing of hyaluronidase isozymes from human urine. *FEBS Lett* **1997***, 417*, 307-310.

(15) Csoka, A. B.; Frost, G. I.; Stern, R. The six hyaluronidase-like genes in the human and mouse genomes. *Matrix Biol* **2001***, 20*, 499-508.

(16) Markovic-Housley, Z.; Miglinerini, G.; Soldatova, L.; Rizkallah, P.; Müller, U. et al. Crystal Structure of Hyaluronidase, a Major Allergen of Bee Venom. *Structure* **2000***, 8*, 1025-1035.

(17) Cherr, G. N.; Yudin, A. I.; Overstreet, J. W. The dual functions of GPI-anchored PH-20: hyaluronidase and intracellular signaling. *Matrix Biol* **2001***, 20*, 515-525.

(18) Lepperdinger, G.; Mullegger, J.; Kreil, G. Hyal2--less active, but more versatile? *Matrix Biol* **2001***, 20*, 509-514.

(19) Lin, G.; Stern, R. Plasma hyaluronidase (Hyal-1) promotes tumor cell cycling. *Cancer Lett* **2001***, 163*, 95-101.

(20) Wolf, R. A.; Glogar, D.; Chaung, L. Y.; Garrett, P. E.; Ertl, G. et al. Heparin inhibits bovine testicular hyaluronidase activity in myocardium of dogs with coronary artery occlusion. *Am J Cardiol* **1984***, 53*, 941-944.

(21) Kuppusamy, U.; Khoo, H.; Das, N. Structure-activity studies of flavonoids as inhibitors of hyaluronidase. *Biochem Pharmacol* **1990***, 40*, 397-401.

(22) Suzuki, A.; Toyoda, H.; Toida, T.; Imanari, T. Preparation and inhibitory activity on hyaluronidase of fully *O*-sulfated hyaluro-oligosaccharides. *Glycobiology* **2001***, 11*, 57-64.

(23) Toida, T.; Ogita, Y.; Suzuki, A.; Toyoda, H.; Imanari, T. Inhibition of hyaluronidase by fully *O*-sulfonated glycosaminoglycans. *Arch Biochem Biophys* **1999***, 370*, 176-182.

(24) Mio, K.; Stern, R. Inhibitors of the hyaluronidases. *Matrix Biol* **2002***, 21*, 31-37.

(25) Akhtar, M. S.; Bhakuni, V. *Streptococcus pneumoniae* hyaluronate lyase contains two non-cooperative independent folding/unfolding structural domains: characterization of functional domain and inhibitors of enzyme. *J Biol Chem* **2003***, 278*, 25509-25516.

(26) Li, S.; Taylor, K. B.; Kelly, S. J.; Jedrzejas, M. J. Vitamin C inhibits the enzymatic activity of *Streptococcus pneumoniae* hyaluronate lyase. *J Biol Chem* **2001***, 276*, 15125-15130.

(27) Klein, E.; Weber, N. In vitro test for the effectiveness of antioxidants as inhibitors of thiyl radical-induced reactions with unsaturated fatty acids. *J Agric Food Chem* **2001***, 49*, 1224-1227.

(28) Mitra, A.; Govindwar, S.; Joseph, P.; Kulkarni, A. Inhibition of human term placental and fetal liver glutathione-S-transferases by fatty acids and fatty acid esters. *Toxicol Lett* **1992***, 60*, 281-288.

(29) Hoechstetter, J.; Oettl, M.; Asen, I.; Molz, R.; Bernhardt, G. et al. The pH activity profile of bovine testicular hyaluronidase depends on the type of assay. *DPhG Jahrestagung*: Berlin, 2003.

(30) Scott, J. E. Secondary structures in hyaluronan solutions: chemical and biological implications. *The Biology of Hyaluronan.*; Ciba Foundation Symposium, 1989; pp 6-14.

(31) Simpson, G. L.; Ortwerth, B. J. The non-oxidative degradation of ascorbic acid at physiological conditions. *Biochim Biophys Acta* **2000***, 1501*, 12-24.

(32) Quiocho, F. A.; Vyas, N. K. *Bioinorganic Chemistry: Carbohydrates*; Oxford University Press: New York, 1999; pp 441-457.

(33) Jedrzejas, M. J.; Mello, L. V.; De Groot, B. L.; Li, S. Mechanism of hyaluronan degradation by *Streptococcus pneumoniae* hyaluronate lyase: Structures of complexes with the substrate. *J Biol Chem* **2002**.

(34) Nishibata, Y.; Itai, A. Automatic creation of drug candidate structures based on receptor structure. Starting point for artificial lead generation. *Tetrahedron* **1991***, 47*, 8985-8990.

(35) Sanchez, R.; Sali, A. Comparative protein structure modeling. Introduction and practical examples with modeller. *Methods Mol Biol* **2000***, 143*, 97-129.

(36) Thompson, J. D.; Higgins, D. G.; Gibson, T. J. CLUSTAL W: improving the sensitivity of progressive multiple sequence alignment through sequence weighting, position-specific gap penalties and weight matrix choice. *Nucleic Acids Res* **1994***, 22*, 4673-4680.

(37) Arming, S.; Strobl, B.; Wechselberger, C.; Kreil, G. In vitro mutagenesis of PH-20 hyaluronidase from human sperm. *Eur J Biochem* **1997***, 247*, 810-814.

(38) Markovic-Housley, Z.; Schirmer, T. Structural Evidence for substrate assisted catalytic mechanism of bee venom hyaluronidase, a major allergen of bee venom. *Carbohydrate Bioengineering: Interdisciplinary Approaches*; RCS: London, 2002; pp 19-27.

(39) Marti-Renom, M. A.; Stuart, A. C.; Fiser, A.; Sanchez, R.; Melo, F. et al. Comparative protein structure modeling of genes and genomes. *Annu Rev Biophys Biomol Struct* **2000***, 29*, 291-325.

(40) Sali, A.; Blundell, T. L. Comparative protein modelling by satisfaction of spatial restraints. *J Mol Biol* **1993***, 234*, 779-815.

(41) Fiser, A.; Do, R. K.; Sali, A. Modeling of loops in protein structures. *Protein Sci* **2000***, 9*, 1753-1773.

(42) Laskowski, R. A.; MacArthur, M. W.; Moss, D. S.; Thornton, J. M. PROCHECK: a program to check the stereochemical quality of protein structures. *J Appl Crystallogr* **1993***, 26*, 283-291.

(43) Morris, A. L.; MacArthur, M. W.; Hutchinson, E. G.; Thornton, J. M. Stereochemical quality of protein structure coordinates. *Proteins* **1992***, 12*, 345-364.

(44) Brameld, K. A.; Shrader, W. D.; Imperiali, B.; Goddard, W. A., 3rd Substrate assistance in the mechanism of family 18 chitinases: theoretical studies of potential intermediates and inhibitors. *J Mol Biol* **1998***, 280*, 913-923.

(45) van Aalten, D. M.; Komander, D.; Synstad, B.; Gaseidnes, S.; Peter, M. G. et al. Structural insights into the catalytic mechanism of a family 18 exo-chitinase. *Proc Natl Acad Sci U S A* **2001***, 98*, 8979-8984.

(46) Cramer, J. A.; Bailey, L. C.; Bailey, C. A.; Miller, R. T. Kinetic and mechanistic studies with bovine testicular hyaluronidase. *Biochim Biophys Acta* **1994***, 1200*, 315-321.

(47) Jedrzejas, M. J.; Mewbourne, R. B.; Chantalat, L.; McPherson, D. T. Expression and purification of *Streptococcus pneumoniae* hyaluronate lyase from *Escherichia coli*. *Protein Expr Purif* **1998***, 13*, 83-89.

(48) Jedrzejas, M. Structural and Functional Comparison of Polysaccharide-Degrading Enzymes. *Crit Rev Biochem Mol Biol* **2000***, 35*, 221-251.

(49) Jedrzejas, M. J.; Chantalat, L.; Mewbourne, R. B. Crystallization and preliminary X-ray analysis of *Streptococcus pneumoniae* hyaluronate lyase. *J Struct Biol* **1998***, 121*, 73-75.

(50) Pace, C. N.; Vajdos, F.; Fee, L.; Grimsley, G.; Gray, T. How to measure and predict the molar absorption coefficient of a protein. *Protein Sci* **1995***, 4*, 2411-2423.

(51) Di Ferrante, N. Turbidimetric measurement of acid mucopolysaccharides and hyaluronidase activity. *J Biol Chem* **1956***, 220*, 303-306.

(52) McPherson, A. *Crystallization of Biological Molecules*; Cold Spring Harbor Laboratory Press: Cold Spring Harbor, New York, 1999.

(53) HamptonResearch Hampton Research Catalog; Hampton Research Inc.: Laguna Hills, CA, 2003.

(54) Otwinowski, Z.; Minor, W. Processing of X-ray diffraction data collected in oscillation mode. *Methods Enzymol* **1997***, 276*, 307-326.

(55) Brunger, A. T.; Adams, P. D.; Clore, G. M.; DeLano, W. L.; Gros, P. et al. Crystallography & NMR system: A new software suite for macromolecular structure determination. *Acta Crystallogr D Biol Crystallogr* **1998***, 54 (Pt 5)*, 905-921.

(56) Jones, T. A.; Zou, J. Y.; Cowan, S. W.; Kjeldgaard Improved methods for building protein models in electron density maps and the location of errors in these models. *Acta Crystallogr A* **1991***, 47 (Pt 2)*, 110-119.

(57) Read, R. J. Improved Fourier coefficients for maps using phases from partial structures with errors. *Acta Cristallograph A* **1986***, 42*, 140-149.

(58) Collaborative Computational Project, N. The CCP4 suite: Programs for protein crystallography. *Acta Cristallograph. D* **1994***, 50*, 760-763.

(59) Kleywegt, G. J. Experimental assessment of differences between related protein crystal structures. *Acta Crystallogr D Biol Crystallogr* **1999***, 55*, 1878-1884.

(60) DeLano, W. L. *The PyMOL Molecular Graphics System at http://www.pymol.org*.

(61) Meyer, M. F.; Kreil, G.; Aschauer, H. The soluble hyaluronidase from bull testes is a fragment of the membrane-bound PH-20 enzyme. *FEBS Lett* **1997***, 413*, 385-388.

(62) Cornell, W. D.; Cieplak, P.; Bayly, C. I.; Gould, I. R.; Merz, K. M., Jr. et al. A Second Generation Force Field for the Simulation of Proteins, Nucleic Acids, and Organic Molecules. *J Am Chem Soc* **1995***, 117*, 5179-5197.

(63) Rarey, M.; Kramer, B.; Lengauer, T. Multiple automatic base selection: protein-ligand docking based on incremental construction without manual intervention. *J Comput Aided Mol Des* **1997***, 11*, 369-384.

(64) Rarey, M.; Kramer, B.; Lengauer, T. The particle concept: placing discrete water molecules during protein- ligand docking predictions. *Proteins* **1999***, 34*, 17-28.

(65) Rarey, M.; Kramer, B.; Lengauer, T.; Klebe, G. A fast flexible docking method using an incremental construction algorithm. *J Mol Biol* **1996***, 261*, 470-489.

(66) Stahl, M.; Rarey, M. Detailed analysis of scoring functions for virtual screening. *J Med Chem* **2001***, 44*, 1035-1042.

(67) Gehlhaar, D. K.; Verkhivker, G. M.; Rejto, P. A.; Sherman, C. J.; Fogel, D. B. et al. Molecular recognition of the inhibitor AG-1343 by HIV-1 protease: conformationally flexible docking by evolutionary programming. *Chem Biol* **1995***, 2*, 317-324.

Chapter 7 3D pharmacophore derivation for structure-based ligand design of hyaluronate lyase inhibitors

7.1 Introduction

The interaction of biologically active ligands with biopolymers, mostly proteins (receptors, enzymes, ion channels), at the molecular level is the fundamental key for rational drug design which at best needs structural information about both of the interacting molecules. Therefore, the preferred starting points for rational drug design are three-dimensional (3D) structures of protein targets.[1,2]

If a 3D structure is available, three distinct design strategies may be pursued depending on additional information about the target of interest. The most laborious case applies if the binding site is unknown. Then pockets or cavities predominating as binding sites may be detected by computational tools like LIGSITE,[3] PASS,[4] SiteID[5] etc. In the second case, the approximate binding region is known, but no specific interactions between ligands and individual amino acids have been identified. This requires a careful search for sites most favourable for interaction. Suitable programmes in that respect are LUDI,[6,7] SUPERSTAR,[8] and GRID[9] etc. which identify ´hot spots´ of binding. This knowledge can be transferred into pharmacophore models for database searching. The most straightforward case applies if the binding site and crystal structures complexed with ligands are known. Based on the exploration of individual interactions and spatial conditions, docking and virtual screening approaches are possible.[1] Recently, the latter approaches were successfully combined in *de novo* ligand design projects using protein-derived 3D pharmacophores in virtual screening.[10-12]

In this chapter, the binding modes of two inhibitors (see Figure 7.1) co-crystallised with *S. pneumoniae* hyaluronate lyase (hylSpn) are compared (see also chapter 6 and reference [13]). In consideration of this analysis and with the help of the programmes LUDI and GRID, hylSpn regions where H-bond donor, H-bond acceptor and hydrophobic moieties of inhibitors most favourably bind are identified and trans-

ferred into a 3D pharmacophore model. This model might serve as basis for a virtual screening approach with UNITY or CATALYST.

7.2 Results and discussion

7.2.1 Comparison of binding modes of a 2-phenylindole based inhibitor and L-ascorbic acid-6-hexadecanoate at *S. pneumoniae* hyaluronidase

The detection of indole-2-carboxylic acid as hit in LUDI searches for bacterial hyaluronate lyase inhibitors (see chapter 3) has inspired us to investigate further 2-substituted indole derivatives.[13] By means of X-ray crystallography, the binding mode of one of these compounds, sulfamic acid 1-decyl-2-(4-sulfamoyloxy-phenyl)-1*H*-indol-6-yl ester (**1**) at hylSpn was elucidated (see Figure 7.2).[13,14] Hydrophobic interactions of the rings and the aliphatic chain as well as hydrogen bonds with the sulfonamide group in position 6 of the indole moiety are obvious. The indole ring is bound on one side by Trp292, with both ring planes stacking at proper distance. The other side of the indole ring is in contact with the guanidinium group of Arg462. Such cation-π interactions can be highly favourable.[15] The phenyl moiety forms an approximately perpendicular ring arrangement with Trp291. The aliphatic tail fits in a surface crevice shaped mainly by the hydrophobic residues Met579, Trp291 and Phe343. The sulfamoyloxy group (attached to the phenyl moiety) for which electron density was completely lacking is presumably oriented outwards and solvent-exposed.

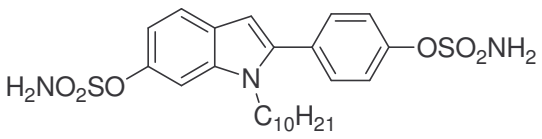

1

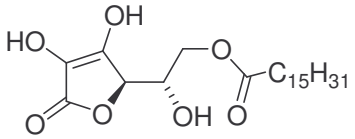

2

Figure 7.1. Chemical structures of the hyaluronate lyase inhibitors sulfamic acid 1-decyl-2-(4-sulfamoyloxy-phenyl)-1*H*-indol-6-yl ester (**1**) and L-ascorbic acid-6-hexadecanoate (**2**).

As shown in chapter 6, the binding mode of L-ascorbic acid-6-hexadecanoate (**2**), the representative member of a series of novel hyaluronate lyase inhibitors, at hylSpn was determined by X-ray crystallography, too. As depicted in Figure 7.2 for comparison with compound **1**, the binding of the different inhibitors causes no significant

conformational changes in the protein structure. The unexpectedly ring-opened vitamin C moiety of **2** (see chapter 6) binds in exactly the same position of the catalytic site as the indole ring of **1**. Also the aliphatic tails of both compounds (in the case of **2** with 16 carbons of which 13 were detected) binds in the same surface crevice with similar orientation. Only the conformations of the aliphatic chains are slightly different due to the presence of the phenyl ring in compound **1**. In particular, the tail of **1** binds closer to Tyr408 and His399. A further difference is evident at the distal end of the chains. The shorter length of the tail of **1** enables the distal end to dock into a surface pocket, whereas the terminus of the palmitoyl group of L-ascorbic acid-6-hexadecanoate is solvent-exposed.

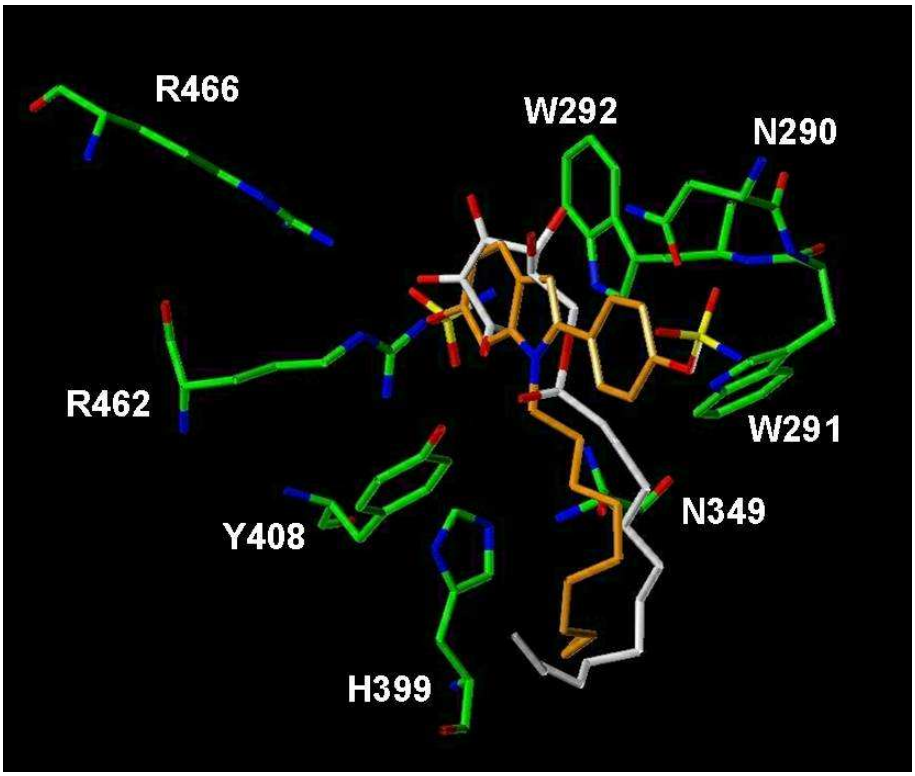

Figure 7.2. Comparison of binding modes of the *S. pneumoniae* hyaluronate lyase inhibitors sulfamic acid 1-decyl-2-(4-sulfamoyloxy-phenyl)-1*H*-indol-6-yl ester (**1**, carbon atoms coloured in orange) and L-ascorbic acid-6-hexadecanoate (**2**, carbon atoms coloured in grey).

7.2.2 Development of a 3D pharmacophore derived from inhibitor binding sites

An important basis of structure-based ligand design is the exact knowledge of the ligand binding sites mostly deduced by crystallographic complexes. Recently, a strategy of virtual database screening using 3D pharmacophores derived from the crystal structures proved to be very efficient with respect to lead finding. In this procedure,

the essential binding features of complexed ligands are considered and favourable interaction sites are calculated, resulting in a complex pharmacophore used for virtual screening.[10,11]

The programmes LUDI[6,7] and GRID version 21[9] were applied to highlight those areas of the binding site where putative ligands can interact with the protein. LUDI places potential interaction sites for hydrogen bond donors, acceptors and hydrophobic groups within the binding pocket according to a set of rules which have been derived from composite crystal-field environments observed in the crystal packing of small organic molecules.[16] GRID is based on a force-field approach. The interaction potential is calculated for a variety of different probes at the intersections of a regularly spaced grid embedded in the binding pocket.

The binding pocket was systematically searched with three probes: a lipophilic probe and two probes representing H-bond acceptors and donors, respectively. LUDI and GRID highlighted qualitatively similar regions called ’hot spots’ but the maps differed quantitatively due to different relative weightings. As shown in Figure 7.3A, placement of an NH group in a ligand is favourable between the amino acid residues Asn349 and His399 as well as below Trp292 (centre of figure). A rather large ‘hot spot’ is situated below Asn349, approximately at the distal end of the decyl tail of compound **1** (see Figure 7.2), resulting from the amino acid residues Glu388 and Asp398 (not shown in Figure 7.3A). This region is only accessible for ligands with rather large substituents like compound **1** (see above). All other ‘hot spots’ lie beyond the ‘inner’ active site of hylSpn, thus probably inaccessible by small lead structures.

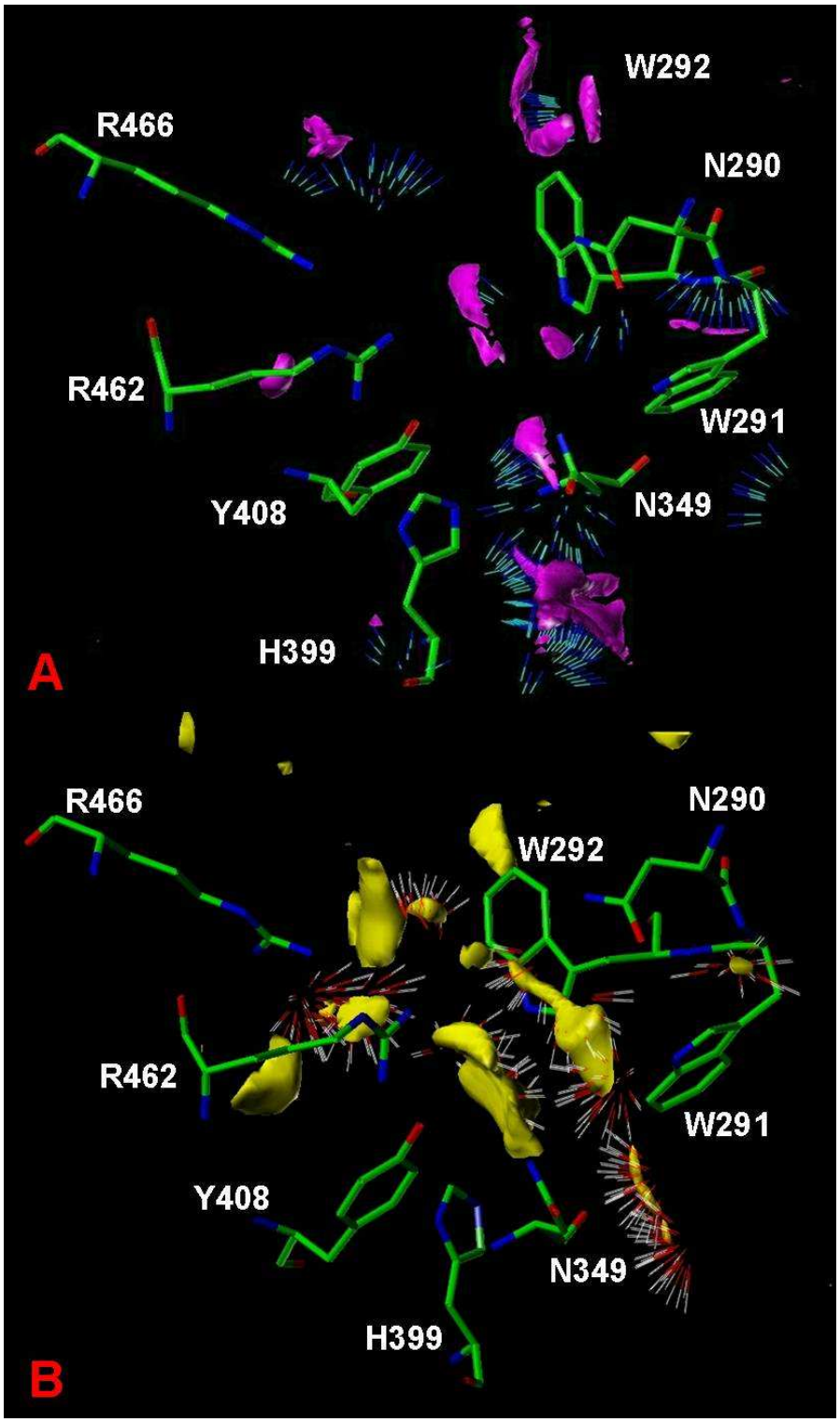

Figure 7.3. Putative binding 'hot spots' in hylSpn. **A**) Possible positioning of hydrogen donor groups in ligands. LUDI interaction sites generated for a NH group are shown as vectors. GRID contour surfaces are coloured in magenta. **B**) Possible positioning of hydrogen acceptor groups in ligands. LUDI interaction sites generated for a C=O group are shown as vectors. GRID contour surfaces are coloured in yellow.

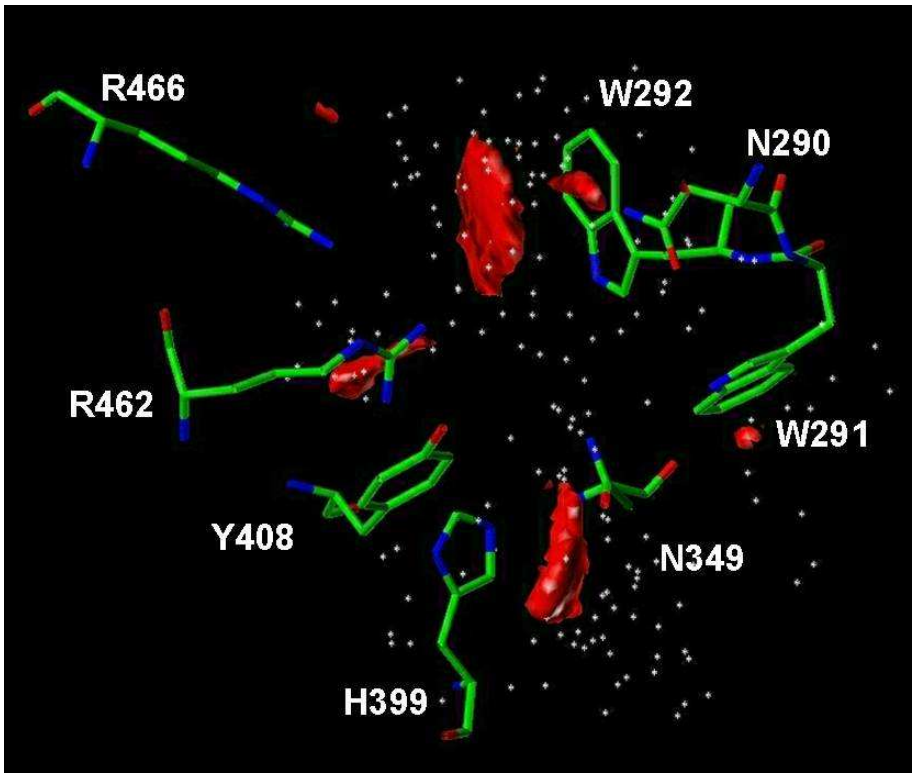

Figure 7.4. Putative hydrophobic 'hot spots' in hylSpn. Possible positioning of lipophilic groups in ligands. LUDI interaction sites generated for a lipophilic carbon atom are shown as dots. GRID contour surfaces are coloured in red.

The H-bond acceptor 'hot spots' induced by Arg462 and Arg466 as well as Arg462, Tyr408 and Asn349 (centre of the figure) are rather distinct. An additional 'hot spot' results from the NH group of Trp291.

The hydrophobic regions can be visualised more easily by the GRID maps (see Figure 7.4) because of the wide scattering of the hydrophobic centres calculated by LUDI. However, increased density of these centres is observed along the side chains and parallel to the ring planes of Trp292 and His399, coinciding with the GRID maps. The lower hydrophobic region is also induced by Met579 (not shown in Figure 7.4).

The 'hot spots' for each of the three probes could be converted into a 3D pharmacophore model that might be queried by the database mining programmes UNITY[5] or CATALYST.[17] A schematic representation of this pharmacophore in relation to the position of compound **1** in the crystal structure is depicted in Figure 7.5. One H-bond donor region is located above the carbonyl group of the side chain of Asn349 (see Figure 7.3A). Four regions for favourable placement of H-bond acceptors in the molecules due to Asn349, Tyr408 and Arg462/Arg466 are placed in the centre of the search sphere (see Figure 7.3B). Additionally, the two large hydrophobic regions (see Figure 7.4) described above are included in the pharmacophore.

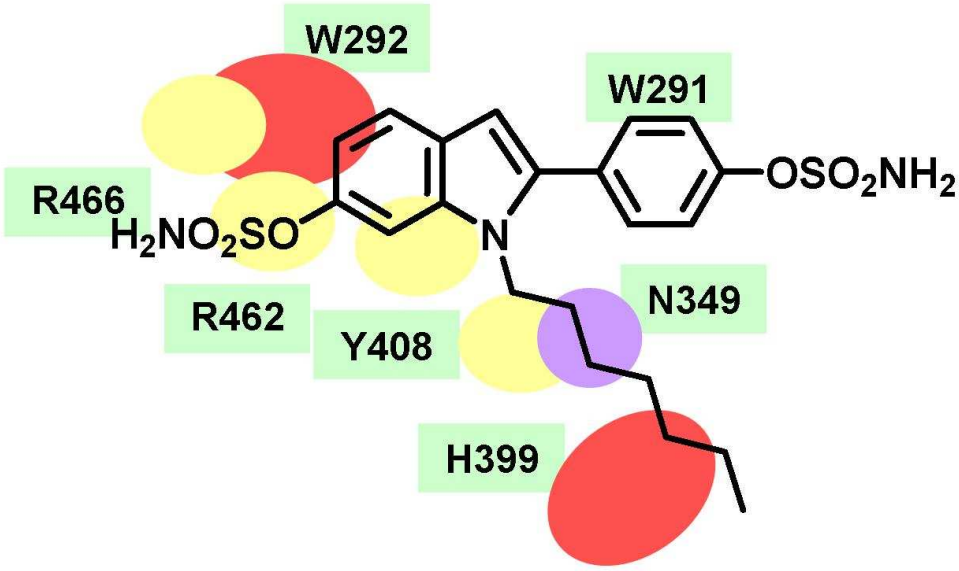

Figure 7.5. Schematic representation of the 3D pharmacophore model derived from the 'hot spots'. Hydrophobic regions (red), hydrogen donor (magenta) and hydrogen acceptor sites (yellow) are depicted as ellipses and arranged in relation to the position of compound **1** in the crystal structure.

7.2.3 Hyaluronate lyase inhibitor design based on known binding modes

For reasons of economy we have not purchased database mining programmes for queries with the 3D pharmacophore described above up to now. However, this model as well as the binding modes of compounds **1** and **2** compared in Figure 7.2 may serve for the design of novel hyaluronate lyase inhibitors on the basis of the following rational considerations, too.

The first question is whether the structure-activity relationships (SAR) of 2-phenylindole derivatives, e.g. compound **1** and compounds **6a-f** (see Table 7.1 and reference [13]) correlate with the pharmacophore model. (Of course, this implies that the binding modes of the inhibitors at hylSpn and $hylB_{4755}$ are similar. This may be anticipated because of the very high sequence identity of the active sites.) Comparing the activities of compounds **6a** and **6b**, the methyl group in position 3 does not lead to significant loss of inhibitory activity. Thus, due to increased compound stability, the 3-Me substituent was retained in compounds **6c-f**.[13]

By simple inspection of Figure 7.2, a binding mode of compounds **6b-f** analogous to that of compound **1** with directly overlaying indole moieties seems to be less probable. Presumably, the additional methyl group would lead to bumps with the amino acid residue Asn290. The distance between the nitrogen atom of the asparagine residue and the carbon atom C-3 of the indole ring is only 2.9 Å, so that the required space for a methyl group would be too small. Possibly the side chain of Asn290 is rotated, thereby eliminating any sterical hindrance. Furthermore, the coplanar orientation of the phenyl and the indole ring as observed for compound **1** in the crystal structure could be more or less distorted. Interestingly, the introduction of a 5-hydroxy substituent in compounds **6a-f** does not generally reduce the inhibitory activity compared to the 6-sulfamoyloxy group in **1**. It may therefore be concluded that the 5-OH oxygen atom occupies one of the H-bond acceptor regions depicted in Figures 7.3B and 7.5. The increasing $hylB_{4755}$ inhibition with increasing chain length of the alkyl substituents at the nitrogen atom of the indole moiety clearly indicates that the binding mode of compounds **6c-f** is similar to that found for compound **1**. Probably, the aliphatic chains occupy the same crevice as the decyl substituent of compound **1**. The 'hot spot' analysis for the hydrophobic map supports the SAR because favourable hydrophobic interactions (see Figure 7.4) were proposed where the aliphatic tails of compounds **1** and **2** are found in the X-ray structures (see Figure 7.2). In conclusion, the SAR of compounds **6a-f** are largely compatible with the 3D pharmacophore model derived above.

Based on the identification of 1,3-diacetylbenzimidazole-2-thione (**3**, Figure 7.6) as hyaluronate lyase inhibitor (see chapter 3), benzoxazole-2-thione derivatives (**4**) were found to inhibit $hylB_{4755}$.[18] All inhibitors of the benzoxazole type (**4**) found to date incorporate an alkoxy chain as substituent at the nitrogen atom (R = CH_3 and C_5H_{11}).[18] The SAR of the 2-phenylindole derivatives are reproduced since $hylB_{4755}$ inhibition is increased with increasing chain length of R. It may therefore be concluded that both benzoxazole-2-thione derivatives have a binding mode similar to that of compound **1**, i.e., the benzoxazole moiety overlays with the indole moiety and the alkoxy substituents of **4** point into the same direction like the aliphatic tail of compound **1**. In this case, the amide oxygen might even occupy one of the hydrogen acceptor sites (see Figures 7.2, 7.3B and 7.5).

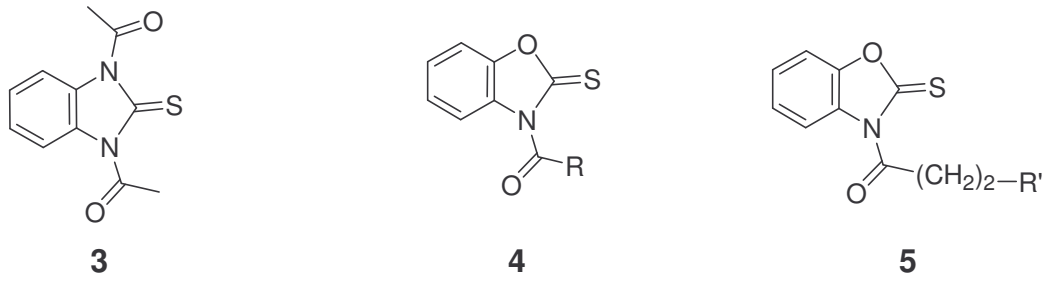

Figure 7.6. Chemical structures of hylB$_{4755}$ inhibitors 1,3-diacetylbenzimidazole-2-thione (**3**), benzoxazole-2-thiones **4** and the proposed derivatives **5**.

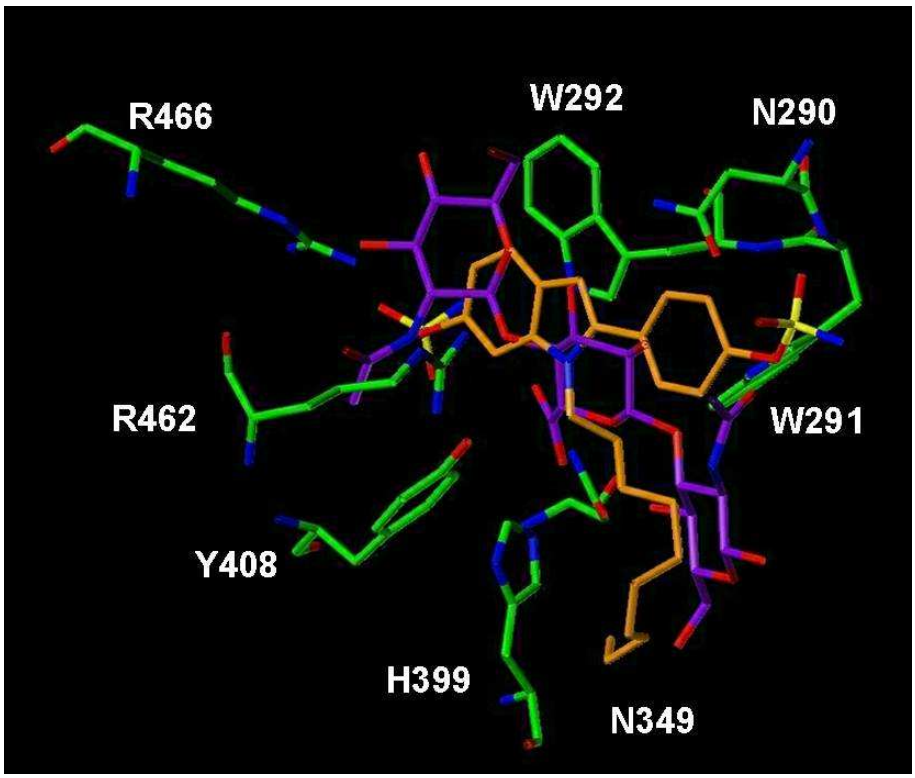

Figure 7.7. Comparison of binding modes of hylSpn inhibitor sulfamic acid 1-decyl-2-(4-sulfamoyloxyphenyl)-1*H*-indol-6-yl ester (**1**, carbon atoms orange) and a substrate-based hexasaccharide (carbon atoms purple, for sake of clarity only a trisaccharide moiety is shown).

Starting from these considerations, a comparison of the binding modes of compound **1** and a substrate-based hexasaccharide was envisaged to rationally derive novel benzoxazole derivatives with the help of observed crystallographic hylSpn data. As shown in Figure 7.7, the depicted trisaccharide overlaps with compound **1**. Focussing on substituents at the nitrogen atom of the benzoxazole moiety, 3-substituted propionic acid derivatives are promising since a *N*-acetylglucosamine residue of the HA substrate is observed in the region where the methylene groups 4 and 5 of the decyl substituent of compound **1** are found (Figure 7.7).

Table 7.1. IC_{50} values of the synthesised 2-phenylindole derivatives (**1**, **6a-f**) determined on the hyaluronate lyase $hylB_{4755}$ (n=3; SEM not larger than 1 %)[13]

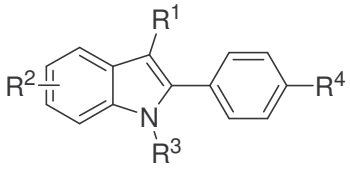

1, 6a-f

No.	Substitution				$hylB_{4755}$ IC_{50}/µM or (% inhibition)[a]	
	R^1	R^2	R^3	R^4	pH 5.0	pH 7.4
1	H	6-OSO_2NH_2	$C_{10}H_{21}$	OSO_2NH_2	**11**	**16**
6a	H	5-OH	H	OH	(75 %)[b]	**160**
6b	CH_3	5-OH	H	OH	**740**	**280**
6c	CH_3	5-OH	CH_3	OH	**480**	**220**
6d	CH_3	5-OH	C_3H_7	OH	**220**	**160**
6e	CH_3	5-OH	C_5H_{11}	OH	**23**	**36**
6f	CH_3	5-OH	C_7H_{15}	OH	**26**	**12**

[a] at concentrations ≤ 100 µM unless otherwise indicated
[b] 1000 µM

Based on this assumption, all proposals should share a common motif (derivatives **5**, Figure 7.6): a benzoxazole moiety as anchor in the upper part of the binding site, a propionic acid as spacer, and a variety of ring-based substituents as R' like morpholine, piperazine, cyclohexyl, phenyl, 4-carboxyphenyl etc. occupying the space of the *N*-acetylglucosamine residue. The synthesis of representative compounds is subject of ongoing work. Very recently, the phenyl derivative of **5** (R' = Ph) was found to be a potent inhibitor of $hylB_{4755}$ with an IC_{50} value of 15 µM at pH 5.0 (optimum pH).[18] This promising result strengthens the proposed structure-based design strategy.

7.3 Summary

Starting from elucidation of two hyaluronate lyase-inhibitor complexes, the binding modes of sulfamic acid 1-decyl-2-(4-sulfamoyloxy-phenyl)-1*H*-indol-6-yl ester (**1**) and L-ascorbic acid-6-hexadecanoate (**2**) were analysed revealing that the unexpectedly ring-opened vitamin C portion of **2** binds in exactly the same part of the catalytic site as the indole ring of **1**. Additionally, the long aliphatic substituents of both compounds bind in the same surface crevice. With the help of the programmes LUDI and GRID, regions where H-bond donor, H-bond acceptor and hydrophobic moieties of inhibitors may bind most favourably were identified and transferred into a 3D pharmacophore model. This model might serve as basis for a virtual screening approach with UNITY or CATALYST.

The analysis of known SAR of 2-phenylindole derivatives with respect to the observed binding mode of compound **1** at hylSpn and to the 3D pharmacophore model led to suggestions for the binding mode of benzoxazole-2-thione derivatives (**4**). Based on the superposition of the crystal structure of hylSpn in complex with compound **1** and a substrate-based hexasaccharide, novel benzoxazole-2-thiones (**5**) with 3-substituted propionic acid groups at the nitrogen atom were predicted as putative hyaluronate lyase inhibitors. Very recently, this design strategy was confirmed by the phenyl derivative of **5** which is a potent inhibitor of $hylB_{4755}$ with an IC_{50} value of 15 µM.

7.4 Theoretical methods

7.4.1 Analysis and comparison of the crystal structures of *S. pneumoniae* hyaluronate lyase in complex with a 2-phenylindole based inhibitor and L-ascorbic acid-6-hexadeacanoate

The crystal structures of *S. pneumoniae* hyaluronate lyase in complex with sulfamic acid 1-decyl-2-(4-sulfamoyloxy-phenyl)-1*H*-indol-6-yl ester[13] and L-ascorbic acid-6-hexadeacanoate (chapter 6) were elucidated in cooperation with M. J. Jedrzejas (Children's Hospital Oakland Research Institute, Oakland, California) and D. Rigden (National Centre of Genetic Resources and Biotechnology, Cenargen/Embrapa, Brasília, Brazil). After superposition of both crystal structures common features of both binding modes were extracted for further structure-based inhibitor design.

7.4.2 Protein-derived pharmacophore

A pharmacophore has been developed by directly extracting favourable interaction sites from the region of the hylSpn crystal structure where the inhibitors bind. To highlight those areas of the binding site where a putative ligand can favourably interact with the protein, we applied LUDI[6,7] and GRID[9] as alternative methods. The active site of hylSpn derived from the binding pockets of the aforementioned co-crystallised ligands (see reference [13] and chapter 6) was systematically searched for favourable interactions with the following functional groups: C=O (H-bond acceptor), an amide NH group (H-bond donor), and a lipophilic group to describe hydrophobic interactions. The centre of the LUDI search sphere with a radius of 10 Å is defined so that both co-crystallised ligands are centred and fully enclosed in the sphere. In the case of GRID, the O and N1 probes as well as the lipophilic DRY probe were selected for the analysis. The side length of the grid box is set to 10 Å, and its centre coincides with that defined for the LUDI calculation. In addition, all lipophilic moieties observed in crystal structures of protein-ligand complexes with hylSpn were superimposed in order to merge the information from the different contouring methods with those of the known binding modes.

7.4.3 References

(1) Sotriffer, C.; Klebe, G. Identification and mapping of small-molecule binding sites in proteins: computational tools for structure-based drug design. *Farmaco* **2002***, 57*, 243-251.

(2) Klebe, G.; Grädler, U.; Grüneberg, S.; Krämer, O.; Gohlke, H. Understanding receptor-ligand interactions as a prerequisite for virtual screening. *Virtual Screening for Bioactive Molecules*; Wiley-VCH: Weinheim, 2000; pp 207-227.

(3) Hendlich, M.; Rippmann, F.; Barnickel, G. LIGSITE: automatic and efficient detection of potential small molecule-binding sites in proteins. *J Mol Graph Model* **1997***, 15*, 359-363, 389.

(4) Brady, G. P., Jr.; Stouten, P. F. Fast prediction and visualization of protein binding pockets with PASS. *J Comput Aided Mol Des* **2000***, 14*, 383-401.

(5) Tripos Inc., St. Louis, Missouri, USA. www.tripos.com.

(6) Böhm, H. J. The computer program LUDI: a new method for the de novo design of enzyme inhibitors. *J Comput Aided Mol Des* **1992***, 6*, 61-78.

(7) Böhm, H. J. LUDI: rule-based automatic design of new substituents for enzyme inhibitor leads. *J Comput Aided Mol Des* **1992***, 6*, 593-606.

(8) Boer, D. R.; Kroon, J.; Cole, J. C.; Smith, B.; Verdonk, M. L. SuperStar: comparison of CSD and PDB-based interaction fields as a basis for the prediction of protein-ligand interactions. *J Mol Biol* **2001***, 312*, 275-287.

(9) Goodford, P. J. A computational procedure for determining energetically favorable binding sites on biologically important macromolecules. *J Med Chem* **1985**, *28*, 849-857.

(10) Grüneberg, S.; Stubbs, M. T.; Klebe, G. Successful virtual screening for novel inhibitors of human carbonic anhydrase: strategy and experimental confirmation. *J Med Chem* **2002**, *45*, 3588-3602.

(11) Brenk, R.; Naerum, L.; Grädler, U.; Gerber, H. D.; Garcia, G. A. et al. Virtual screening for submicromolar leads of tRNA-guanine transglycosylase based on a new unexpected binding mode detected by crystal structure analysis. *J Med Chem* **2003**, *46*, 1133-1143.

(12) Greenidge, P. A.; Merette, S. A.; Beck, R.; Dodson, G.; Goodwin, C. A. et al. Generation of ligand conformations in continuum solvent consistent with protein active site topology: application to thrombin. *J Med Chem* **2003**, *46*, 1293-1305.

(13) Salmen, S. Inhibitors of bacterial and mammalian hyaluronidases: synthesis and structure-activity relationships; University of Regensburg: Regensburg, 2003.

(14) Rigden, D. personal communication, 2003.

(15) Gallivan, J. P.; Dougherty, D. A. Cation-pi interactions in structural biology. *Proc Natl Acad Sci U S A* **1999**, *96*, 9459-9464.

(16) Klebe, G. The use of composite crystal-field environments in molecular recognition and the de novo design of protein ligands. *J Mol Biol* **1994**, *237*, 212-235.

(17) Gorham, S. D.; Olavesen, A. H.; Dodgson, K. S. Effect of ionic strength and pH on the properties of purified bovine testicular hyaluronidase. *Connective Tissue Research* **1975**, *3*, 17-25.

(18) Braun, S. personal communication, 2003.

Chapter 8 Summary

Hyaluronan and hyaluronidases have been used in several medical fields for many years. For example, sodium hyaluronate is frequently applied in the treatment of osteoarthritis, whereas preparations of bovine testicular hyaluronidase are useful in the therapy of different diseases in internal medicine, ophthalmology and orthopaedia. It has been reported that some hyaluronidases play a role in, e.g., meningitis, septicaemia, arthroses and cancer. To further investigate the function of hyaluronic acid and hyaluronidases in physiological and pathophysiological processes, selective and potent hyaluronidase inhibitors are required. Originated by the lack of such compounds, the main goal of this thesis was the prediction and selection of lead-like structures by *de novo* ligand design and virtual screening of generated compound libraries.

For structure-based ligand design with the *de novo* design programme LUDI, a homology model of *S. agalactiae* strain 4755 hyaluronate lyase was constructed starting from two crystal structures of the related enzymes from *S. pneumoniae* and *S. agalactiae* strain 3502. Screening of the three databases LeadQuest® Vol. 1&2, Accelrys and the adapted ChemACX database (ChemACXF) resulted in 1275 hits. Of the 19 compounds selected for synthesis and testing, 13 were active on S. *agalactiae* strain 4755 hyaluronan lyase in the milli- and submillimolar range.‡‡‡ 1,3-Diacetylbenzimidazole-2-thione was identified to be one of the most potent inhibitors of hyaluronate lyases described to date (IC_{50} values of 5 µM and 160 µM at physiological pH and optimum pH, respectively). Based on the results of all investigated compounds, an additional approach combining virtual screening by pharmacophore filters with validation of scoring functions was applied. Using the re-scoring scheme with X-Score and subsequently the automated flexible docking programme FlexX, a double-docking-double-scoring strategy was derived which seems to improve the selection and lead optimisation of hyaluronate lyase inhibitors.

‡‡‡ Purchase, synthesis and pharmacological investigations of the selected compounds were subject of the PhD thesis of Sunnhild Salmen, Universität Regensburg, 2003.

To validate the usage of the LeadQuest® (Vol. 1&2 and Vol. 1-3), the Accelrys and the ChemACXF databases in further virtual screening approaches, the distribution of six (physico)chemical properties (molecular weight, log P, numbers of H-bond donor and acceptor atoms, numbers of rotatable bonds and of rings) within these databases were analysed with respect to drug-likeness. The analysis revealed that the further development of the LeadQuest® database from Vol. 1&2 to Vol. 1-3 led to a compound selection which contains more drug-like molecules than its ancestor with respect to all examined properties except for molecular weight. Furthermore, the rather raw pre-filtering of the ChemACX database as compound selection of commercially available molecules by elimination of reactive compounds and of entities outside a certain molecular weight range resulted in a database with property distributions significantly different from those of the LeadQuest® databases, though covering the essential pharmacological space. Thus, the LeadQuest® databases Vol. 1-3 as well as the reduced ChemACX database are likewise suited for the selection of potential drugs and provide a robust basis for virtual screening with the programme LUDI.

A property analysis for the potential hyaluronate lyase inhibitors, i.e., the *de novo* design hits from the LeadQuest® and ChemACXF databases, in comparison to the property distributions in the original databases should give insights into the capability of the programme LUDI to extract molecules meeting the LUDI-derived pharmacophore features with similar (physico)chemical properties. Obviously the screening filter of LUDI (the pharmacophoric properties of the hyaluronate lyase binding site) generates a constrained but allowed pharmacological space represented by typical ranges of molecular weights, log P values, numbers of H-bond donor and acceptor atoms, and numbers of rotatable bonds. Thus, these ranges are subranges with respect to the property distributions of the databases used which cover most of the ‘potential pharmacological space’.

For *de novo* design of inhibitors of bovine testicular hyaluronidase (BTH) with the programme LUDI, a homology model of the enzyme based on crystal structures of bee venom hyaluronidase was constructed with the help of MODELLER. Filtering of the LeadQuest® databases Vol. 1-3 and the ChemACXF database resulted in more than 5500 hits. Five compounds were selected for testing hyaluronidase inhibition.

Unfortunately, none of the compounds inhibited BTH, probably due to their poor solubility. To possibly overcome this failure by less lipophilic compounds, an additional, ligand-based approach was performed. The superposition of the active sites of the BTH model, the crystal structures of bee venom hyaluronidase and the bacterial chitinases A and B in complex with inhibitors revealed a very good overlap of the amino acids involved in catalysis and of the co-crystallised ligands (HA tetrasaccharide fragment, allosamidin and CI-4). By considering essential substructures mimicking the proposed intermediate of hyaluronic acid hydrolysis and by introducing suitable substituents suggested to interact with amino acids of the active site of the bovine enzyme, two compounds were proposed as potential inhibitors of BTH.

Based on the finding that vitamin C weakly inhibits *S. pneumoniae* hyaluronidase, the more hydrophobic vitamin C derivative L-ascorbic acid-6-hexadecanoate was investigated and proved to be a potent inhibitor of *S. agalactiae* hyaluronidase, *S. pneumoniae* hyaluronidase and BTH with IC_{50} values of 4 µM, 100 µM and 56 µM, respectively. L-ascorbic acid-6-hexadecanoate is the most potent inhibitor of bacterial and bovine hyaluronidase described to date.

The binding mode of L-ascorbic acid-6-hexadecanoate at *S. pneumoniae* hyaluronidase was determined by X-ray analysis[§§§], supporting the hypothesis that additional hydrophobic interactions with Trp291, Phe343, His399, and Thr400 in the active site contribute to the high affinity. To predict the potential binding mode of L-ascorbic acid-6-hexadecanoate at BTH, flexible docking of the compound with FlexX was performed suggesting two alternative binding modes. With respect to potential hydrophobic interactions, that binding mode seems to be clearly favoured where the long alkyl chain of L-ascorbic acid-6-hexadecanoate favourably interacts with an extended, strongly hydrophobic channel formed by the mostly conserved amino acids Ala84, Leu91, Tyr93, Tyr220 and Leu344.

Starting from elucidation of two hyaluronate lyase-inhibitor complexes, the binding modes of sulfamic acid 1-decyl-2-(4-sulfamoyloxy-phenyl)-1*H*-indol-6-yl ester and L-ascorbic acid-6-hexadecanoate were analysed indicating that the vitamin C portion of

[§§§] These studies were performed in cooperation with M. J. Jedrzejas (Children's Hospital Oakland Research Institute, Oakland, California 94609, USA). The X-ray structure of the complex was solved by D. Rigden (National Center of Genetic Resources and Biotechnology, Cenargen/Embrapa, Brasília, D.F. 70770-900, Brazil).

L-ascorbic acid-6-hexadecanoate binds in exactly the same region of the catalytic site as the indole ring of sulfamic acid 1-decyl-2-(4-sulfamoyloxy-phenyl)-1*H*-indol-6-yl ester. Additionally, the long aliphatic substituents of both compounds bind in the same surface crevice. With the help of the programmes LUDI and GRID, regions where H-bond donor, H-bond acceptor and hydrophobic moieties of inhibitors may interact most favourably were identified and transferred into a 3D pharmacophore model. This model might serve as basis for a virtual screening approach with UNITY or CATALYST.

The analysis of known SAR of 2-phenylindole derivatives with respect to the observed binding mode of sulfamic acid 1-decyl-2-(4-sulfamoyloxy-phenyl)-1*H*-indol-6-yl ester at *S. pneumoniae* hyaluronate lyase and to the 3D pharmacophore model led to suggestions about the binding mode of benzoxazole-2-thione derivatives. Based on the superposition of the crystal structure of this bacterial lyase in complex with the co-crystallised indole derivative and a substrate-based hexasaccharide, novel benzoxazole-2-thiones with 3-substituted *N*-propanoyl groups were predicted as putative hyaluronate lyase inhibitors. This design strategy was confirmed by the activity of the 3-phenylpropanoyl derivative which potently inhibits *S. agalactiae* strain 4755 hyaluronate lyase with an IC_{50} value of 15 µM.

In summary, ligand-based and structure-based approaches led to the identification of hyaluronidase inhibitors with (sub)micromolar activity. Especially by *de novo* design, potent hyaluronate lyase inhibitors were obtained. Further work is necessary to design inhibitors of mammalian hyaluronidases which can be used as pharmacological tools to study the role of the enzyme and its substrate, hyaluronic acid, in physiological and pathophysiological processes.

Chapter 9 Appendix

List of abbreviations

2D	two-dimensional
3D	three-dimensional
ACD	Available Chemical Directory
ADMET	absorption, distribution, metabolism, excretion, toxicity
BSA	bovine serum albumin
BTH	bovine testicular hyaluronidase
BVH	bee venom hyaluronidase
CADD	Computer-aided drug design
CTAB	cetyltrimethylammonium bromide
ChiA	chitinase A
ChiB	chitinase B
CI-4	cyclo-(L-Arg-D-Pro)
CMC	Comprehensive Medicinal Chemistry
DMSO	dimethylsulfoxide
DTT	dithiothreitol
HA	hyaluronic acid
HTS	high-throughput screening
hylSpn	*S. pneumoniae* hyaluronidase
$hylB_{3502}$	*S. agalactiae* strain 3502 hyaluronate lyase
$hylB_{4755}$	*S. agalactiae* strain 4755 hyaluronate lyase
IC_{50}	concentration of an inhibitor required to give 50 % inhibition of enzyme activity
IU	international units
K_d	equilibrium dissociation constant
K_i	inhibition constant
K_m	Michaelis constant; concentration of a substrate at which reaction rate is half maximal
lg	log

log P	logarithm of the partition coefficient
M	mol/L
min	minute
MW	molecular weight
NCE	database of New Chemical Entities
PMF	potential of mean force
QSAR	quantitative structure-activity relationships
rms	root mean square
SAR	structure-activity relationships
SCR	structurally conserved regions
UV	ultra violet

List of publications and abstracts

Braun, S., Botzki, A., Schneider, L., Bernhardt, G., Dove, S., Buschauer, A. Benzimidazoles and analogues as hyaluronidase inhibitors. Frontiers in Medicinal Chemistry, Erlangen, Germany, March **2004**.

Radons J., Dove S., Neumann D., Altmann R., Botzki A., Martin M.U., Falk W. The interleukin 1 (IL-1) receptor accessory protein Toll/IL-1 receptor domain: analysis of putative interaction sites in vitro mutagenesis and molecular modeling. *J Biol Chem.* **2003**;278(49):49145-53.

Böhmer F.D., Karagyozov L., Uecker A., Serve H., Botzki A., Mahboobi S., Dove S. A single amino acid exchange inverts susceptibility of related receptor tyrosine kinases for the ATP site inhibitor STI-571. *J Biol Chem* **2003**; 278(7):5148-55.

Mahboobi, S., S. Teller, H. Pongratz, H. Hufsky, A. Sellmer, A. Botzki, A. Uecker, T. Becker, S. Baasner, C. Schächtele, F. Überall, M. U. Kassak, S. Dove, F.-D. Böhmer, Bis(*1H*-2-indolyl)methanones as a novel class of inhibitors of the platelet-derived growth factor receptor kinase, *J Med Chem* **2002**, 45(5):1002-18.

Botzki A., Braun S., Ridgen D.J., Nukui M., Bernhardt G., Dove S., Buschauer A., Jedrzejas M.J.: L-ascorbic acid-6-hexadecanoate as potent inhibitor of hyaluronidases. Jahrestagung der DPhG, Würzburg, Germany, 8.-11. Oktober **2003**.

Botzki, A., Salmen, S., Schneider, L., Bernhardt, G., Dove, S., Buschauer, A.: Structure-based design of bacterial hyaluronidase inhibitors. Jahrestagung der DPhG, Germany, 9.-12. October 2002, *Arch. Pharm. Pharm. Med. Chem.* 335, Suppl.1, **2002**.

Salmen, S., Botzki, A., Walter, G., Schreiber, E., von Angerer, E., Bernhardt, G., Dove, S., Buschauer, A.: Indole derivatives as inhibitors of bacterial hyaluronidase. Jahrestagung der DPhG, Germany, 9.-12. Oktober 2002, *Arch. Pharm. Pharm. Med. Chem.* 335, Suppl.1, **2002**.

Braun, S., Botzki, A., Jedrzejas, M., Bernhardt, G., Dove, S., Buschauer, A.: Vitamin C derivatives as inhibitors of bacterial hyaluronidase. Jahrestagung der DPhG, Germany, 9.-12. October 2002, *Arch. Pharm. Pharm. Med. Chem.* 335, Suppl.1, **2002**.

Hoechstetter, J., Asen, I., Botzki, A., Fischer, D., Geyer, A., Bernhardt, G., Buschauer, A.: Biochemical characterisation of a hyaluronate lyase preparation from *Streptococcus agalactiae*. Jahrestagung der DPhG, Germany, 9.-12. Oktober 2002, *Arch. Pharm. Pharm. Med. Chem.* 335, Suppl.1, **2002**.

Dove, S., Karagyosov, L., Uecker, A., Serve, H., Botzki, A., Mahboobi, S., Böhmer, FD.: Molecular determinants for the selectivity of the tyrosine kinase inhibitor STI-571 (Gleevec^{TM}). Jahrestagung der DPhG, Germany, 9.-12. Oktober 2002, *Arch. Pharm. Pharm. Med. Chem.* 335, Suppl.1, **2002**.

Mahboobi, S., Teller, S., Pongratz, H., Hufsky, H., Sellmer, A., Botzki, A., Uecker, A., Beckers, T., Baasner, S., Schächtele, C., Überall, F., Kassack, MU., Dove, S., Böhmer, FD.: Bis(*1H*-2-indolyl)methanones as a novel class of inhibitors of the PDGF receptor kinase. Jahrestagung der DPhG, Germany, 9.-12. Oktober 2002, *Arch. Pharm. Pharm. Med. Chem.* 335, Suppl.1, **2002**.

Salmen, S., Botzki, A., Schneider, L., Bernhardt, G., Dove, S., Buschauer, A., Inhibitors of bacterial hyaluronidases: structure-based lead discovery, Poster, 17th International Symposium on Medicinal Chemistry Barcelona, Spain. Abstract, *Drugs Fut.*; 27 (Suppl A), 432, **2002**.

Botzki, A., Salmen, S., Schneider, L. , Bernhardt, G., Dove, S. , Buschauer, A., Inhibitors of bacterial hyaluronidases: structure-based lead discovery, Lecture, Moderne Aspekte der Medizinischen Chemie, Travemünde, Germany, Oktober **2002**.

Botzki, A., Salmen, S., Schneider, L., Bernhardt, G., Dove, S., Buschauer, A., Structure-based design of bacterial hyaluronidase inhibitors, Lecture, Jahrestagung der DPhG in Berlin, Germany, September 2002, Lecture, *Arch. Pharm*. 335. **2002**.

Salmen, S., Botzki, A., Schneider, L., Bernhardt, G., Dove, S., Buschauer, A., Structure-based design and synthesis of hyaluronate lyase inhibitors, Poster, Summer School Medicinal Chemistry in Regensburg, Germany, 15.-18. September **2002**.

Botzki, A.: *De novo* Design von Inhibitoren der bakteriellen Hyaluronidasen; Weihnachtskolloquium des Organischen Instituts der Universität Regensburg am 18.12.2002, Vortrag.

Botzki, A., Dove, S.: Docking studies on inhibitors of the receptor tyrosine kinases PDGFR-β and FGFR-1. 21. Sommerkurs in Pharmazeutischer Chemie und Nationalsymposium für Doktoranden ‚E. Duranti', Urbino, Italien, 1.-5. Juli **2001**.

Botzki, S. Dove: Binding models for inhibitors of the receptors tyrosine kinases PDGFR-β and FGFR-1, *Arch. Pharm. Pharm. Med. Chem.* 333, Suppl.2, **2000**.

Erklärung

Ich erkläre hiermit an Eides statt, dass ich die vorliegende Arbeit ohne unzulässige Hilfe Dritter und ohne Benutzung anderer als der angegebenen Hilfsmittel angefertigt habe; die aus anderen Quellen direkt oder indirekt übernommenen Daten und Konzepte sind unter Angabe des Literaturzitats gekennzeichnet.

Regensburg, März 2004

(Alexander Botzki)